ELECTROCHEMISTRY OF PROTON-EXCHANGE-MEMBRANE ELECTROLYTE FUEL CELL (PEMFC) ELECTRODES

NENGYOU JIA

Electrochemistry of Proton-Exchange-Membrane Electrolyte Fuel Cell (PEMFC) Electrodes

by

Nengyou Jia

A thesis submitted to the school of Graduate Studies in partial fulfilment of the requirements for the degree of Master of Science

Department of Chemistry

Memorial University of Newfoundland

January 1999

St. John's Newfoundland

To my wife and son

ABSTRACT

The purpose of this research is mainly focused on four areas of the electrochemistry of PEMFCs: (1) developing a fast method to screen catalysts, (2) modifying carbon-supported Pt catalysts to improve their performance; (3) demonstrating a new method to accurately measure the catalyst active surface area by cyclic voltammetry; (3) reducing MeOH crossover in direct methanol fuel cells by modifying the electrolyte membrane.

In order to achieve the above goals, a new electrochemical apparatus was designed to study the oxygen reduction reaction (ORR) on gas diffusion electrodes. Different kinds of electrode & membrane assemblies (MEA) were made at various platinum loadings and different catalysts (10 % and 20 % Pt on Vulcan XC-72R) using the hot bonding method. Several electrochemical techniques (cyclic voltammetry, transient and steady state polarization, and ac impedance) have been used to evaluate the key parameters that determine the oxygen reduction performance of the electrodes, such as active catalyst surface area, Tafel slope, and resistance. Polarization results indicate that a self-written program for collecting current provides useful data for both transient and steady state polarizations. The transient (10s) polarization can fully represent the electrode performance rapidly and reliably. AC impedance is a useful technique for measurement of the cell performance.

Commercial carbon-supported Pt catalysts were modified by chemical oxidation (HNO_3, H_2SO_4, H_3PO_4, $HClO_4$, NaClO, H_2O_2, or $(NH_4)_2S_2O_8$) to enhance the catalytic

activity for oxygen reduction reaction. Catalysts modified by either acidic or non-acidic oxidants can significantly improve ORR performance. The catalysts treated by acids, especially by HNO_3, increase the number of carbon surface functional groups such as -OH and – COOH allowing protons more easy access to the catalyst surface. The improved ionic conductivity on the catalyst surface leads to a higher performance based on the triple contact mechanism for the ORR in the catalyst layer.

Furthermore, a technique using CO_2 electroreduction/reoxidation was evaluated to accurately measure the active surface area of carbon-supported catalysts as an alternative to the conventional use of hydrogen adsorption. The reduced CO_2 oxidation charge can be used to compare the active surface areas of different catalysts although charge should be used due to the complexity of the products of CO_2 reduction. This method retains the resolution advantage of the CO stripping method, and avoids the overestimation of the active surface area. Moreover, peak and onset potentials for reduced CO_2 oxidation are shown to be representative parameters for explaining catalyst tolerance to MeOH and CO, especially the oxidation onset potentials.

Finally, membranes modified with conducting polymers by different polymerization methods such as Fe^{3+}, $(NH_4)_2S_2O_8$, H_2O_2, and O_2 with UV irradiation were evaluated in terms of ionic conductivity and permeability to methanol. Electrochemical measurements showed that the modified membranes can significantly reduce methanol crossover. The inhibition of methanol crossover is realized by a lower methanol diffusion coefficient in the membrane as measured by chronoamperometry. The

stability of modified membrane needs to be evaluated under practical operating conditions of direct methanol fuel cells.

TABLE OF CONTENTS

Chapter 2

Electrochemical Evaluation of Commercial Catalysts and Modified Carbon-Supported Catalysts

LIST OF FIGURES

LIST OF TABLES

LIST OF ABBREVIATIONS AND SYMBOLS USED

Symbol	Meaning	Unit
A	electrode area	cm^2
AC	alternating current	
CV	cyclic voltammetry or cyclic voltammogram	
PEMFC	proton-exchange-membrane fuel cell	
DOE	Department of Energy of the USA	
FC	Fuel cell	
PAFC	phosphoric acid fuel cell	
AFC	alkaline fuel cell	
DMFC	direct methanol fuel cell	
MCFC	molten carbonate fuel cell	
SOFC	solid oxide fuel cell	
PFSA	polyfluoronated sulfonic acid	
YSZ	yttria stabilized zirconia	
PTFE	polytetrafluoroethylene	
MEA	membrane & electrode assembly	
IFC	International Fuel Cells, Inc.	
ORR	oxygen reduction reaction	
E_r	reversible potential for oxygen reduction	V

E	cell potential	V
I	current density	A/cm^2
b	Tafel slope	V/dec.
i_0	exchange current	A/cm^2
α	symmetry factor	
F	Faraday constant	96484.5 C/mol
GIC	graphite intercalation compound	
SCE	saturated calomel electrode	
EIS	electrochemical impedance spectroscopy	
R_{cell}	resistance of cell	
σ	conductivity of the catalyst	s/cm
d	sample thickness (catalyst or membrane)	cm
R_u	bulk resistance	Ω
R_{ct}	the charge-transfer resistance	Ω
C_{dl}	double layer capacitance	$\mu F/cm^2$
FTIR	Fourier transform infrared	
$Q_{H,s}$	the quantity of charge corresponding to saturation hydrogen coverage	
CO_{2r}	reduced CO_2	
SP	starting potential for reduced CO_2 oxidation	V
PP	peak potential for reduced CO_2 oxidation	V
PBI	polybenzimidazole	

PPy	polypyrrole	
PMPy	poly(N-methylpyrrole)	
C_m	methanol concentration in the membrane	mol/L
D_m	diffusion coefficient of methanol in the membrane	cm^2/s
i_{lim}	limiting current	A/cm^2
n	electrons per molecule involved in a redox process	
t	time	s
v	scan rate	V/s
Z'	real impedance	Ω
Z''	imaginary impedance	Ω
RT	room temperature	^0C
$E_{1/2}$	half-wave potential	V

ACKNOWLEDGEMENT

I would like to express my sincere appreciation to my supervisor Dr. Peter G. Pickup for his inspiring supervision and patient guidance through the course of the degree programme. His personal advice and help are greatly appreciated.

I would also like to give thanks to Dr. Zhigang Qi for his help on the treatment of some catalysts and membranes. Special thanks are extended to my colleagues: Colin Cameron, Brian Maclean, Huan Huang. Special appreciation also extended to my wife, Yuehua and my son, Ray Jia. I thank Ballard Power Systems, Inc. for the provision of some of the experimental materials.

For my financial support, the Graduate Fellowship from School of Graduate Studies of Memorial University of Newfoundland, the Teaching Assistantship from the Department of Chemistry, and the supplements from an NSERC Strategic Grant are gratefully acknowledged.

Chapter 1

1. General Review of Proton-Exchange-Membrane Fuel cells (PEMFCs)

1.1 History of Fuel Cells

The world energy perspective has changed since the first oil crisis of 1973. Increasing focus is being placed on clean energy alternatives for satisfying growing energy demands. The problem of atmospheric pollution has led to strict emission legislation in Japan and California. Over the last few years, discussions on the greenhouse effect have led to general acceptance of the theory that carbon dioxide (CO_2) emission causes global warming, and global studies have conclusively shown that the earth's fossil fuel resources should be better maintained in order to secure a sustainable future. In the USA, these concerns have led to the enactment of major laws. The Clean Air Act Amendment of 1990 reduced the volume of allowable emissions of pollutants and imposed strict regulation on pollution sources. The Energy Policy Act of 1992 set energy efficiency standards for industrial equipment and specifically calls for DOE (Department of Energy) programs to develop fuel cells. The increased interest in cleaner fuels strongly affects the automobile industry, and people now realize that the limited

fossil fuel reserves should be used as efficiently as possible. Therefore, in the last few years, this has resulted in a trend toward decentralization of power production with a strong emphasis on energy savings at the end-user's level (mainly household appliances and lighting systems)(1).

The development of the fuel cell (FC) covers 150 years since its invention in 1839, in which it has experienced ups and downs. A fuel cell is defined as an electrochemical device that can continuously convert the chemical energy of a fuel and oxidant to electrical energy without chemical combustion (2). Fuel cells work at a high efficiency with emissions far below the strictest industrial standards, and are not subject to the Carnot limitation as Gibbs energy can in principle be converted at 100% efficiency. For this reason, the fuel cell is considered to be the solution to the future problem of energy conservation. The hydrogen fuel cell is bound to be one of the alternative power sources of the future. It provides clean non-polluting energy, and produces only water and heat as byproducts. It is expected that the commercialization of fuel cells, and their use in homes, offices, hospitals (3, 4), shopping complexes, automobiles (5) and space missions will usher in the beginning of the hydrogen economy.

Although the fuel cell has received much attention in recent years, the underlying concept is by no means a product of the twentieth century (6, 7). A more detailed review of the background of the development of fuel cells can be found in reference (8). The first fuel cell was described by Grove in 1842 (9). However, Grove was troubled by the poor performance achievable at that time. Performance is still the major issue requiring improvement in present-day fuel cells. Throughout the first half of the twentieth century

several attempts were made to build fuel cells that could convert coal or carbon directly to electricity. None succeeded due to a lack of understanding of electrode kinetics.

The first major fuel cell development project that eventually led to a successful device was embarked upon in 1932 by Francis T. Bacon. In order to obtain a sufficiently large active electrode area with three-phase contact (triple contact), and therefore obtain high current densities, porous gas diffusion electrodes were used. However, no practical applications were realized until the 1960s (10), when systems were first used for the Apollo and Gemini space programs. Fuel cell technology was used for terrestrial systems by the 1970s, and tested by gas companies, electric utilities and electricity consumers by the 1980s. During this period, most of the development of fuel cells was in the experimental and demonstration stages. Not until 1990 was the decision taken, by three fuel cell companies, to start commercial production (11-13). Fuel cells continue to show outstanding promise as pollution-free energy sources of the future for power and transportation applications (14, 15)

There are five main types of fuel cell named according to their electrolyte materials, which have reached varying stages of development (16-19). All five fuel cells are designed to work on hydrogen or hydrogen-rich reformates as the fuel and oxygen or air as the oxidant. These five fuel cells are the phosphoric acid fuel cell (PAFC) working at approximately 200 ^{0}C with concentrated (103 wt %) phosphoric acid as the electrolyte, the alkaline fuel cell (AFC) working below 100 ^{0}C with 30 wt % KOH as the electrolyte, the proton exchange membrane fuel cell (PEM) with a water-swollen perfluorinated sulfonic acid ionomer as the electrolyte (this cell is used with a particularly modified

electrocatalyst for direct methanol fuel cells (DMFCs)), the molten carbonate fuel cell (MCFC) which most frequently uses a eutectic melt containing 38/62 mole % potassium and lithium carbonate and less frequently 48/52 mole % lithium and sodium carbonate, and the solid oxide fuel cell (SOFC) which uses oxygen ion conducting yttria stabilized zirconia (YSZ) as the electrolyte. Among these fuel cells, the phosphoric acid fuel cell (PAFC) is the most developed, and a number of 250 kW stacks have been produced in the USA and Japan for field demonstration with very promising results (20, 21). At the same time, the alkaline fuel cells are still operating in the Space Shuttle as an auxiliary power supply (22, 23). These alkaline fuel cell power plants (manufactured by International Fuel Cells – United Technologies Corporation) have a well-established record in NASA's space flights, although they have only been used for short durations (less than two weeks). The polymer electrolyte fuel cell is now a strong competitor for a hydrogen energy system for NASA's proposed long – range space missions (lunar, Mars and space stations).

1.2 Proton-Exchange-Membrane Fuel Cells (PEMFCs)

Proton-exchange-membrane fuel cells (PEMFCs) have attracted much interest recently, which is attributed to their unique advantages (24) which are as follows:

- high power density and efficiency
- fast startup and shutdown
- no liquid electrolyte and therefore less corrosion

- insensitive to differential pressures
- less sensitive to CO_2
- no carbonate formation
- long life and potable liquid product (water)
- versatility of application

The PEMFC is very attractive from the point of view that all components in the fuel cell are solid, and that its operational conditions are relatively mild (the temperature range is 50-90 ^{0}C, and the pressure is 3-6 atm). Thus, the PEMFC system would be an excellent candidate for commercial viability. The need for an efficient, nonpolluting power source for vehicles in urban environments emphasized by recent legislative initiatives has resulted in increased attention to the use of fuel cells to power vehicles with high efficiency and low tail-pipe emissions. In fact, it is this application which has stimulated PEMFC technology research and development.

In PEMFCs, the heart of the cell is the so-called membrane/electrode assembly (MEA). In its simplest form, the electrode component of the MEA would consist of a thin layer (5-50 μm thick) containing a dispersed platinum catalyst. This catalyst layer is in good contact with the ionomer membrane (typically 50-175 μm thick) that serves as the electrolyte and gas separator. Teflonized porous carbon paper or carbon cloth serves as a gas distributing layer and current collector. Therefore, a MEA will always have the following structure when viewed from either the anode or cathode side: porous wet-proofed carbon backing/catalyst layer//ionomer membrane//catalyst layer/porous wet-

proofed carbon backing. With the help of the catalyst, hydrogen is electrochemically ionized and broken down into positive hydrogen ions (protons) and negatively charged electrons at the hydrogen electrode (anode) as shown in **Eqn (1.1)**.

$$H_2 \longrightarrow 2H^+ + 2e^- \qquad (1.1)$$

The protons are attracted to the negatively charged sulfonic acid groups of the ionomer membrane. These sulfonic acid groups provide sites for the hydrogen ions that are then allowed passage through the membrane to the oxygen electrode (cathode). There, the hydrogen ions electrochemically combine with oxygen and electrons, that have been transported through the external load from the anode to the cathode, to produce water according to **Eqn (1.2)**.

$$O_2 + 4e^- + 4H^+ \longrightarrow 2H_2O \qquad (1.2)$$

The catalyst used in the PEMFC was originally platinum black, and a high loading was required to provide high performance. More recently, the application of carbon supported catalysts is the most important breakthrough in fuel cell development for catalyst cost reduction (25).

The membrane commonly employed in most recent PEMFC technology developments is made of a perfluorocarbon sulfonic acid ionomer. Nafion™ made by DuPont is the best-known example of this type of membrane. Nafion has a 130 ^{0}C glass

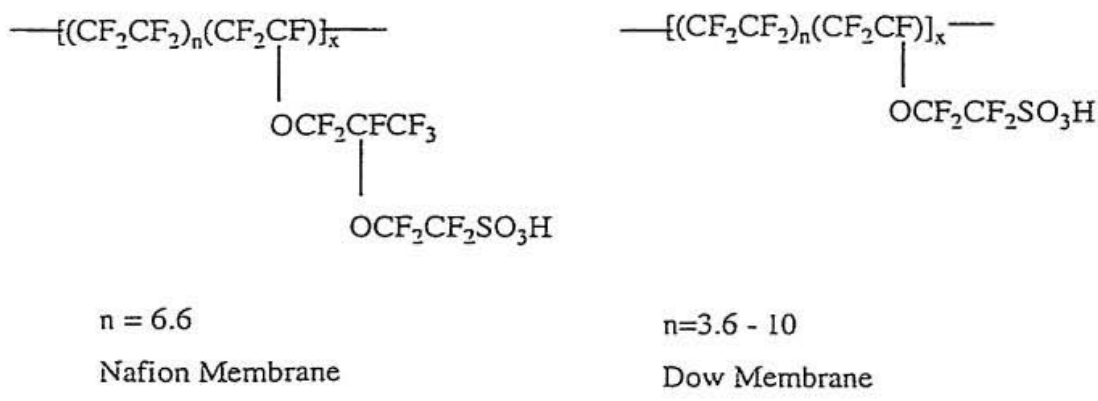

Fig. 1.1 The skeleton structures of Nafion and Dow membranes (26, 27).

transition temperature, which indicates that higher temperatures will change the polymer to the gel state in which it can flow. Both polymers (Nafion and Dow) have the following desirable properties: high oxygen solubility, high proton conductivity, high chemical stability, low density, and high mechanical strength.

The porous backing layer placed behind the catalyst layer fulfills important tasks in the PEMFC. It must provide the combined requirements of effective reactant gas supply to the catalyst layer and effective water supply or removal. Wet-proofing by PTFE is required to ensure that at least part of the pore volume in the cathode backing remains free of liquid water in an operating cell, so as to enable rapid gas-phase transport. Obviously, the backing layer has to be made of a material of high and stable electronic conductivity in a wet environment. Although some porous metal structures have been suggested, most of PEMFC backings to date have been based on porous carbon paper or cloth.

1.3 Development of PEMFCs

The development of PEMFCs up to the middle of the 1960s has been reviewed by Niedrach and Grubb (28), Magnet (29), and Liebhavsky and Cairns (8). Appleby and Foulkes (30) have reviewed PEMFC technology with respect to its early development, membrane structure and functioning. The research pursued on PEMFCs mostly covers three fields including the development of reliable electrolyte membranes and the improvement of catalyst performance as well as the development of membrane and electrode assemblies (MEAs). The early research on PEMFCs enhanced the basic understanding of fuel cells, i.e., "the electrochemistry of fuel cells". During the 1980s, new initiatives in the development of PEMFC stacks and power systems emerged. The present status of the solid polymer electrolyte fuel cell technology is summarized in several recent articles (31-38).

The performance of fuel cells was increased significantly by the development of the MEA structure and engineering design, and the platinum loading was reduced greatly from 4 mg/cm^2 down to 0.4 mg/cm^2 without compromising performance. The size of stacks had reached the kilowatt level. In recent years, PEMFC performances have been improved by a number of approaches which include system design, stack operating conditions, stack hardware and MEA design, but all options have to be assessed from an engineered system point of view (39). Most of the system designs concentrated on water management in the stack (40-44). Performance loss due to flooding is mainly on the cathode and at high current densities, typically greater than 0.8 A/cm^2, where mass

transport effects dominate. The low concentration of oxygen in air, the reaction kinetics associated with oxygen reduction, the formation of liquid water resulting in water flooding of active sites and restriction of oxygen transport to the active electrocatalyst layer, all result in substantial cathode overpotentials, particularly at high current densities. By appropriate cell design and operating conditions, liquid water accumulated in the cathode can be drawn by a concentration gradient across the membrane to the anode and removed by the fuel stream at the anode.

In spite of improved system designs and operating conditions, the improvement of fuel cell performance also relies on the optimization of MEA structure that plays a very important role in PEMFC performance. Therefore, a lot of work has been concentrated on this area. The earliest method of the MEA preparation was based on bonding of platinum black to the polymeric membrane. A US patent (45) described catalytically active layers prepared from finely divided metal powders (blacks) mixed with a binder such as polytetrafluoroethylene (PTFE). The catalysts were applied to a substrate, and bonded to the membrane using appropriate combinations of temperature and pressure. This technique has remained to date the method of choice in the preparation of MEAs. The drawback of this mode is low catalyst utilization as there is a lack of efficient access of protons to a large fraction of catalyst particles (those located away from the membrane electrolyte), and also lack of efficient gas access to another fraction of the catalyst sites (those deeply embedded in the membrane). Therefore, the combined result of limited dispersion and low utilization in such Pt/PTFE mixtures requires a high platinum loading, typically 4 mg Pt/cm^2, to obtain satisfactory cathode performance, particularly for

operation with air. At such loadings the catalyst cost inhibits the commercialization of PEMFC.

Based on the working mechanism of the PEMFC, the cathode must be effectively accessed simultaneously by all three reactants: oxygen gas, electrons, and protons for the Pt sites to be active for oxygen reduction. The first move toward substantially lowering the platinum loading in PEMFCs, while maintaining comparable cell performance, was described by Raistrick (46). Raistrick used a mixture of carbon-supported platinum (Pt/C) and PTFE deposited onto a carbon paper that was pretreated with PTFE to make it hydrophobic. Compared with catalysts based on platinum black, an important advantage of the carbon-supported platinum catalyst is the higher degree of dispersion. Particle diameters of 2 nm are easily obtained in carbon-supported form by various protocols described in the patent literature. However, this MEA still suffers poor performance when electrodes are bonded by hot-pressing onto an ionomeric membrane as there is a lack of proton access to the majority of catalyst sites which are not in intimate contact with the membrane. This understanding of the limitations in the MEA for PEMFCs was important. In a catalyst layer comprising Pt/C (or platinum black) mixed with PTFE, the two first requirements are effectively met due to the good connectivity within the carbon support/carbon powder (or platinum black) and the hydrophobic pores generated by the PTFE component, respectively. The third requirement, effective proton access, cannot be met adequately.

To overcome this critical limitation, Raistrick (47) impregnated the Pt/C/PTFE catalyst layer on the carbon cloth with a solution of Nafion prior to hot-pressing the

electrode onto the membrane. Impregnation of the catalyst layer in this way with recast ionomer resulted in a very significant increase in performance and demonstrated, for the first time, significant PEMFC performance with platinum loadings as low as 0.4 mg/cm^2, i.e., an order of magnitude lower than that employed in the GE/Hamilton (an USA fuel cell company) standard technology. This first result of Raistrick with impregnated gas-diffusion electrodes (47) was a breakthrough in PEMFC technology in two senses. The main idea in this method is to extend the three-dimensional reaction zone by impregnation of a proton conductor (for example, Nafion) into the active layer of an electrode with a low platinum loading. Firstly, it demonstrated that PEMFCs could be effectively operated with Pt/C catalysts of loading similar to the ones employed in the phosphoric acid fuel cells, thus bringing the loading and cost of the precious metal catalyst down by an order of magnitude. In addition, and perhaps even more importantly for developments to follow, this innovative experiment revealed the great importance of "triple access" (gas, electrons, protons) to each active catalyst site and, with that, it opened the way to further optimization of catalyst layers in PEMFCs with the desired combination of low loadings and high performance. Although PTFE is usually effective as a binder and imparts hydrophobicity to the gas diffusion regime of the electrode, no particular advantage is realized by the presence of PTFE in the immediate vicinity of the catalyst sits. Moreover, a penalty is paid in the catalytic region due to the lack of utilization of catalyst in completely dry and/or Teflon-coated pores.

Based on the above considerations, a new structure for PEMFC electrodes was developed by Wilson et al. (48), which attempted to improve upon the previous

construction by significantly increasing the contact area between the polymer electrolyte and the platinum clusters. This was achieved in two ways. First, the supported catalyst and the ionomeric additive are cast together to form the catalytic layer. This ensures that the thickness of the catalyst layers coincides with the depth of the ionomer impregnation. Second, the contact area between the ionomer additive and catalyst is increased by completely eliminating the PTFE component and by improving the dispersion of the ionomer through the catalyst layer. In the absence of PTFE, the recast Nafion provides the structural integrity. The gas diffusion portion of the electrode consists of a separate Teflonized carbon cloth backing that is placed behind the thin catalyst film to provide support and to provide a hydrophobic distribution network for the gases. The two-part construction of the electrode – hydrophobic backing and hydrophilic catalyst layer – allows each of the two regions to be fabricated separately with the properties that best suit the function of each.

Oxygen reduction at the platinum/Nafion interface has recently been the subject of active research (49-52). Such fundamental investigations are immediately relevant to an understanding of the operation of the oxygen electrode of proton-membrane fuel cells (53).

Further significant improvements of the initial idea described by Raistrick were achieved by Srinivasan, Ticianaelli and their co-workers. They described successful attempts to increase the performance of impregnated Pt/C layers on carbon supports and hot-pressed to the membrane by increasing the temperature and gas pressure (54), optimizing the percentage of Nafion impregnant (55), replacing the 10% Pt/C with a 20%

Pt/C (56), and adding a thin layer of platinum on the front surface of the electrode by sputter deposition and an electrochemical catalyzation (ECC) prior to impregnation (57-59). The last two modifications shorten the average distance traveled by protons to access the platinum catalyst sites and generate, particularly in the case of the sputtered film, a significant number of active Pt sites very close to the membrane. The objectives of these methods are to use relatively thin electrocatalytic layers in the gas diffusion electrodes and to localize further the platinum near the front surface of the electrodes to minimize activation, ohmic, and mass transport overpotentials. The electrodes performance by those methods have demonstrated that it is possible to achieve current densities of about 2 A/cm^2 at cell potentials of close to 0.6 V with H_2/O_2 as the reactants and of about 0.45 – 0.5 V at the same current density with H_2/air as the reactants (60). An optimum configuration of the electrode was found to be the one fabricated with 20 wt% Pt/C in the supported electrocatalyst onto which was sputtered a 50 nm film of platinum.

Another mode of application of platinum catalyst to a porous carbon structure has been described by Taylor et al. (59). This special mode involves impregnation of the porous carbon structure with ionomer, exchange of the cations in the ionomer by a cationic complex of platinum, $Pt(NH_3)_4^{4+}$, and electrodeposition of platinum from this complex onto the carbon support. The result of such a procedure is the deposition of platinum only at sites that are accessed effectively by both the electronic conductor (carbon) and the ionic conductor (recast Nafion). In this regard, this mode of catalyst preparation seems to offer an important advantage of catalyst utilization. Indeed,

significant PEMFC performances can be obtained with cathodes prepared in this way with loading as low as 0.05 mg Pt/cm^2, as reported by Taylor and co-workers (59).

1.4 Current Challenges for PEMFCs

The successful development and commercialization of low- to medium-temperature fuel cells, particularly for terrestrial applications, depends on enhancing the kinetics of the electroreduction of oxygen. The major challenges in reaching this goal have been and, to some extent still are, as follows:

(i) The first challenge is to attain the reversible potential. The oxygen electrode has an exchange current density at Pt of 10^{-9} A/cm^2 or lower at low to medium temperatures. Due to competing reactions, even on the best metallic electrocatalyst (Pt), it is practically impossible to attain the reversible potential. The competing reactions are metal dissolution, oxide formation, and oxidation of the carbon support and organic impurities. The net result is that the observed rest potential is a mixed potential which is lower than the reversible potential of the oxygen electrode reaction by typically ca. 0.2 V. This loss in cell potential has a primary effect of reducing the efficiency of fuel cells by as much as 16% before any current is drawn. Therefore, further improvement in Pt based catalyst technology would be desirable to increase the efficiency of fuel cells and reduce catalyst loadings, and new types of catalyst also need to be developed to meet cost

reduction targets. Moreover, these advances must also be amenable to useful, high-volume production

(ii) The second challenge is to enhance the electrode kinetics of oxygen reduction with alloy electrocatalysts. The best results to date have been obtained with alloys of platinum with chromium, vanadium, cobalt, or nickel. The non-noble metal component is more corrodible than the noble one. Thus, preferential dissolution of the former may occur, which causes a degradation in performance of the oxygen electrode. Worse still is that the transition metal can migrate to the hydrogen electrode and inhibit its electrocatalytic activity. By optimizing the composition and structure of the alloy, these problems can be minimized. Therefore, the modification of Pt based catalysts to enhance their catalytic activity becomes practical.

Although several new techniques have been applied to increase fuel cell performance and reduce platinum loading, the slowness of oxygen reduction on the cathode catalyst still limits fuel cell efficiency. Therefore, further efforts need to be taken to improve the catalytic activity of the catalyst. Since carbon has widely been used as the catalyst support, it can be modified to increase its surface proton conductivity without sacrificing electronic conductivity. The proton conductivity of the carbon support can extend the three-dimension reaction zone without the involvement of foreign ionic conductors leading to less inhibition of diffusion of the reactive oxidant gas.

2. Direct Methanol Fuel Cells (DMFCs)

In respect to fuel cell commercialization in vehicle applications, electrochemists are challenged to use a fuel that is easily transported and converted into energy from the liquid state. Although the PEMFC is the most promising candidate to replace gasoline engines in vehicles, gaseous fuels such as hydrogen suffer serious storage and transportation problems, and are incompatible with present fuel distribution systems. In order to fit the existing gasoline system, a liquid fuel such as methanol is a favored choice (61). The direct methanol/air fuel cell (DMFC) uses aqueous methanol solutions. The overall reaction for methanol oxidation can be written as follows:

$$CH_3OH + H_2O \longrightarrow CO_2 + 6H^+ + 6e^- \qquad (1.3)$$

With E^0=0.029 V/SHE (62).

The advantages of the methanol liquid-feed fuel cell over cells designed for gas-feed may be summarized as follows:

- elimination of fuel vaporizer and its associated heat source and controls,
- elimination of complex humidification and thermal management systems,
- dual-purpose use of the liquid methanol/water as fuel and as an efficient stack coolant, and
- significantly lower system size, weight and temperature than existing fuel cell systems.

Recent advances in DMFC research and development have been quite dramatic, with the methanol/air fuel cell achieving a power density which is a very significant fraction of that achieved with methanol reformate/air fuel cells. Recent DMFC work has strongly focused on cells with polymeric (primarily PFSA) membrane electrolytes. More applied work, aim primarily at the demonstration of enhanced, stable performance of DMFC single cells or stacks has taken place in the USA in research institutes including the Jet Propulsion Laboratory (63, 64). Case Western Reserve University (65), and Los Alamos National Laboratory (66) in collaboration with industries such as International Fuel Cells (IFC) and Giner, Inc. Similar efforts in Europe resulted in a demonstration at Siemens (67) of a high performance polymer electrolyte DMFC operating at temperatures above 120 ^{0}C. The performance was such that 0.5 V was reached at the 270 mA/cm^{2} design point (68).

In spite of the DMFC's advantages, however, the DMFC remains poorly developed compared to other fuel cells. Great difficulties have also been encountered in improving the efficiency of DMFC itself. These problems may be summarized as:

- Similar electrocatalysts have been proposed for both anode and cathode, leading to the problem of mixed potentials at both electrodes and a marked reduction in efficiency. The anode reaction is very slow near the thermodynamic potential, at least on the catalysts currently used. A large overpotential loss is therefore encountered (69).

- the catalysts currently used for the anode are all based on high platinum content. These catalysts are easily poisoned both by impurities and (more seriously) by products of the anodic reaction.
- MeOH crossover from the anode to the cathode is a major problem that needs to be solved in order to commercialize DMFCs (70). MeOH crossover will depolarize the cathode so as to drastically decrease cell performance, and waste a large amount of fuel.

3. The Objectives of This Thesis

The main purpose of the work described in chapter 2 was to develop a reliable and fast screening technique to characterize carbon-supported catalysts. In order to improve the performance of commercial catalysts, chemical oxidation methods, especially in acidic environments, have been investigated. The mechanisms by which the modified catalysts show improved performance are also discussed in this chapter.

When carbon is used as a catalyst support, it can increase the degree of dispersion of the catalyst to provide better performance than platinum black at low loadings. But, it also creates a problem, in that, it becomes very difficult to determine the active surface area as the minimum potential for hydrogen adsorption is not pronounced. The active platinum surface area of the catalyst is an intrinsic property of the catalyst. Therefore, it is necessary to accurately determine it. The present method involving hydrogen

adsorption or desorption needs to be modified to achieve that accuracy. These subjects will be addressed in Chapter 3.

In order to prevent MeOH crossover in DMFC, Nafion membranes have been modified with conducting polymers such as polypyrrole and polymethylpyrrole by different polymerization methods. A potential step method was employed to evaluate inhibition of crossover by the modified membranes. Preliminary results are presented in Chapter 4.

References

(1) S. A. Weiner, J. Power Sources, 71, 61 (1998).

(2) G. T. Young, " Fuel Cells," Rheinhold Publishing, New York, Vol.1: Symposium of Am. Chem. Soc., 1959 (1960); Vol. 2: Symposium of Am. Chem. Soc., 1961 (1963).

(3) T. A. Pamberger, J. Power Sources, 71, 45 (1998).

(4) F. Panik, J. Power Sources, 71, 36 (1998).

(5) S. G. Chalk, J. Milliken, J. F. Miller, S. R. Venkateswaren, J. Power Sources, 71, 26 (1998).

(6) B .J. Crowe, Fuel Cells: A survey, NASA Rep. (sp-5115) , Washington, DC (1973).

(7) J. B. O'Sullivan, Historical Review of Fuel Cell Technology, Proc. 25th Power Sources Symp., 149 (1992).

(8) H. A. Liebhavsky and E. J. Cairns, Fuel Cells and Batteries, Interscience, New York,

1968, pp. 587-619.

(9) W. R. Grove, Phil. Mag., 21, 417 (1842).

(10) Pratt & Whitney Aircraft, Design and Development of H_2-O_2 Fuel Cell Power Plants for Apollo Command Module, NASA/Houston, Final Report 6/16/1962.

(11) K. B. Prater, J. Power Sources, 61, 105 (1996).

(12) R. Whitaker, J. Power Sources, 71, 71 (1998).

(13) K. Hassmann, and R. Rippel, J. Power Sources, 71, 75 (1998).

(14) K. B. Prater, J. Power Sources, 51, 129 (1994).

(15) P. F. Howard and C. J. Greenhill, Proc. 1993 Future Transportation Technical Conf., San Antonio, TX. USA, 9-12 Aug. 1993, SAE Special Publication No. 984, Warrandale, PA, USA, 1993, pp. 113 – 119.

(16) Alfa, Research Chemicals, Metals and Materials, 1997-98

(17) Supramaniam Srinivasan, Electrochemistry in Transition- From the 20th to the 21st century, Edited by O. J. Murphy, Supramaniam Srinivasan and Brian E. Conway (1992).

(18) K. V. Kordesch and G. R. Simader, Chemical Reviews, 95, 191 (1995).

(19) H. Wendt, T. Brenscheidt, and A. Fischer, Phil. Trans. Roy. Soc. Lond. A, 354, 1627 (1996).

(20) A. J. Appleby, and F. R. Foulkes, Fuel Cell Handbook, Krieger Publishing Company, 1993.

(21) International Fuel Cells (IFC), "The PC 25 200kW Fuel Cell Plant", CEC-Italian Fuel cell Workshop, Proceedings (P. Zegers, ed.) Taormina, Italy, 1987, p. 81.

(22) K. Kordesch, J. Gsellman, P. Kalal, J. C. T. Oliveira, and K. H. Steininger, Proceedings of the 33rd International Power Sources Symposium, p. 817, The Electrochemical Society, Inc. Pennington, NJ. 1988.

(23) M. Warshay and P. R. Prokopius, J. Power Sources 29, 193 (1989).

(24) K. Straber, Ber. Bunsenges. Phys. Chem. 94, 1005 (1990).

(25) P. Stonehart, "State-of-the-Art for Dispersed Platinum Electrocatalysts", p. 96, Extended Abstracts, 31st Meeting ISE, Venice, Italy 1980.

(26) W. A. Titterington, and A. D. Fickett, Proc. 8th Intersoc. Energy Conv. Eng. Conf., 574 (1973).

(27) H. L. Yeager, and A. Steck, Anal. Chem. 51, 862 (1979).

(28) L. W. Niedrach and W. T. Grubb in W. T. Michell Jr. (Ed.), Fuel Cells, Academic Press, New York, 1993, p. 253.

(29) H. J. R. Magnet in C. Berger (Ed.), Handbook of Fuel Cell Technology, Prentice-Hall, Englewood Cliffs, NJ, 1967, pp. 425-491.

(30) J. Appleby and R. R. Foulkes, Fuel Cell Handbook, Van Nostrand Reinhold, New York, 1989.

(31) S. Srinivasan, D. J. Manko, H. Koch, M. A. Enayetullah and A. J. Appleby, J. Power Sources, 29, 367 (1990).

(32) S. Srinivasan, O. A. Velev, A. Parthasarathy, D. J. Manko and A. J. Appleby, J. Power Sources, 36, 299 (1991).

(33) H. P. Dhar, J. Electroanal. Chem., 357, 237 (1993).

(34) S. Mukerjee and S. Srinivasan, J. Electroanal. Chem., 357, 201 (1993).

(35) Leo. J. M. Blomen and Michael N. Mugerwa , Fuel Cell Systems, Plenum Press, New York, 1993.

(36) K. Kordesch and G. Simader, Fuel Cells and Their Applications, VCH, 1996, p. 72.

(37) J. P. Shoesmith, R. D. Collins, M. J. Oakley and D. K. Stevenson, J. Power Sources, 49, 129 (1994).

(38) S. Gottesfeld and T. A. Zawodzinski in: Advances in Electrochemical Science and Engineering, edited by R. C. Alkire, H. Gerischer, D. M. Kolb and C. W. Tobias, WILEY-VCH, Vol. 5, 1997, p.195.

(39) D. H. Swan, O. A. Velev, I. J. Kakwan, A. C. Ferreira, S. Srinivasan and A. J. Appleby, Tech. Proc. Hydrogen '91 Conf. (Edited by T. N. Veziroglu), Independence, Missouri (1991).

(40) T. E. Springer, M. S. Wilson and G. Gottesfeld, J. Electrochem. Soc. 140, 3513 (1993).

(41) D. Bernardi, J. Electrochem. Soc. 137, 3344 (1990).

(42) S. Srinivasan, O. V. Velev, A. Parthasarathy, D. J. Manko and A. J. Appleby, J. Power Sources 36, 299 (1991).

(43) D. M. Bernardi and M. W. Verbrugge, AIChE J. 37, 1151 (1991).

(44) K. Prater, J. Power Sources 29, 239 (1990).

(45) Niedrash, US Patent 3, 297, 484 (1967).

(46) D. Raistrick, in: Diaphragms, Separators, and Ion Exchange Membrane, J. W. Van Zee, R. E. White, K. Kinoshita, H. S. Burney, (eds.). The Electrochemical Society Softbound Proc. Series, Pennington, NJ (1986), PV 86-13, p. 172.

(47) I. D. Raistrick, U.S. Patent 4,876,115 (1989).

(48) M. S. Wilson, S. Gottesfeld, J. Appl. Electrochem., 22, 1 (1992).

(49) A. Parthasarathy, C. R. Martin, and S. Srinivasan, J. Electrochem. Soc. 138, 916 (1991).

(50) A. Parasarathy, B. Dave, S. Srinivasan, A. J. Appleby, and C. R. Martin, J. Electrochem. Soc. 139, 1634 (1992).

(51) D. R. Lawson, L. D. Whiteley, C. R. Martin, M. N. Szentirmay, and J. I. Song, J. Electrochem. 135, 2247 (1988).

(52) W. Paik, T. E. Springer, and S. Srinivasan, J. Electrochem. 136, 644 (1989).

(53) A. J. Appleby, and E. B. Yeager, in Assessment of Research Needs for Advanced Fuel Cells by the DOE AFCWG, Solid Polymer Electrolyte Fuel cells, chap. 4, S. S. Penner, Editor, U.S. Dept. of Energy, Washington, D. C. (1985).

(54) S. Srinivasan, E. A. Ticianelli, C. R. Derouin, A. Redondo, J. Power Sources 22, 359 (1988).

(55) E. A. Ticianelli. C. R. Derouin, A. Redondo, S. Srinivasan, J. Electrochem. Soc. 135, 2209 (1988).

(56) E. A. Ticianelli. C. R. Derouin, S. Srinivasan, J. Electroanal. Chem. 251, 275 (1988).

(57) S. Mukerjee, S. Srinivasan, A. J. Appleby, Electrochim. Acta, 38, 1661 (1993).

(58) M. F. Weber, S. Maniche-Afra, M. J. Dignam, L. Pataki and R.D. Verter, J. Electrochem. Soc., 134, 1416 (1987).

(59) E. J. Taylor, E. B. Anderson, and N. R. K. Vilambi, J. Electrochem. Soc. 139, L45

(1992).

(60) R. Mosdale and S. Srinivasan, Electrochim. Acta, 40, 413 (1995).

(61) R. Metkmeijer, P. Achard, Int. J. Hydrogen Energy, 19, 535 (1994).

(62) A. J. Bard, R. Parsons, J. Jordan, "Standard Potentials in Aqueous Solution", Marcel Dekker Inc., New York, 1985.

(63) S. Surampudi, S. R. Narayanan, E. Vamos, H. Frank, G. Halpert, A. LaConti, J. Kosek, G. K. Surya Prakash, G. A. Olah, J. Power Sources 47, 377 (1994).

(64) I. A. Kosek, C. C. Cropley, G. Wilson, A. B. LaConti, S. Narayan, E. Vamos, S. Surampudi, H. Frank in: Proc. 28th Intersociety Energy Conversion Engineering Conference (IECEC), Atlanta, GA (1993), Vol. 1, p. 1209.

(65) R. F. Savinell, E. Yeager, D. Tryk, U. Landau, J. S. Wainright, D. Weng, K. Lux, M. Litt, C. Rogers, J. Electrochem. Soc. 141, L46 (1994).

(66) X. Ren, Mahlon S. Wilson, S. Gottesfeld in: Proton Conducting Membrane Fuel Cells I, S. Gottesfeld, G. Halpert, A. Landgrebe (eds.), The Electrochemical Society, Pennington, NJ 1995, p. 252.

(67) H. Grune, G. Luft, K. Mund, M. Waidhas, Program and Abstracts, Fuel Cell Seminar, San Diego, CA, Nov. 28 – Dec. 1, 1994, p. 474.

(68) D. L. Maricle, B. L. Murach, L. L. Van Dine, "Direct Methanol Fuel Cell Stack Development", Proc. of the 36th Power Sources Conference, 6-9 June, 1994, p.99.

(69) R. Parsons, T. V. D. Noot, J. Electroanal. Chem., 257, 9 (1988).

(70) D. Chu and S. Gilman, J. Electrochem. Soc., 141, 1770 (1994).

Chapter 2

Electrochemical Evaluation of Commercial Catalysts and Modified Carbon-Supported Catalysts

2.1 Introduction

2.1.1 Current Catalyst Status for the Oxygen Reduction Reaction (ORR) in PEMFCs

The cathodic reduction of oxygen is one of the most widely studied electrochemical reactions. The kinetics and mechanisms of oxygen reduction have been investigated with a wide range of cathode materials and in a variety of aqueous and solid polymer electrolytes. Much of the impetus for the extensive studies of oxygen reduction can be attributed to the strong interest in low-temperature (below 200 ^{0}C) fuel cells. The high overpotential for oxygen reduction in low-temperature fuel cells with acidic electrolytes is one major block in the drive for commercialization of this technology, particularly for PEMFCs. In this regard, a major effort is being devoted to discovering electrocatalysts that can enhance oxygen reduction rates. Despite all the attention devoted

to electrocatalysis of oxygen reduction at low and moderate temperatures in acidic electrolytes, the kinetic overpotential for oxygen reduction with Pt-based catalysts is still relatively high (i.e., typically > 0.3 V). Thus the challenge still remains to reduce the overpotential of oxygen electrodes in such applications as fuel cells.

The important role of electrode kinetics on the performance of fuel cells (particularly those operating at low and intermediate temperatures, 25-200 ^{0}C) is best illustrated by a typical cell potential versus current density plot (**Fig. 2.1**). Three distinct regions are illustrated in this plot showing the kinetic, ohmic, and mass transport losses. The cell potential (E) versus current density (I), from a current density of 0 to the value at the end of the linear region, may be expressed by the relation

$$E = E_r + b \log i_0 - b \log I - R\,I \qquad (2.1.1)$$

Where E_r is the reversible potential for oxygen reduction (V); E is the cell potential (V); I is the current density (A/cm^2); The parameters b and i_0 are the Tafel slope and exchange current density for the oxygen reduction reaction, and R accounts for the linear variation of overpotential (predominantly ohmic) with current density that is observed in the intermediate range.

The slow kinetics of oxygen reduction is one factor that limits the performance of electrochemical systems utilizing oxygen electrodes, and the requirement for high catalyst loadings leads to cost problems. From the perspective of electrode performance, the cost problem can be solved by reduction of the catalyst loading with improvement of

catalyst utilization and performance. Following the discussion by Damjanovic (1), a generalized

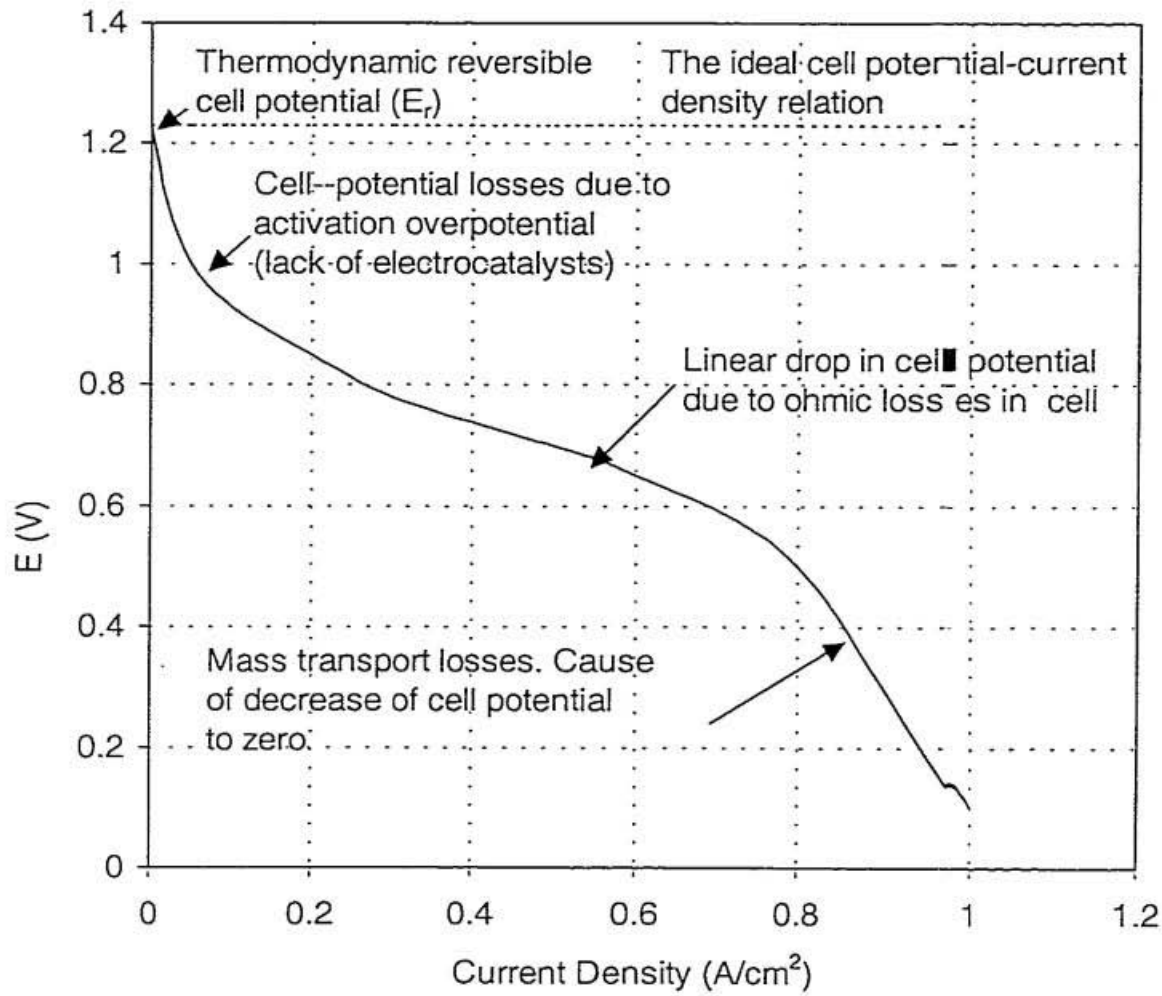

Fig. 2.1 A typical cell potential-current curve in a PEMFC

rate expression for oxygen reduction, with the rate-determining step as the first electron transfer, is given by

$$O_2 + H^+ + e^- = O_2H_{ads} \quad \text{(the r.d.s)} \qquad (2.1.2)$$

$$I = k[P_{O2}]^n [H^+]^m \exp(-\alpha FE/RT) \qquad (2.1.3)$$

Where n and m are the reaction orders for O_2 and H^+, respectively, and α is the symmetry factor. k is a constant, and the other terms have their usual electrochemical significance. Damjanovic (1) reported that n and α are both equal to 1, and that m is close to 1.5 with oxide-free platinum in acid electrolytes. Experimental studies with solid metal electrodes (2-3) and with porous gas-diffusion electrodes of PTFE-bonded Pt supported on carbon (4) showed that the reduction current at a given potential varies linearly with oxygen pressure, which is indicative of a first-order dependence with respect to oxygen pressure. It is very clear that an increase of either H^+ or O_2 concentration would enhance the ORR (oxygen reduction reaction) on the Pt surface, especially for H^+ concentration because of its 1.5 power index. In order to improve the ionic conductivity of the catalyst, an ionomer (Nafion) solution is usually added to the catalyst ink, which results in a large performance gain (5). Significant cost reduction by decreasing the catalyst loading has also been reported by optimizing the electrode structures (6-12). The underlying concept of reducing catalyst loading is to enhance catalyst utilization in the gas diffusion electrode.

Most attempts concentrated on the impregnation of an ionic conductor into the catalyst layer to extend the ionic conductivity. However, the involvement of a foreign ionic conductor like Nafion in the catalyst layer can restrict oxygen diffusion, and decrease the electronic conductivity in the layer. The most important facet of maximizing catalyst utilization in fuel cells is to maximize the volume of the catalyst/electrolyte interface without unduly limiting the gas permeability and electronic conductivity. Based on the ORR mechanism in PEMFCs, a balance between the electronic and ionic conductivity of the catalyst should be maintained in the catalyst layer to achieve a high performance. Therefore, it has always been a goal to find a way to improve the ionic conductivity of catalysts without the compromising their electronic conductivity. If the ionic conductor can be created *in situ* on the Pt catalyst, carbon support, without affecting the other properties of carbon support, then fast ORR kinetics can be achieved by increasing the proton and oxygen concentrations in the absence of (or with less) Nafion in the catalyst layer.

2.1.2 Modification of the Surface of the Carbon Support by Chemical Oxidation

Numerous methods such as electrochemical, chemical, and thermal methods have been applied to activate electrocatalysts for oxygen reduction (13). Presently, graphitized carbon is used as the catalyst support to increase Pt dispersion resulting in a higher catalytic activity. The graphitized carbon is more hydrophobic in comparison to carbon

black, which causes a difficulty for proton access to the platinum catalyst. A highly catalyzed carbon layer should not be too hydrophobic, otherwise it would not achieve a good interfacial contact with the electrolyte (14). Therefore, it should be a fruitful approach to increase the proton conductivity by modifying the hydrophobicity of the carbon support in order to increase the ORR performance of the catalysts.

Carbon-oxygen complexes are by far the most important surface groups influencing the physicochemical properties of carbon black such as wettability, catalysis, electrical conductivity, and chemical reactivity. Moreover, the carbon surface properties also affect metal electrocatalyst-carbon support interactions, adsorption of reactive species, and carbon-polymer binder adhesion. A schematic representation of surface oxides on carbon is presented in **Fig. 2.2.**

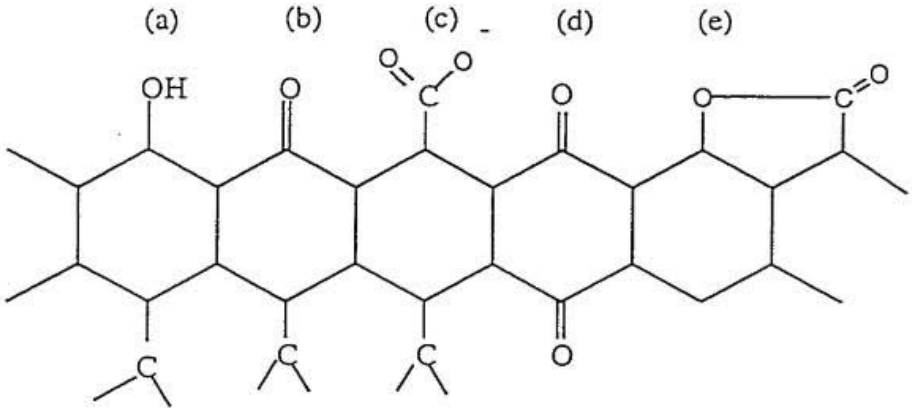

Fig. 2.2 Schematic representation of the oxygen surface functional groups on carbon. (a) phenol; (b) carbonyl; (C) carboxyl; (d) quinone; (e) lactone.

Graphite intercalation compounds (GICs) are prepared by inserting atomic or molecular layers of guest chemical species into the host graphite layer to give unique properties such as the high conductivity and catalytic activity. The term "intercalate" refers to a substance that is inserted between the layer planes. A discussion on the nomenclature and terminology for graphite intercalation compounds was recently published (15). For highly graphitic materials, the extent of intercalation or chemical doping depends on the particle size, the amount of volatile matter, the extent of porosity, the extent of heat treatment, the use of chemical oxidation, and other factors.

Various processes are used to produce graphite intercalation compounds. These include the two-zone treatment technique, the liquid intercalation method, the electrochemical method, and the cointercalation technique. Each of these techniques was reviewed recently by Dresselhaus and Dresselhaus (16-17). Several short summaries of the reactants and experimental conditions used to prepare graphite oxide were presented in references (18-24). The two requirements that seem necessary for synthesis of graphite oxide are a strong oxidizing agent and/or an acid environment. Graphite can accommodate oxy-acids in its lattice structure to form intercalation compounds that are saltlike and ionic, and with conductivity approaching that of metals. Perhaps the most widely studied acid compound is graphite bisulfate although a number of other acid compounds have been examined (e.g., intercalates such as HNO_3, HSO_3F, $HClO_4$, H_3PO_4, $H_4P_2O_7$, H_2SeO_4, H_3AsO_4, HBF_4, CF_3COOH, and HF). The only acid compound that is isolated from acids as a solid is graphite nitrate. The possible intercalates by several acids are given in **Table 2.1**.

Table 2. 1 Graphite intercalation compounds and their limiting compositions.

Intercalate	Limiting Composition
H_2SO_4	$C_{25}^{+}\bullet HSO_4^{-}\bullet 2H_2SO_4$
HNO_3	$C_{24}^{+}\bullet NO_3^{-}\bullet 3HNO_3$
HF	$C_{24}^{+}\bullet HF_2^{-}\bullet 2\ H_2F_2$

If milder oxidizing conditions are used, oxidation of carbon to give acidic surface groups is achieved in a liquid-phase environment without completely destroying the carbon structure (25-28). Oxidation of carbon black in HNO_3 appears to produce a large increase in the concentration of surface oxide groups but it has only a marginal effect on the surface area. The large decrease in the pH of carbon slurries that is obtained by oxidation in HNO_3 indicates that acidic surface oxides are formed by the treatment. Puri and Bansal (28) also confirmed the formation of surface oxides on carbon blacks that are oxidized in HNO_3. It is well known that the formation of the intercalation compounds such as graphite oxide occurs only with highly graphitized carbon samples.

The extensive research effort to date on the chemical modification of carbon surfaces has resulted in an improved understanding of the role of carbon surface properties in electrochemistry. Nevertheless, considerable research is still needed to determine the influence of surface groups on the electrochemical behavior of carbon, and investigate phenomena at carbon surfaces, particularly with regard to the influence of polymers and liquid/gas interfaces on porous electrodes. In order to make better use of

chemical oxidation techniques, further research is required to elucidate the importance of electrocatalyst-carbon support interactions in electrocatalysis, to determine how to modify such interactions to improve electrocatalyst activity, and to identify techniques to modify the carbon surface in order to add oxygen functional groups that enhance the sensitivity and activity of carbon-supported catalysts.

2.1.3 Objectives of This Work

Graphite intercalation has been used for a long time in the battery and supercapacitor industries to improve performance. It has not been used in the fuel cell field although it has the potential to improve the ionic conductivity of carbon supports while maintaining their electronic conductivity. It is also a big challenge to utilize graphite intercalates in fuel cells which requires a large current density range. In the work described in this chapter, chemical oxidation was used to obtain GICs, and the treatment conditions were evaluated. An electrochemical half-cell technique was used to achieve fast and reliable screening. An electrode apparatus was designed to study the ORR at gas diffusion electrodes (the cathode of a practical PEMFC). Methodologies such as cyclic voltammetry, potentiostatic steady state and transient polarization, and impedance spectroscopy were used to measure the key parameters that determine the performance of the electrode including the active catalyst surface area and Tafel slope.

These methodologies were employed to test the ORR performances of carbon-supported catalysts modified by different acidic and non-acidic chemicals. IR

spectroscopy was also used to investigate the carbon surface functional groups produced by chemical oxidation. The four-probe method was applied to measure the electronic conductivities of the modified catalysts. The mechanism for the improved performance of the modified catalysts is discussed, based on the triple contact theory.

2.2 Experimental

2.2.1 Electrochemical Apparatus for Catalyst Evaluation

A schematic of a self-designed gas diffusion electrode holder is shown in Fig. 2.3 (a).

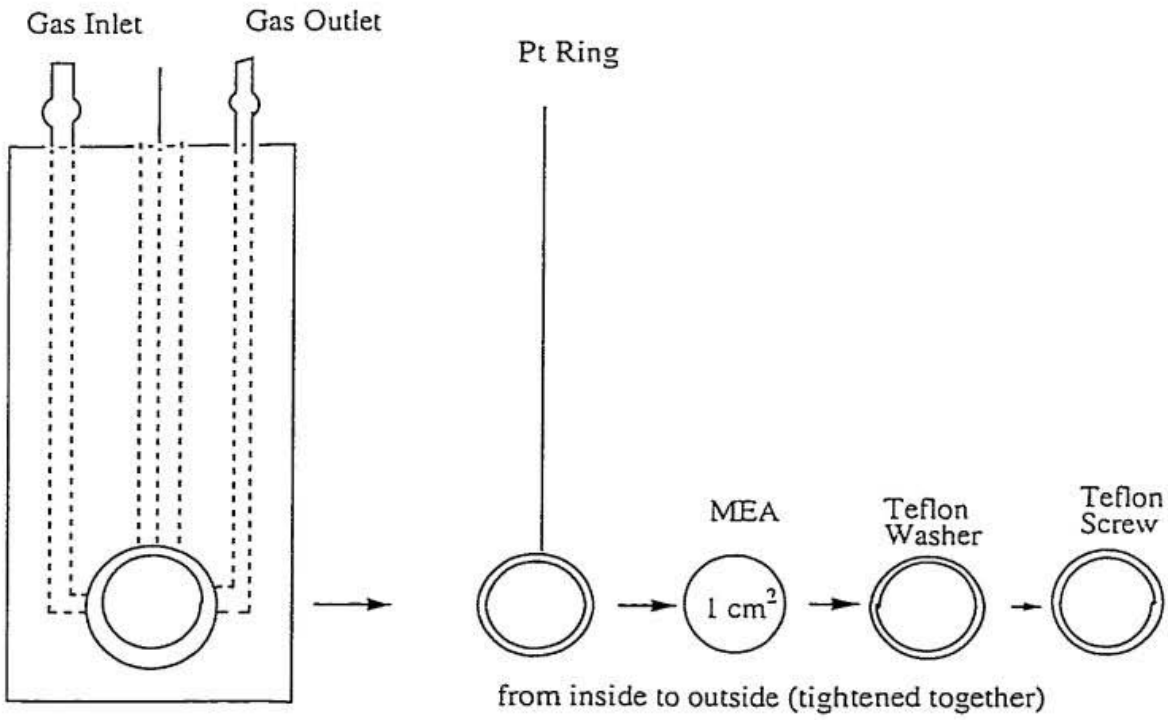

Fig. 2.3 (a) Schematic of a gas diffusion electrode holder

A platinum electrode and a saturated calomel electrode (SCE) were used as counter and reference electrodes, respectively, for all electrochemical measurements. The working electrode (1 cm^2 geometric area gas diffusion electrode) was inserted into a holder (**Fig. 2.3 (a)**), which exposed the membrane side to 1 M H_2SO_4 solution and the backside to flowing oxygen or nitrogen for polarization and cyclic voltammetric measurements, respectively.

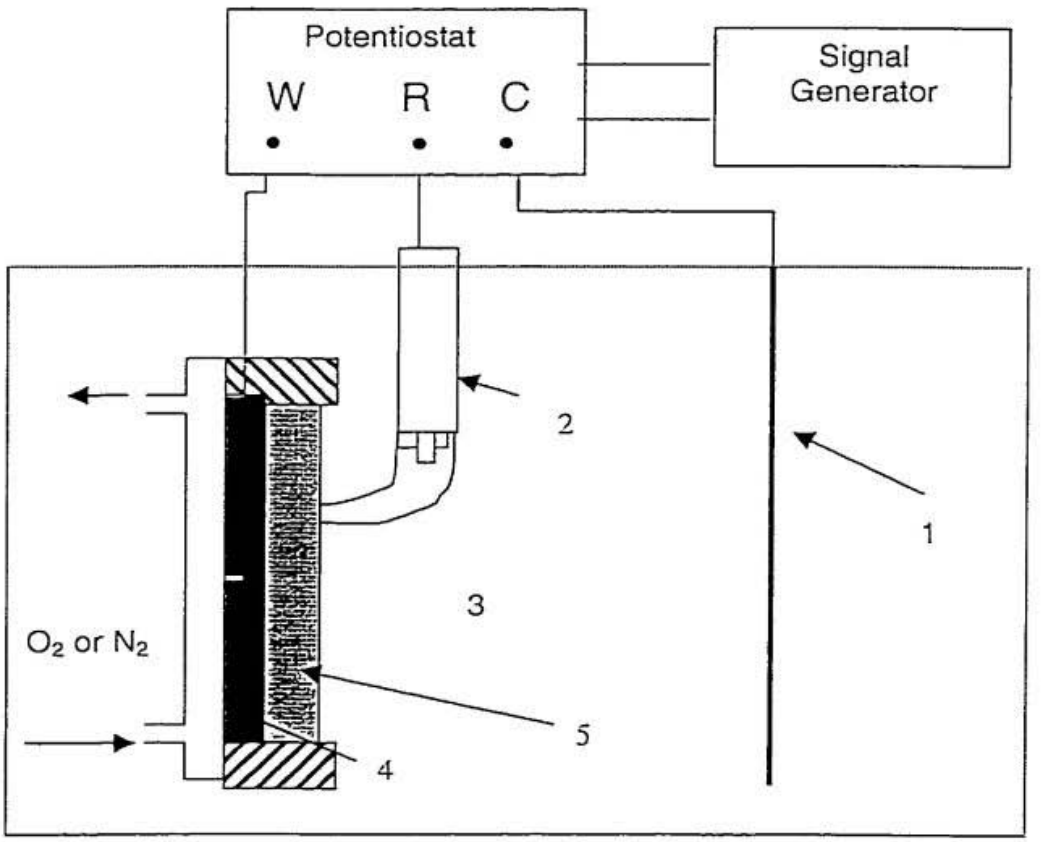

Fig. 2.3 (b) Experimental setup for evaluating catalyst performance. 1. Counter electrode; 2. Reference electrode (SCE); 3. Electrolyte: 1 M H_2SO_4; 4. Carbon paper; 5. Nafion membrane. (4 + catalyst + 5 = MEA).

A Luggin capillary was used to bring the reference electrode close to the test electrode to minimize the solution resistance (**Fig. 2. 3 (b)**). In order to avoid the flooding of the electrodes and oxidant starvation, a large excess of oxygen was employed. All electrochemical experiments were conducted at room temperature (23 ± 1 ^{0}C) in 1.0 M sulfuric acid (Fisher, ACS grade, > 95.0%) unless otherwise indicated.

2.2.2 Techniques for Catalyst Evaluation

2.2.2.1 Polarization

A program was written to collect transient and steady state polarization data at fixed potentials. The transient data was sampled at the end of a ten-second interval of polarization, which was followed by a switch back to the initial open circuit potential (rest potential) for 10 seconds. The purpose of this setup is to avoid the electrode flooding as a long polarization would generate a large amount of water. Currents sampled following 30 minutes of polarization were considered to be steady state values. The average of three readings over one second period at each potential was taken to minimize the error due to noise. The polarization performance for each electrode was tested twice, for the purpose of reproducibility, with oxygen supplied at atmospheric pressure (Canadian Liquid Air Ltd., >99%).

2.2.2.2 Cyclic Voltammetry

Cyclic voltammetry was carried out using a Model 1286 Solartron Electrochemical Interface connected to a computer. CV profiles were recorded at different scan rates between the potential limits for hydrogen (- 0.30 V vs. SCE) and oxygen evolution (1.5 V vs. SCE). Conventionally, the cyclic voltammetric technique has been used to ascertain the electrochemically active surface areas of Pt electrodes (29-31). The electrochemically active surface area can be computed by integrating the current in the hydrogen adsorption region of the CV as shown in **Fig. 2.4**. To obtain the true active area, the double-layer charging current must be accurately subtracted and the appropriate minimum potential, which is usually taken as the potential of the cathodic current minimum before the onset of H_2 evolution, must be selected correctly. From the coulombic charge required for hydrogen adsorption (shaded area in **Fig. 2.4**), the catalyst active surface area can be calculated by assuming a coulombic charge of 210 $\mu C/cm^2$ (32). This calculation is based on the assumption that atomic hydrogen adsorption on the Pt surface is monolayer, which is quite close to the real situation.

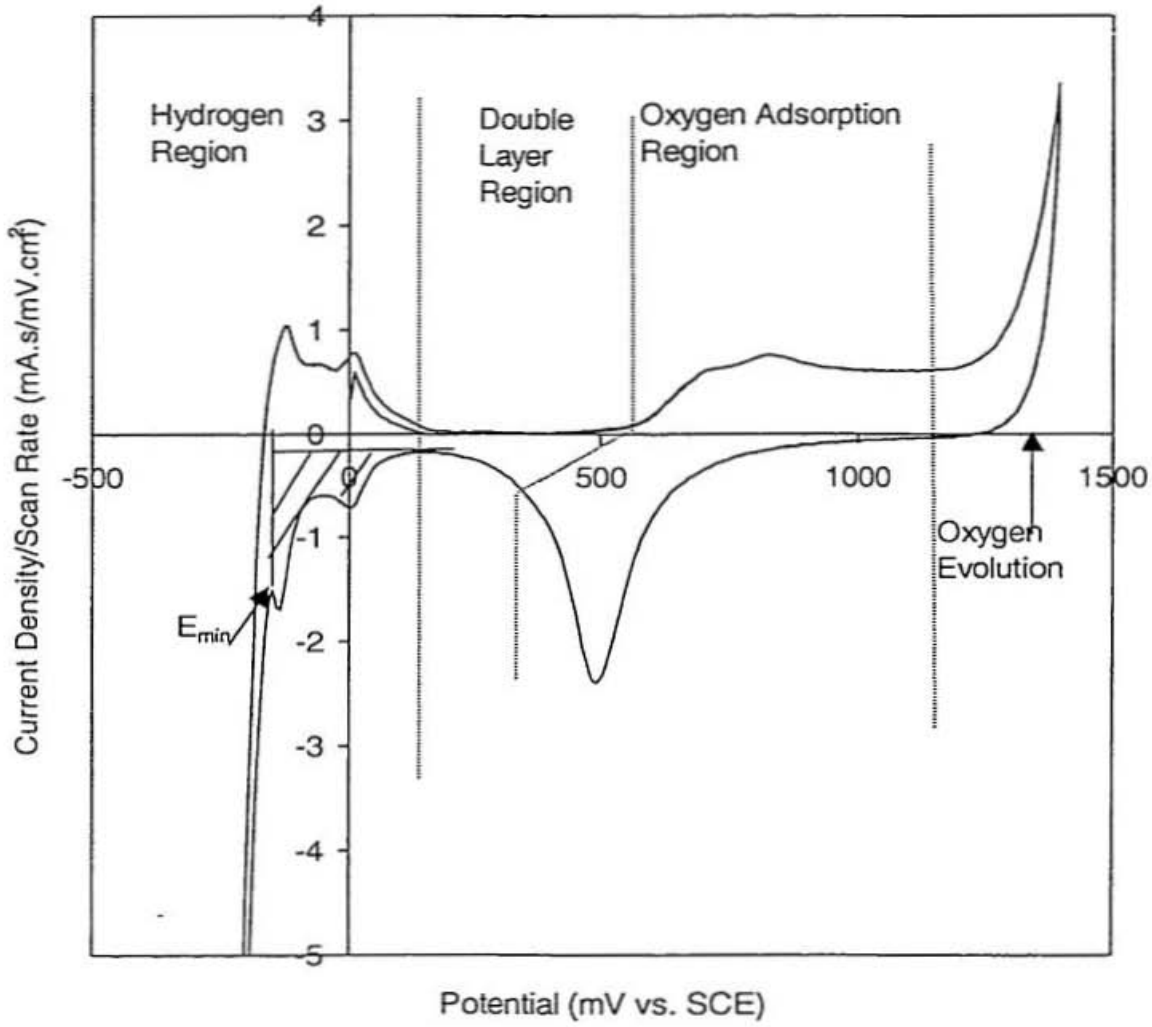

Fig. 2.4 Cyclic voltammogram of a 4 mg Pt/cm^2 (Pt black) electrode at a scan rate of 10 mV/s.

2.2.2.3 AC impedance

The instrumentation for electrochemical impedance spectroscopy (EIS) consisted of an electrochemical interface (Solartron Instruments model 1286 and an impedance phase analyzer Solartron Instruments Model 1250) connected to a computer. The EIS measurements were carried out at the initial open circuit potential, and data were analyzed with ZPLOT software (Scribner Associates). An alternating sinusoidal signal of 5 mV peak-to-peak was superimposed on the dc-potential. The impedance spectra were collected over the range of frequency between 65 kHz and 1 Hz. The cell resistance (R_{cell}) was measured as the high-frequency real-axis intercept of the complex plane impedance plot.

AC impedance plots show the relationship between Z' (real impedance) and Z'' (imaginary impedance). AC impedance spectra can be used to investigate the reaction mechanism of reactive species in catalyzed gas diffusion electrodes, and are useful to separate and to discern the contributions to the kinetic behavior from different electrocatalyst materials or preparation procedures (32-34). Moreover, AC impedance is also used to determine the double-layer capacitance of the electrode allowing us to measure the effective, electrochemically used inner surface and the degree of wetting of the inner surface of the electrode (35). To interpret the cell resistance measurements, a simplified equivalent circuit similar to that reported by Parthasarathy et al. (36) was adopted (**Fig. 2.5**). The equivalent circuit contains two RC parallel circuits in series. The first circuit corresponds to the behavior of the electrode/electrolyte interface in the

activation – controlled region (0.55 ~ 0.70 V vs. SCE), and is linked to the charge – transfer process for oxygen reduction at the Pt/Nafion interface. The second RC parallel circuit pertains to the membrane itself and is representative of the membrane relaxation process. From the circuit pertaining to the membrane, membrane properties such as the uncompensated resistance, R_u, grain – boundary or "intercluster" resistance, R_{gb}, and membrane grain – boundary capacitance, C_{gb}, were obtained. The uncompensated resistance, R_u is the sum of the solution resistance, R_l, and the bulk membrane resistance.

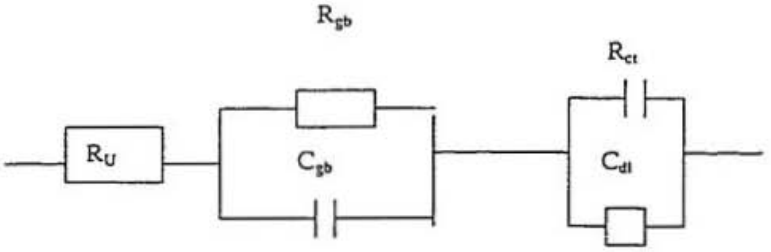

Fig. 2.5 Equivalent circuit for the electrolyte/electrode interface. R_u is the bulk resistance; R_{ct} is the charge-transfer resistance; C_{dl} is the double layer capacitance.

2.2.2.4 Infrared spectroscopy

IR spectra were obtained from pressed discs of mixtures of small quantities of carbon-supported catalysts with KBr. The typical concentration of carbon in the KBr disks was in the range of from 0.01 to 0.5 wt %. IR spectroscopy was used to identify the

surface functional groups on the carbon before and after treatment in acid and non-acidic chemicals. A major problem with carbon materials is their strong absorption of radiation in the IR region.

2.2.3 Preparation of Catalyzed Gas Diffusion Electrodes

The desired amount of catalyst (10 % and 20 % Pt /Vulcan XC-72R, Electrosynthesis Co., Inc.) was mixed with the required amount of 15 wt % PTFE suspension (diluted from 60 wt % PTFE, E. I. Du Pont De Nemours) to control the PTFE content in the catalyst layer. Several drops of 1 M H_2SO_4 solution were added into the composition to reduce the surface tension of the catalyst. The catalyst paste was then sonicated for about 30 minutes at room temperature to form a homogeneous mixture that was finally spread on teflonized carbon paper (Torey TGP-090 carbon paper teflonized with PTFE, Toray Industries) to form the catalyzed gas diffusion electrode. The catalyzed electrodes were sintered at 400 ^{0}C to melt the PTFE binder. The catalyst loading (mg Pt/cm^2) and PTFE content for the resulting catalyzed electrode can be determined by gravimetry according to the following equations, respectively:

$$\text{Pt loading} = (W_{cat} \times C_{cat}/A) \times [(\Delta W_{cp})/(W_{PTFE} \times C_{PTFE} + W_{cat} + W_{acid})] \qquad (2.2.1)$$

$$\text{PTFE \%} = (W_{PTFE} \times C_{PTFE}) \times 100/\Delta W_{cp} \qquad (2.2.2)$$

Where ΔW_{cp} is the carbon paper mass difference after and before casting the catalyst (mg); W_{PTFE} is the mass of PTFE solution added into the catalyst paste (mg); C_{PTFE} is PFFE concentration (15 %); C_{cat} is the Pt percentage on the carbon support, and W_{cat} is the mass of the catalyst used to make the catalyst ink (mg); W_{acid} is the mass of H_2SO_4 added into the catalyst (mg); A is the area covered by the catalyst (cm^2).

The half MEA (membrane & electrode assembly) was fabricated by hot pressing the electrode onto Nafion®117 (E. I. Du Pont De Nemours) at 125 ^{0}C and 50 atmosphere pressure for 90 seconds. The membrane was first subjected to a pretreatment in order to remove organic and metallic impurities. Briefly, this pretreatment consisted of heating the membrane in 10 % H_2O_2 to about 80 ^{0}C for ca. 1 h to remove organic impurities. This was then followed by treatment in boiling 1 M H_2SO_4 30 min to remove metallic impurities. The membranes were stored in deionized water after treatment. Two pieces of thin PTFE film were applied to prevent the MEA from sticking to the hot stainless steel plates used for bonding. After the MEA was taken away from the press, the PTFE films were peeled from the MEA surface. Commercial electrodes (4 mg Pt/cm^2 (Pt black), Ballard Power Systems, Inc.) were used as received except when the effect of Nafion loading was evaluated, for which Nafion was brush-coated onto the electrode surface with a 5 % Nafion solution (5 % solution, 1100 EW, Solution Technology, Inc.). The hot-press apparatus for MEA fabrication is shown in **Fig. 2.6**.

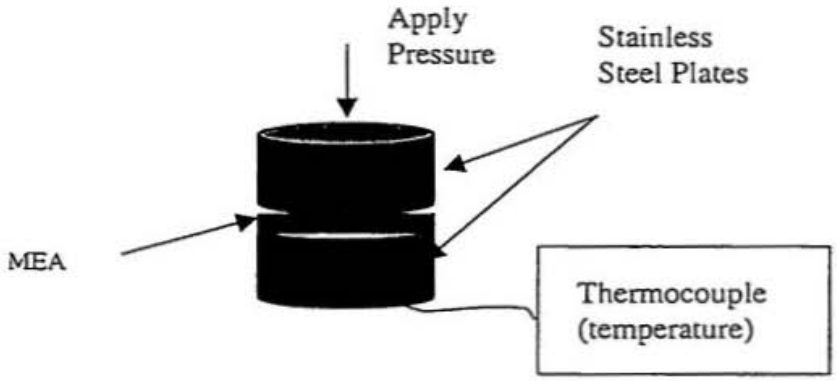

Fig. 2.6 The hot-press apparatus for MEA fabrication.

2.2.4 Catalyst Treatment by Chemical Oxidation

The 20 % Pt carbon-supported catalysts were refluxed with different chemical solutions including concentrated HNO_3 (BDH, 71 %), H_2SO_4 (Fisher, ACS ,98.0%), 30 % H_2O_2 (ACP, ACS), 0.2 M $(NH_4)_2S_2O_8$ (Fisher, ACS), 5.25 % NaClO (BHC, ACS) or concentrated H_3PO_4 (Anachemia, 85.0 %) for a certain period of time. Concentrated $HClO_4$ (Fisher, ACS, 70.0 %) was only used to treat the catalysts at room temperature as high temperatures may cause an explosion. The treated catalysts were filtered through sintered glass under vacuum, and washed several times with deionized water. The catalysts were dried under vacuum at 80 ^{0}C overnight, and were ground before use.

2.2.5 Measurement of Conductivity of Modified Catalysts

A four-point probe method was employed to measurement the conductivity of various carbon powders and catalysts (37-38). A schematic diagram of the conductivity measurement is shown in **Fig. 2.7**. A pressure of 82 psig was applied to test the catalysts during the measurement.

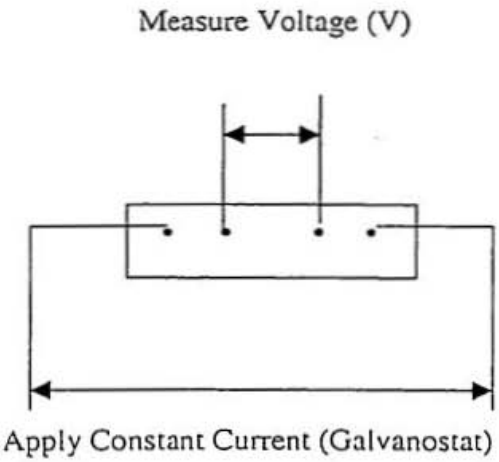

Fig. 2.7 Schematic of the conductivity measurement with a four-probe method.

The electronic conductivity (σ) of the catalyst can be computed by **Eqn (2.2.4)**:

$$\sigma = I/(4.27\ V\ d) \qquad (2.2.4)$$

Where I: the applied current (A); V: the measured voltage (V); d: sample thickness (cm); σ: conductivity of the catalysts (S/cm).

2.3 Results and Discussion

2.3.1 Characterization of Methodologies for Catalyst Evaluation

2.3.1.1 Characterization of cyclic voltammetric technique

A set of cyclic voltammograms for a 4 mg Pt/cm^2 (Pt black) electrode with 10 % teflonized carbon paper as substrate at different scan rates from 10 mV up to 100 mV/s are shown in **Fig. 2.8**. Several characteristic regions, including the hydrogen region, double layer region, oxygen adsorption region, and oxygen evolution region, were well defined. In the hydrogen region, the typical peaks associated with hydrogen adsorption and desorption could be clearly observed. Two adsorbed hydrogen oxidation peaks reversibly matched the two reduction peaks. Since the double layer charging current and minimum potential are dependent on the scan rate and potential scan range, the electrode needs enough time to reach steady state. Otherwise, the current density in the double layer region may include some faradaic current leading to underestimation of real active surface area. CVs for different scan rates and potential ranges are displayed in **Fig. 2.8** and **Fig. 2.9**.

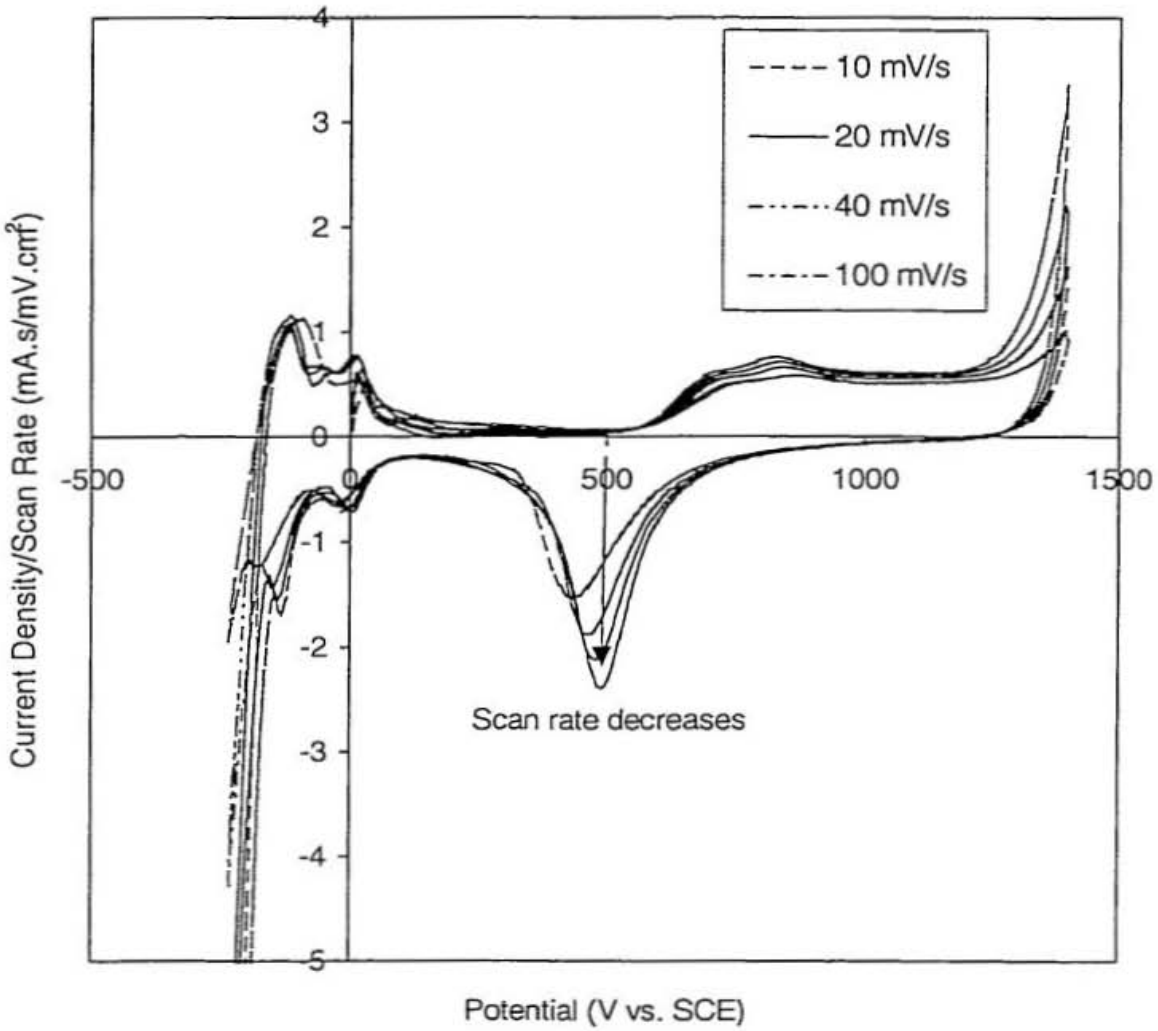

Fig. 2.8 CVs at different scan rates for 4 mg Pt/cm^2(Pt black) over the potential scan range of - 0.30 V to 1.4 V vs SCE.

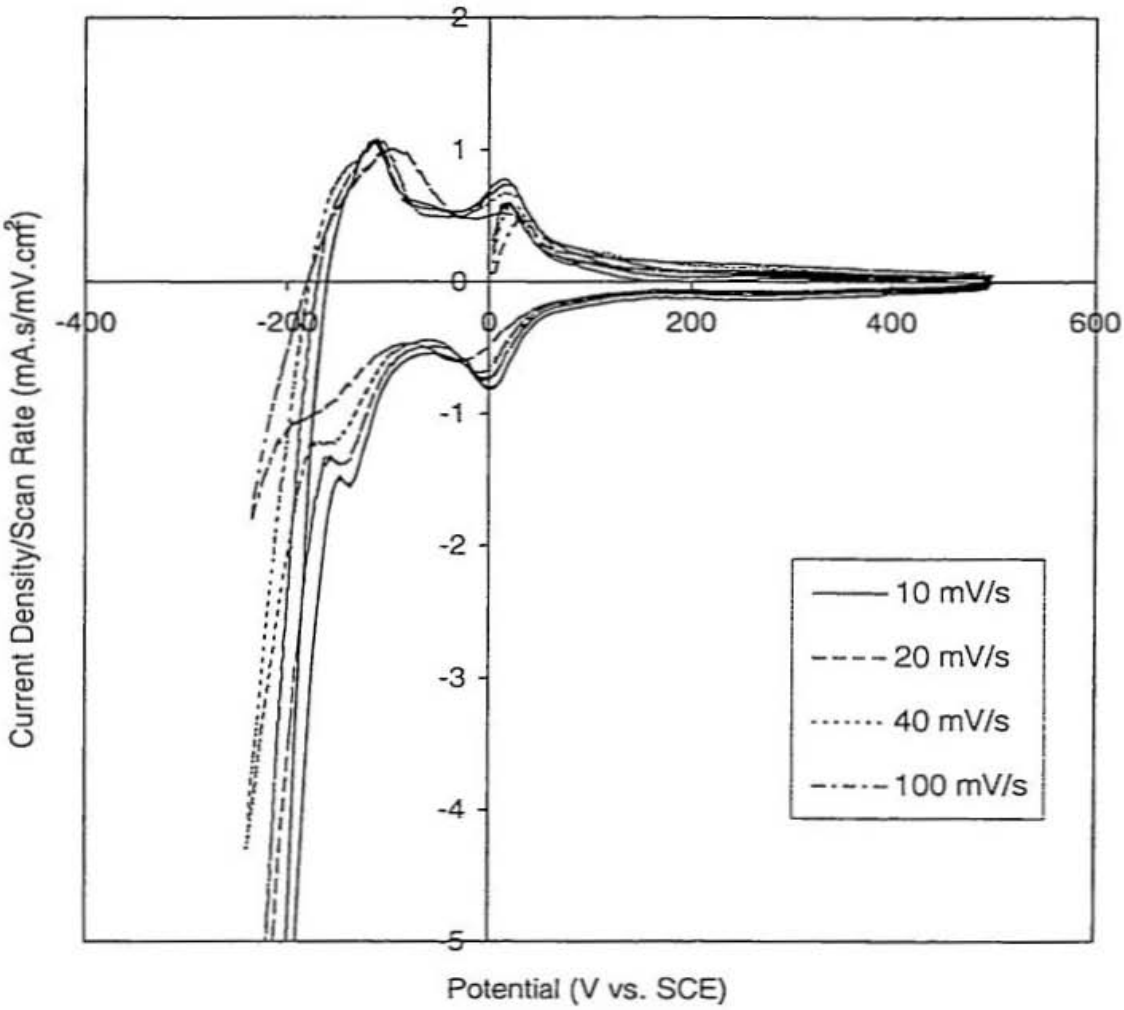

Fig. 2.9 CVs at different scan rates for 4 mg Pt/cm^2 (Pt black) over the potential range of - 0.3 V to 0.5 V vs SCE.

It can be seen from **Figs. 2.8 & 2.9** that the current density in the double layer region (0.2 V ~ 0.5 V/SCE) depends on scan rate and potential scan range. The dependence of the hydrogen adsorption charge on scan rate and potential range is illustrated in **Fig. 2.10**, which indicates that the true double-layer charging current can be measured at low scan rate, such as 10 mV/s. This point is strongly supported by the similarity of the integration curves for narrow and wide potential ranges for 10 mV/s. The electrode with 4 mg Pt/cm^2 Pt black had a minimum potential of 0.155 V/SCE at a scan rate of 10 mV/s corresponding to a true active surface area of 670 cm^2.

Fig. 2.11 shows CVs for 10 % and 20 % carbon-supported catalysts at 0.40 mg Pt/cm^2 loading. Most of the features in the CVs are also well defined. However, poor resolution was observed for the hydrogen adsorption-desorption peaks. At the same catalyst loading, the electrode with 20 % Pt/C has a larger surface area than that with 10 % Pt/C. From the area under the hydrogen adsorption peak, the electrodes have approximate active areas of 260 cm^2/per geometric cm^2 and 60 cm^2/per geometric cm^2, respectively. As there is a larger double-layer charging current due to the carbon support (39), the hydrogen adsorption peaks are masked by carbon features leading to difficulty in determining the minimum potential for hydrogen adsorption. This problem remains to be discussed in detail in Chapter 3. In spite of this problem, the cyclic voltammetric technique proved to be useful for estimating the active surface area of gas diffusion electrodes. From the measurement of electrochemically active surface areas for Pt black and carbon-supported catalysts, it was proved that our experimental setup with the CV

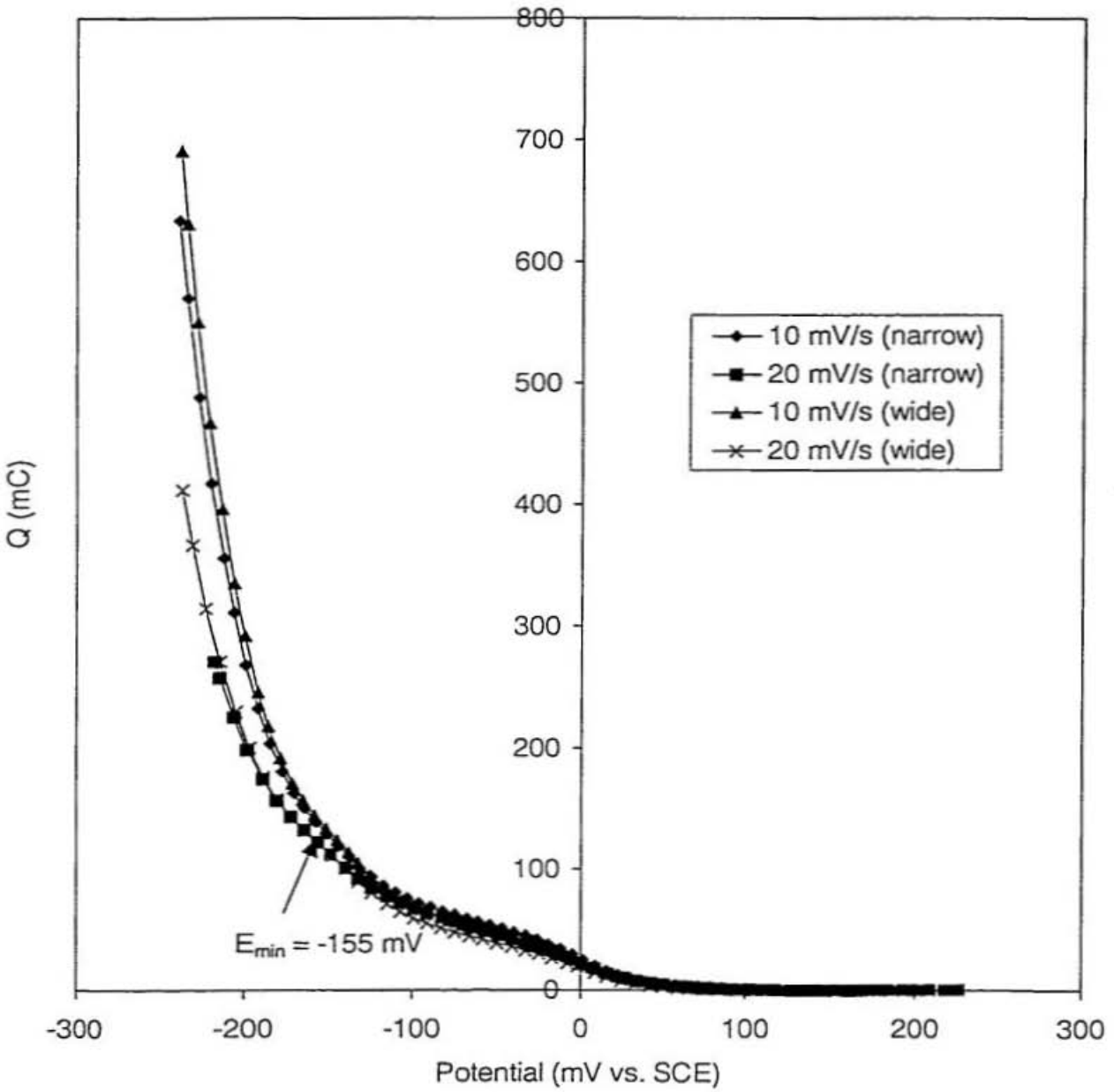

Fig. 2.10 The relationship between charge and potential for wide and narrow potential ranges. Charge was integrated from 220 m V to - 250 m V (SCE) with correction for the double-layer charge.

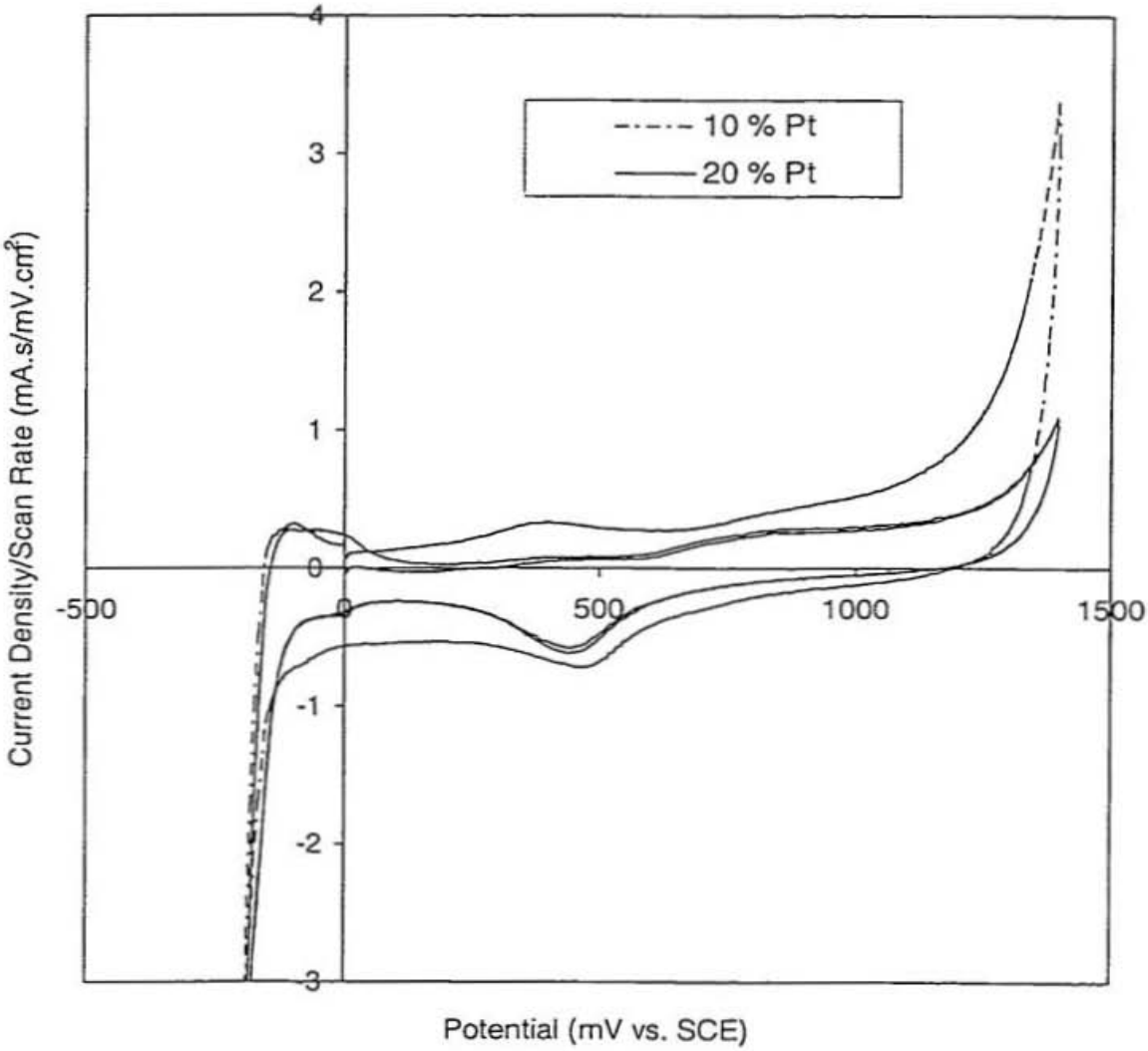

Fig. 2.11 Cyclic voltammograms for 10 % and 20 % Pt /C catalysts at 0.40 mg Pt/cm^2. Scan rate: 10 mV/s.

technique is valid for evaluating the active surface area of catalyst, which is one of important parameters for the catalyst.

2.3.1.2 AC impedance

AC impedance spectra for three different catalysts at the initial open circuit potential and over the frequency range between 1 Hz and 65 kHz are collected in **Fig. 2.12.**

The AC impedance spectrum of Pt black is different from those for 10 % and 20 % Pt/C catalysts that show quite similar behavior. The different behaviors between Pt black and the carbon-supported catalysts suggests that the Pt black catalyst may have a different reaction mechanism for reactive species in the catalyzed gas diffusion electrode in comparison to the carbon-supported catalysts (**Fig. 2.12**). However. both types of catalyst showed diffusion control at low frequencies as represented by a straight line close to 45^0. The detailed analysis of the kinetic mechanism of the catalysts involves many factors, and it is not our intention to do this kind of analysis here. Our focus is on the measurement of the cell resistance so as to compensate the IR drop in polarization measurements. Therefore, the high frequency impedance can be used as representative of the total cell resistance, which were measured as 0.28 Ω, 0.38 Ω, and 0.40 Ω for Pt black (4 mg Pt/cm^2), 10 % Pt/C (0.4 mg Pt/cm^2), and 20 % Pt/C (0.4 mg Pt/cm^2), respectively from the data in **Fig. 2.12.**

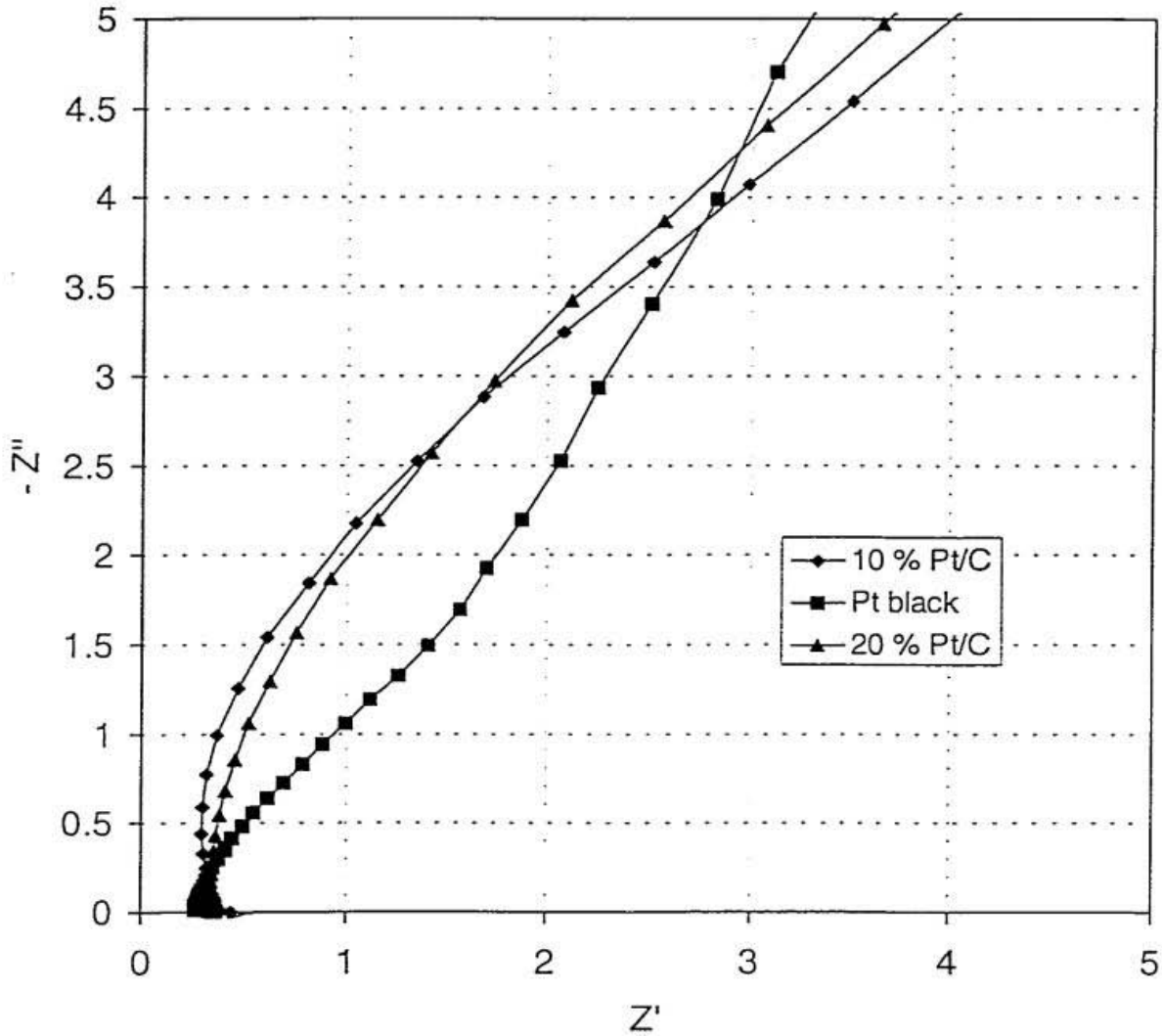

Fig. 2. 12 AC impedance spectra for different catalysts at initial open circuit potential. Frequency: 1 Hz ~ 65 kHz; Pt loading: 4 mg/cm^2 for Pt black, and 0.4 mg/cm^2 for both 10 % and 20 % Pt/C catalysts.

2.3.1.3 Characterization of polarization techniques

(1) Potentiostatic transient and steady state polarization

A program was written to collect the current at certain potentials with a short polarization time (10 seconds) or at steady state by measuring the current at long times (30 minutes). The potentiostatic transient polarization possesses a speed advantage if it can reasonably represent the steady state value. **Fig. 2.13** shows a performance comparison between transient polarization and steady state polarization experiments for three different catalysts including Pt black, 20 % Pt/C (original), and 20 % Pt/C treated by HNO_3 at 4 mg Pt/cm^2, 0.2 mg Pt/cm^2, and 0.2 mg Pt/cm^2, respectively.

To avoid complications at high current densities, ohmic drop effects on the polarization data were carefully compensated using the AC impedance results. It is seen from this figure that the Pt black and 20 % Pt/C electrodes showed good performance. No oxygen diffusion limitation occured even at current densities of 1 A/cm^2. The overpotentials (after IR compensation) of these three electrodes at 1 A/cm^2 were about 0.3 V, 0.4, and 0.5 V, respectively. The steady state polarizations were quite close to the transient values except in the low current density region where the steady state value is slightly higher than that from transient polarization. This kinetic gain may be caused by a temperature rise resulting from a long polarization in the O_2 environment. Except for this small difference, all three catalysts behaved similarly in transient and steady state experiments. Therefore, transient polarization experiments can be used to evaluate the catalyst performance for oxygen reduction reaction without sacrificing accuracy.

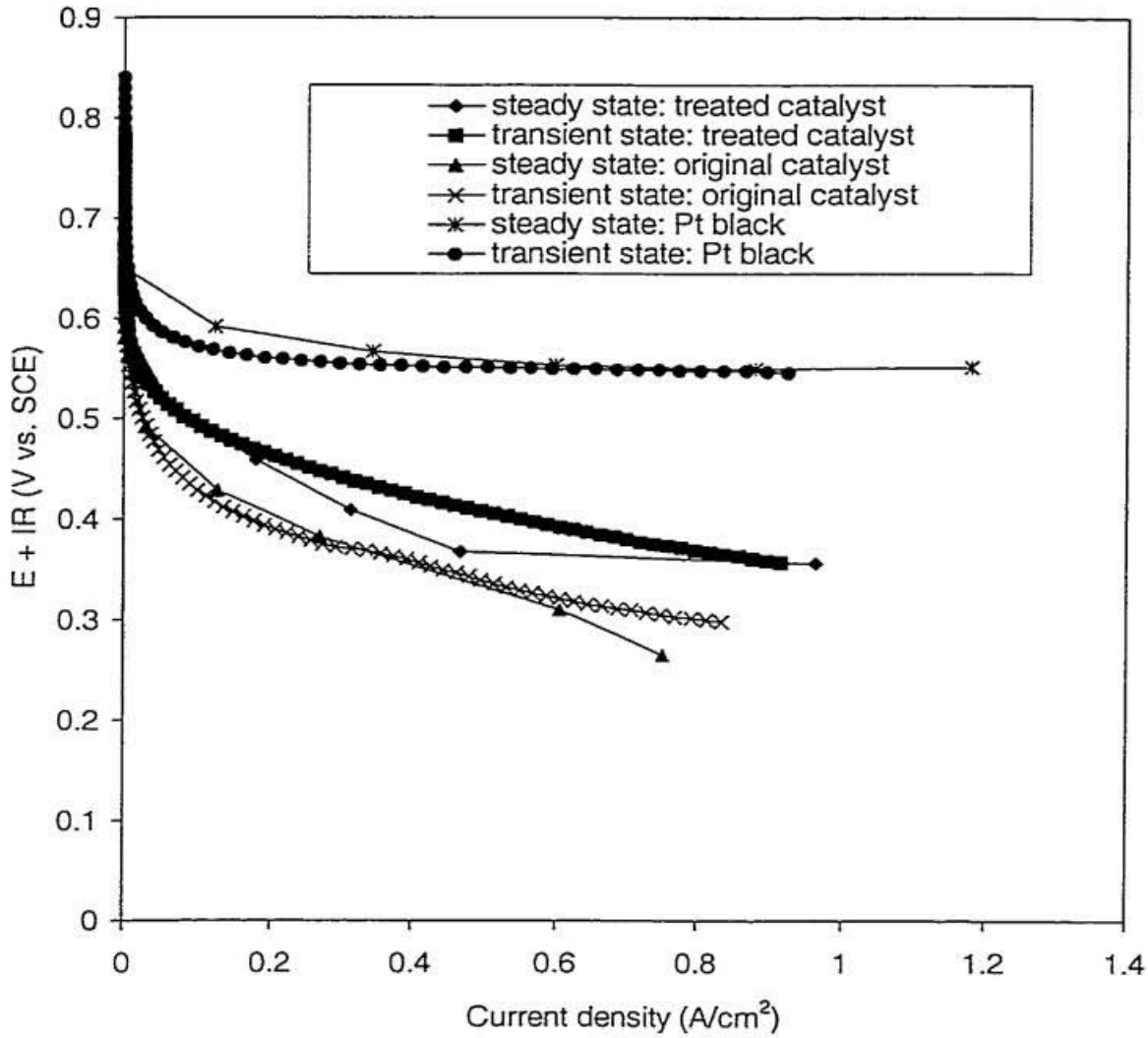

Fig. 2.13 ORR performance comparison between transient and steady state polarizations for Pt black and 20 % Pt/C. Pt black: 4 mg Pt/cm^2; original 20 % Pt/C and 20 % Pt/C treated by HNO_3: 0.20 mg Pt/cm^2.

(2) Tafel plots

Fig. 2.14 shows a set of the Tafel plots for the ORR using the transient polarization data for three different catalysts (Pt black, 20 % Pt/C, and 10 % Pt/C). The slope of a Tafel plot can be used to systematically identify the oxygen adsorption mechanism on the Pt surface (40). The Pt black catalyst showed a Tafel slope (b) of 72 mV/decade (close to 60 mV/decade). However, the values of the Tafel slopes for the carbon-supported catalysts (10 % and 20 % Pt/C) were observed to be 85 mV/decade and 140 mV/decade at lower and higher current densities, respectively. At the low current densities, i.e., the high potentials, the Tafel plot would be expected to deviate from linearity due to the presence of platinum oxide on the platinum surface (41, 42). The Tafel slope for this oxide region was 72 mV/decade. The deviation for the carbon-supported catalysts could be larger due to the interaction between Pt and carbon support. At the high current densities, two Tafel regions for O_2 electroreduction on Pt electrode surface in acid electrolyte have also been observed by many research groups (41-47).

According to Sepa et al. (40), the existence of these two Tafel slopes in H_2SO_4 solutions can be explained in terms of the degree of coverage of the platinum surface by adsorbed oxygen, which follows a Temkin isotherm at high electrode potential, leading to b = 60 mV/decade (2.3 RT/F) at 25 ^{0}C, and a Langmuir isotherm at lower electrode potentials, leading to b = 120 mV/decade (2 (2.3 RT/F)). It also implies different rate-determining steps over the different potential ranges (48). The Tafel slope of ~ 60 mV

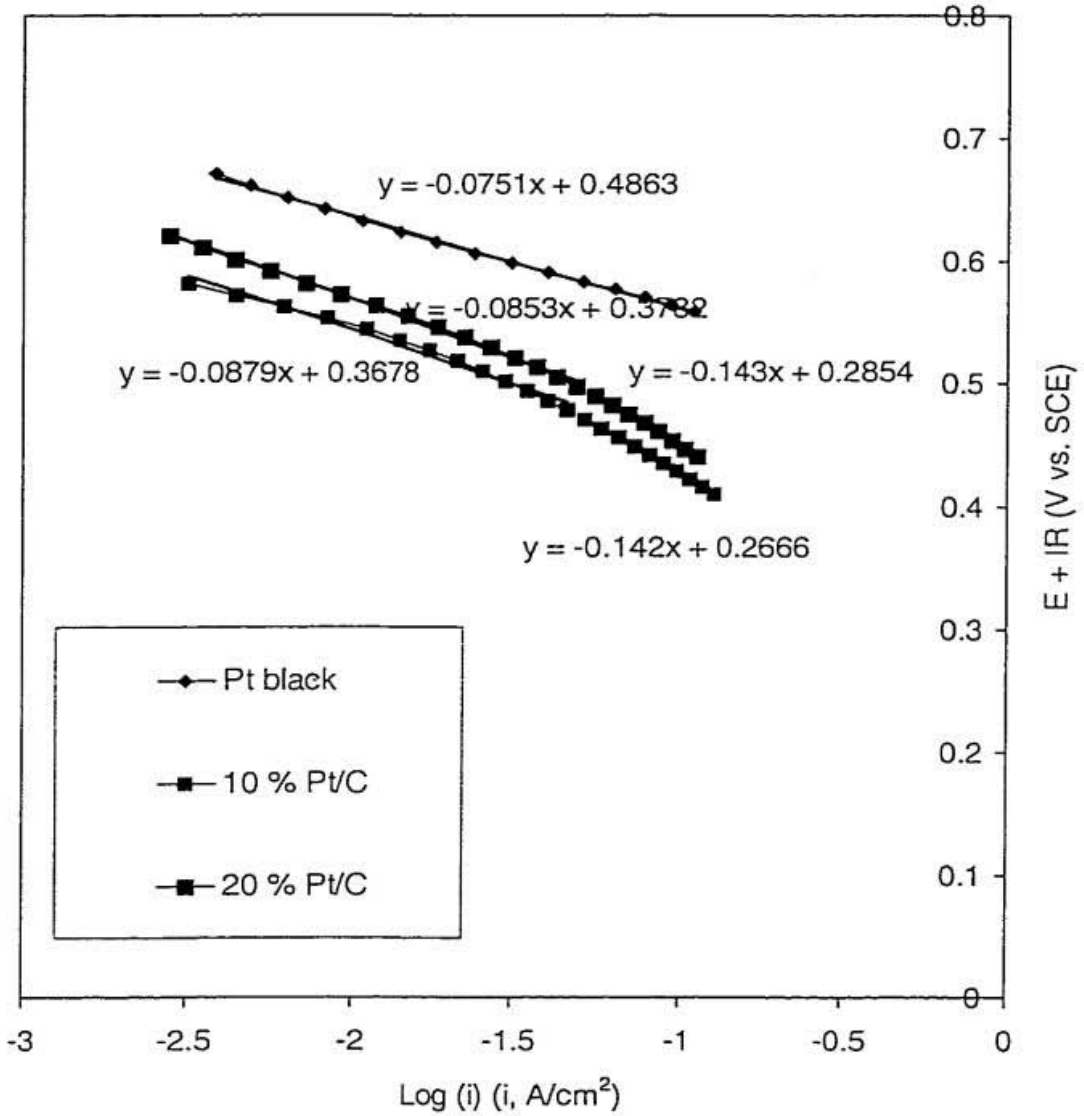

Fig. 2.14 Tafel plots for different catalysts. Pt black: 4 mg Pt/cm^2; 10 % and 20 % Pt/C: 0.4 mg Pt/cm^2.

MV/decade is possible for a rate-determining charge-transfer step following **Eqn (2.2.4)** under Temkin conditions (49).

$$O_2 + H^+ + e^- = O_2H_{ads.} \qquad \textbf{(2.2.4)}$$

The exchange current density i_0 can be obtained by extrapolating the Tafel plot to the reversible electrode potential E_r. However, this calculation involves considerable error because of the mixed open circuit potential. Therefore, the i_0 values become meaningless. The current density at a certain potential, however, can valuably be used to represent the catalytic activity of the catalysts, e.g., at a potential of 0.6 V (SCE), the electrode with 4 mg Pt/cm^2 (Pt black) has a current density of 29 mA/cm^2, and both electrodes made with carbon-supported catalysts give a small current (3 mA/cm^2). This means that the Pt catalyst with a high loading possesses a higher catalytic activity for the ORR.

(3) Effect of Nafion content on ORR performance

In order to test the sensitivity of our experimental setup to change in the properties of the gas diffusion electrode, electrodes impregnated with different Nafion loadings were evaluated. The results are shown in **Fig. 2.15** which indicates that Nafion

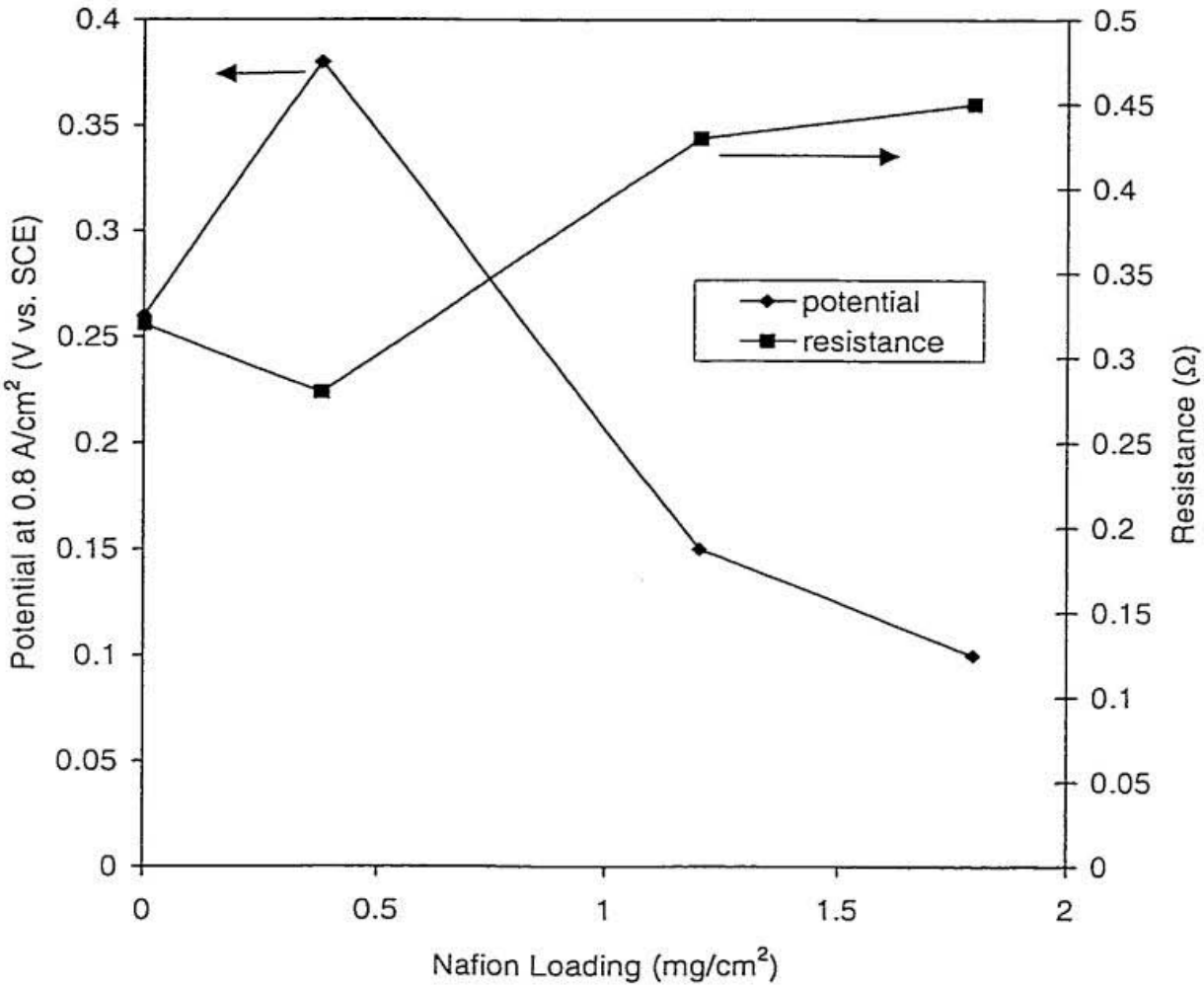

Fig. 2.15 The relationship of electrode performance and resistance with Nafion loading. Electrode: 4 mg Pt/cm^2.

loading in the catalyst layer had an optimum value of 0.38 mg/cm^2 in this case. The electrode performance has a volcano shape relationship with Nafion loading as shown in reference (50).

From a structural point of view, Nafion loading mostly influences the ionic resistance of the catalytic layer. At 0.38 mg/cm^2 Nafion, a maximum in electrochemical activity was found, and correspondingly, the ionic resistance of the electrodes reached its lowest value. This phenomenon has been explained according to a physical model in which a low amount of Nafion is located within the pores of the electrodes, and resistance decreases when the pores fill with Nafion. Above 0.38 mg/cm^2, due to the hydrophobic-hydrophilic properties of the Nafion structure, a further supply of Nafion does not fill the pores but forms a film on the external surface of the electrodes. The film can be represented as a series resistance with ionic conductor contained within the catalyst layer to give an additional contribution to the overall resistance. Moreover, excess Nafion added into catalyst layers lowers the performance of PEMFCs because the diffusion of reactant gases to Pt catalyst sites is disturbed. The excess addition leads to reduction of reaction currents due to lowering of the diffusion rate of reactant gases in Nafion film covering Pt catalyst particles. Although the performance is reduced by excess addition of Nafion, an increase in electrochemically active surface area was observed with increasing Nafion loading since the ionic conductivity of the catalyst layer increases. This increase is due to non-operating measurement of the active surface area, and not much related to the resistance and gas diffusion limitation.

2.3.2 Electrochemical Evaluation of Modified Catalysts

2.3.2.1 Modification of catalysts by nitric acid

Fig. 2.16 shows the results for 20 % Pt on Vulcan XC-72R (Electrosynthsis) modified by refluxing in concentrated HNO_3 for 30 minutes at 0.2 and 0.4 mg Pt/cm^2 loadings. It was found that the ORR performance for both non-treated and treated catalysts increase slightly with Pt loading on the electrode. The treated catalyst had a significantly higher performance than that for non-treated catalyst at the same Pt loading, e.g., 0.2 V higher at a current density of 800 mA/cm^2. As well as lower resistive (linear) losses in the high current density region, the treated catalyst also demonstrated a large performance gain in the kinetic region (low current region) including a higher open circuit potential. The Tafel slope for the modified catalyst changed to 0.090 V/decade, and there is only one Tafel slope over the current range. This indicates that the treatment of the catalyst may change the adsorption mechanism of oxygen on the Pt surface. The lower Tafel slope indicates improved electron transfer on the catalyst surface leading to facile kinetics.

The reaction time has been investigated to determine the optimum conditions for HNO_3 treatment. The results are shown in **Fig. 2.17**, which illustrates that the catalysts modified for different reaction times all obtained a performance gain although the modified catalyst with 5 hours treatment had the lowest value. This is probably due to

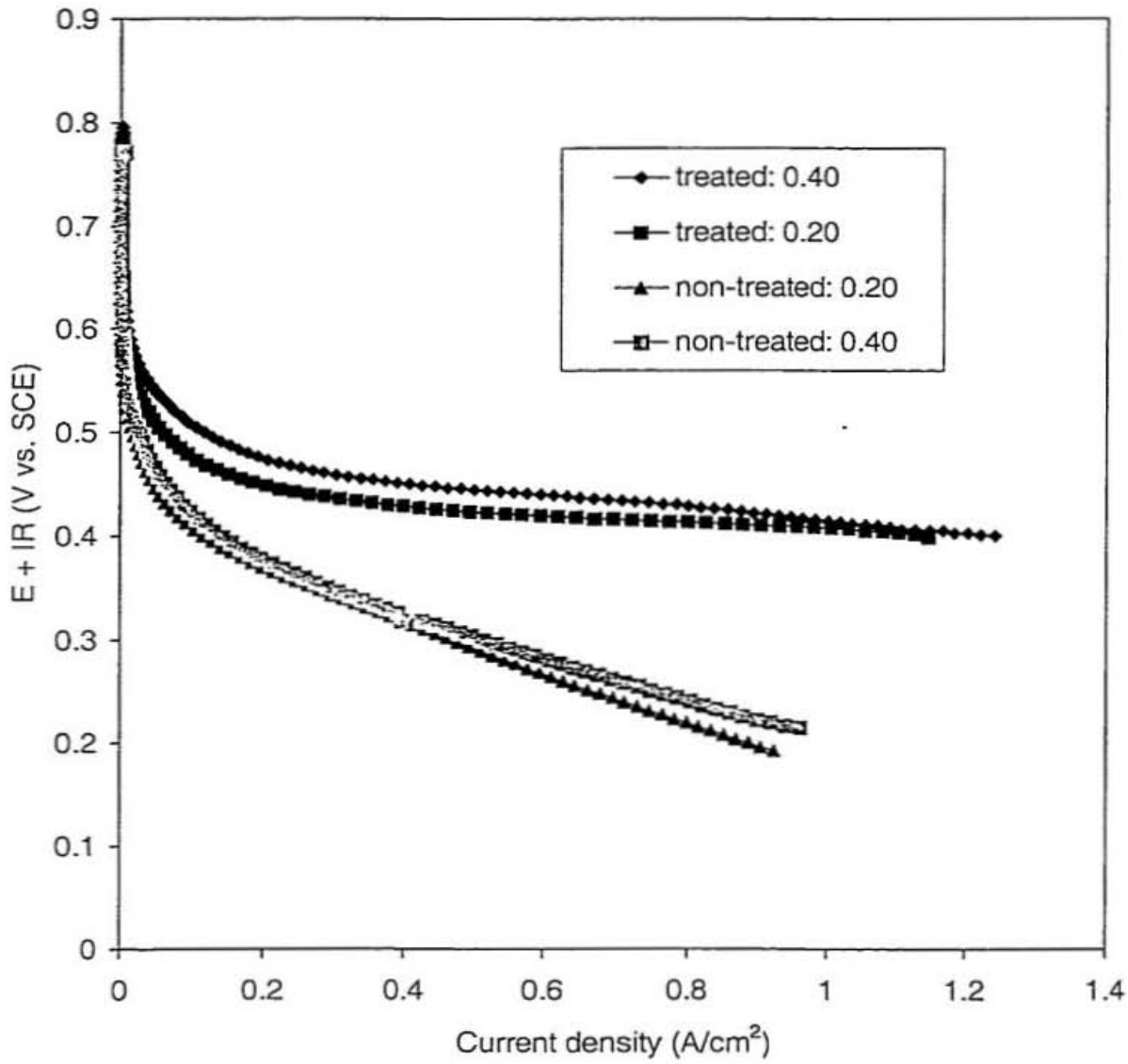

Fig. 2.16 Polarization curves for catalysts modified with nitric acid. Modified catalyst is 20 % Pt/C refluxed in 71 % nitric acid for 30 min. Pt: 0.2 & 0.4 mg Pt/cm^2, respectively.

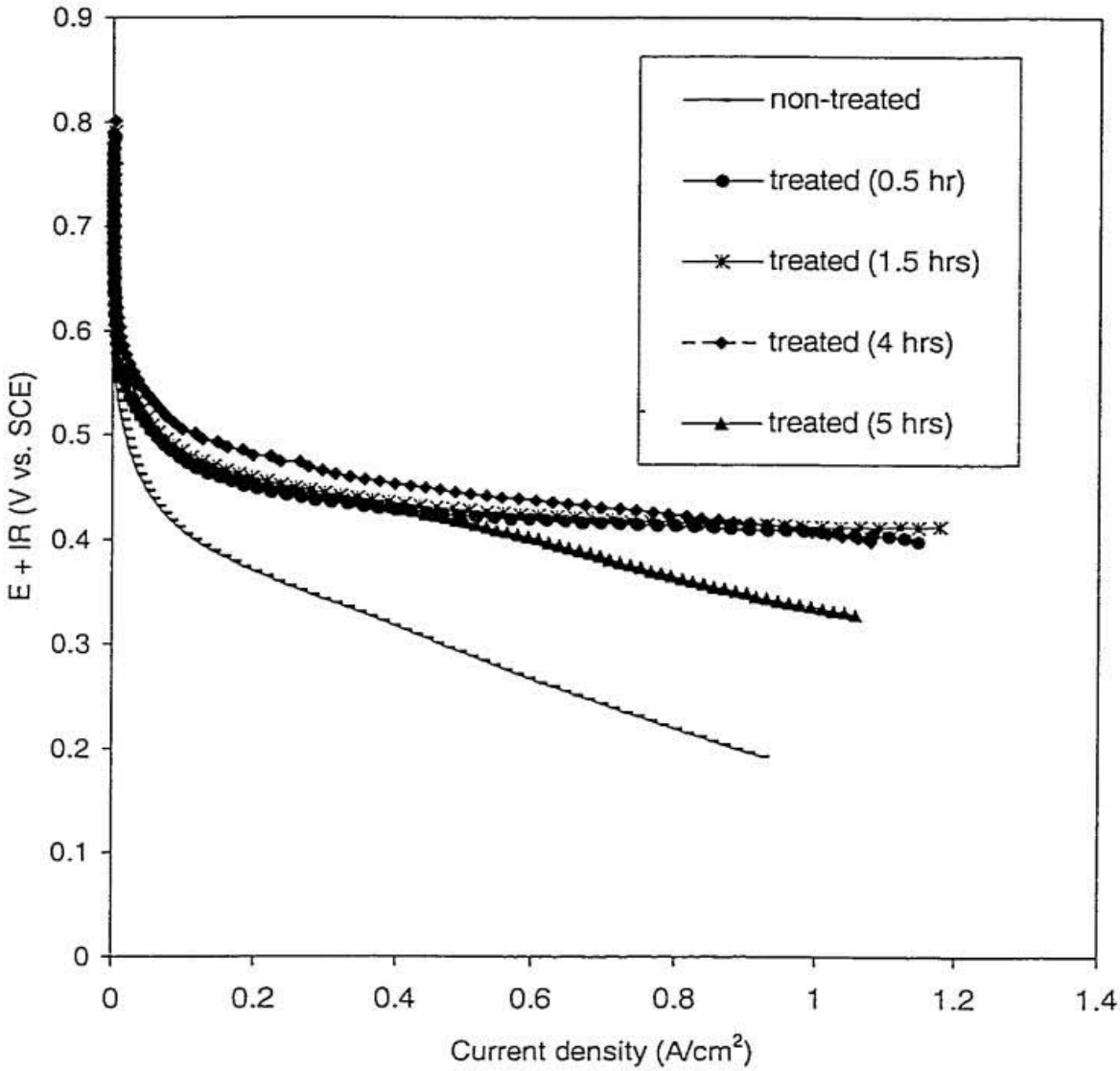

Fig. 2.17 Oxygen reduction performance for catalysts modified by HNO_3 for different treatment times (0.2 mg Pt/cm^2).

structural damage to the carbon support by overoxidation with HNO_3. This leads to the conclusion that a reaction time in HNO_3 less than 5 hours should be applied in order to achieve optimum performance.

Power density is defined as the product of current density and cell voltage, i.e., power = IV. If it is assumed that the performance achieved for the modified catalysts can be achieved in a H_2/O_2 PEMFC, projected power densities can easily be obtained by using this relationship. The relationship between power density and cell voltage is shown in **Fig. 2.18**. This relationship behaves like a parabolic curve, which indicates that a maximum power exists in PEMFCs. The maximum power is not achieved at maximum voltage. It occured at about 0.4 V. It is clear that the modified catalyst can provide nearly twice the power of the original catalyst.

2.3.2.2 Modification of catalysts by different acids

Different acids such H_2SO_4, H_3PO_4, and $HClO_4$ have been used to treat the carbon-supported catalyst. HNO_3 has also been used to treat the catalyst at room temperature to obtain a higher yield. **Fig.2.19** shows the results for these treated catalysts at 0.2 $mgPt/cm^2$ loadings. It can be seen that the catalysts treated by $HClO_4$ and HNO_3 at room temperature achieved improved performances comparable to those obtained with hot HNO_3 treatment. Treatment at room temperature by $HClO_4$ and HNO_3 provided a higher yield; 95 % in comparison to 85 % for refluxing 3 hours in HNO_3 because hot acid

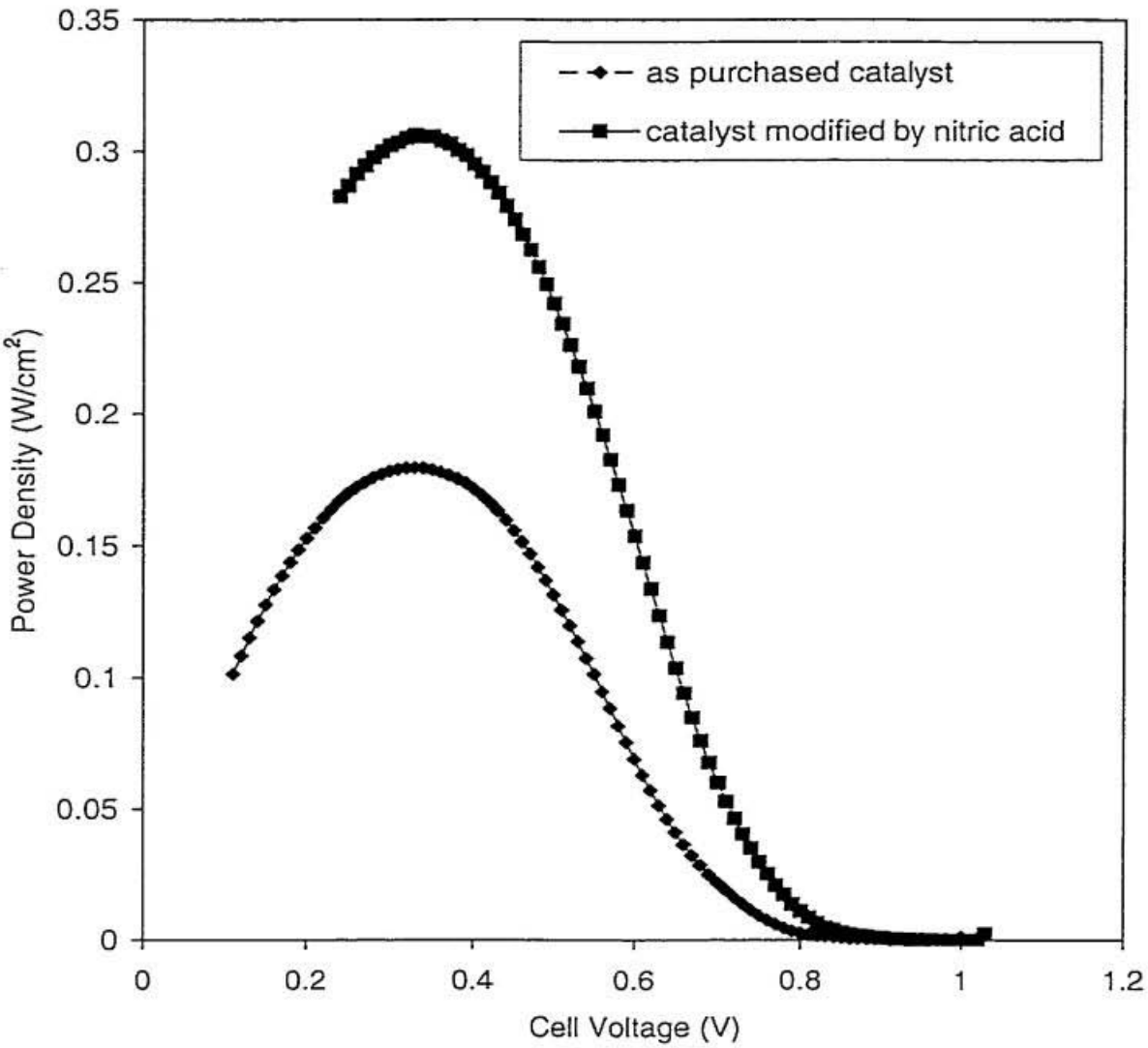

Fig. 2.18 Projected power density curves for hydrogen/oxygen fuel cells. Pt loading: 0.2 mg/cm^2 (20 % Pt/C).

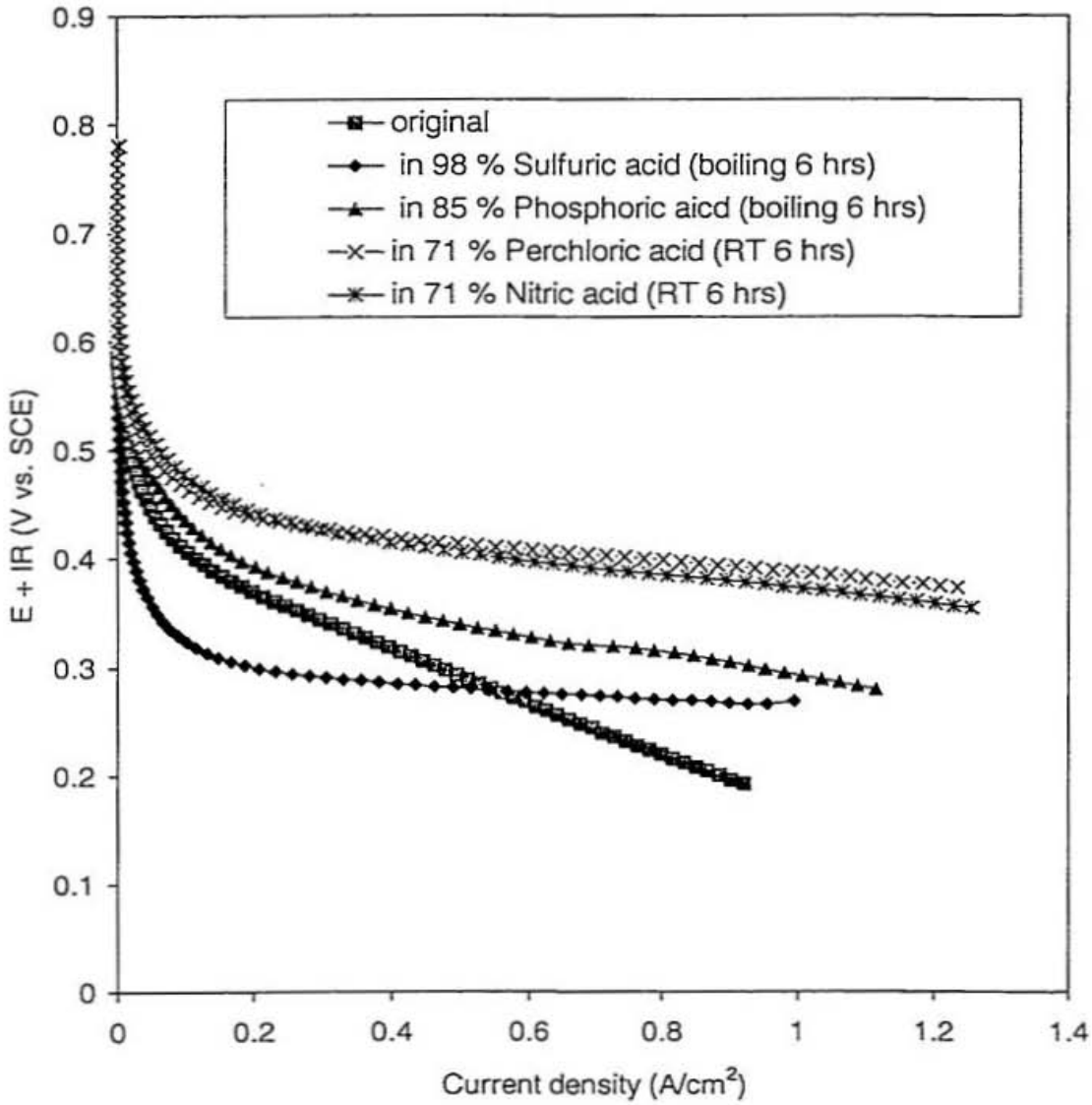

Fig. 2.19 Oxygen reduction performances for catalysts modified by different acids at 0.2 mg Pt/cm^2 loading for all electrodes. Original catalyst is 20 % Pt on Vulcan XC-72R.

oxidized carbon more quickly. The catalyst yield was determined by weight difference before and after treatment. Treatment of the catalyst with H_3PO_4 only slightly increased the ORR performance, which may be due to PO_4^{3-} adsorption on the Pt surface resulting in blocking of sites active for O_2 reaction (31, 51). On the other hand, at temperatures beyond the boiling point of water, orthophosphoric acid becomes successively dehydrated forming pyrophosphate polymer chains and resulting in a higher ionic conductivity (31). This may be the major reason why the treatment with H_3PO_4 still slightly improved the performance, even with the detrimental effect of PO_4^{3-} adsorption. Conversely, H_2SO_4 treatment decreased the catalyst's performance, especially in the kinetic region (low current region). In order to further investigate this phenomenon, the same MEA was polarized in O_2 for a long time (about 1 hour) with a large amount of water being produced. It was observed that after the long time polarization, the ORR performance for this MEA recovered significantly, particularly in the kinetic region (**Fig. 2.20**). It seems that the catalyst had been poisoned by the treatment with H_2SO_4. In acid electrolyte, the most widely accepted reason for lower electrode kinetics is the dominance of anion adsorption effects (e.g., sulfate or phosphate) (52-53). The long time polarization removed the poison on the Pt surface leading to an improved performance. In regard to all treatments, it can be concluded that most of the oxidizing acids, except those with anions that can poison the catalyst, can be used to modify the carbon support to increase the ORR performance of the catalyst.

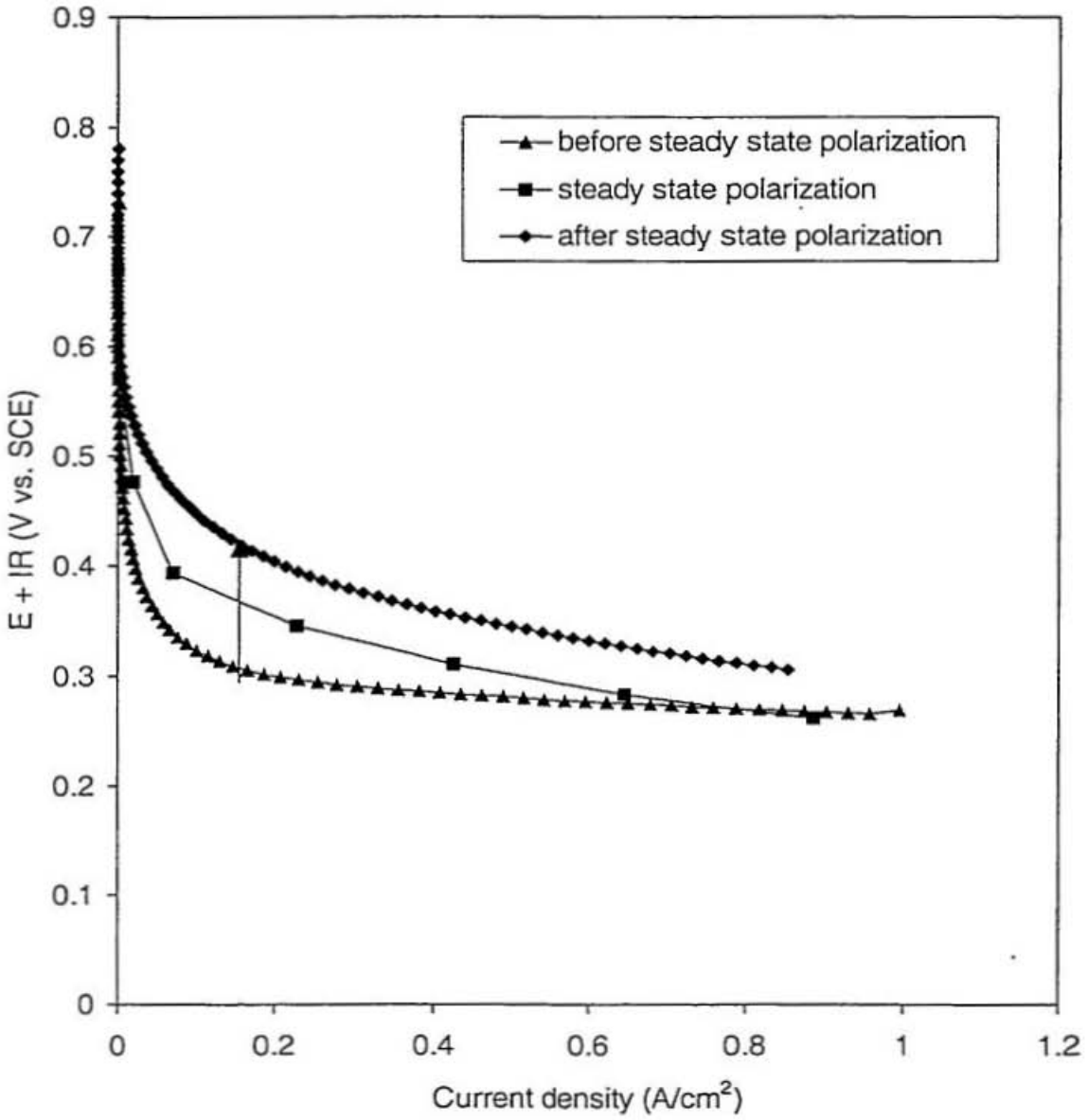

Fig. 2.20 The effect of polarization time on oxygen reduction performance for the H_2SO_4 modified catalyst at 0.20 mg Pt/cm^2. 20 % Pt/C treated by H_2SO_4 (boiling 6 hours).

2.3.2.3 Modification of catalysts by non-acidic oxidants

The 20 % Pt/C catalyst was treated with non-acidic oxidants such as NaClO, $(NH_4)_2S_2O_8$, and H_2O_2. **Fig. 2.21** shows the results indicating that both H_2O_2 and $(NH_4)_2S_2O_8$ slightly improved the original catalyst performance, but by less than the HNO_3 treated catalyst. Treatment with NaClO decreased the catalyst's performance.

The performance gains with H_2O_2 and $(NH_4)_2S_2O_8$ were achieved mostly in the high current region, i.e., ohmic region. Significant kinetic gains have not been realized by non-acidic oxidant treatment. The results for non-acidic oxidants just slightly changed the catalyst ORR performance showing that non-acidic oxidants are not strong enough to change the carbon surface to increase ionic conductivity of the carbon support that may be a main reason for the improved performances with treated catalysts.

2.3.3 Mechanisms of Improvement for the Modified Catalysts

2.3.3.1 Effect of PTFE content on ORR performance

The PTFE content in the catalyst greatly affects MEA performance by changing the amount of active Pt sites available to protons and O_2 as well as the water distribution (54). It appears that PTFE used for binding and wet-proofing the electrodes disturbs the diffusion of reactant gases in the porous catalyst layers, and also the conduction of proton in ionomer within the layer resulting in a reduction of Pt catalyst utilization. Therefore, it

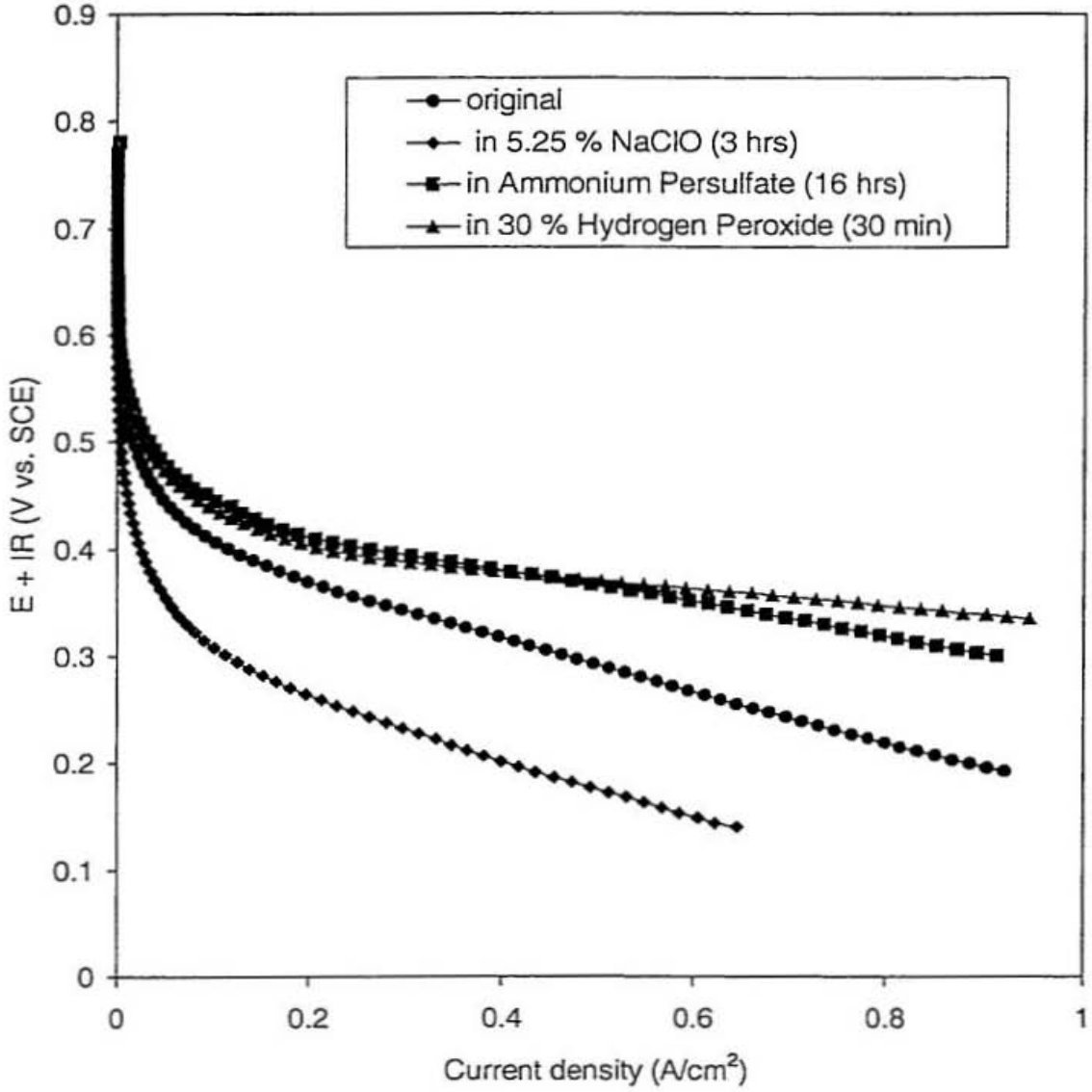

Fig. 2.21 Performances for catalysts modified by non-acidic oxidants at 0.2 mg Pt/cm^2.

is of great importance to determine the optimum PTFE content in the catalyst layer for accomplishment of the best performance.

Fig. 2.22 shows the relationship between the ORR performance and PTFE content. It was found that 20 % PTFE in the modified catalyst gave the highest performance in comparison to 10 % and 35 %, while for the original catalyst the optimum PTFE loading was found to be 15 %. Lower PTFE contents such as 10 % caused mass transport problems in the catalyst layer. At low PTFE content, the proportion of the main gas channels to the catalyzed reaction volume is small, and product water fills not only the reaction volume but also the gas channels. This resulted in diffusion control problems. As the PTFE content increased to ca. 20 %, the gas channels and the active sites increased which, in turn, shift control from diffusion to activation, thereby enhancing the activity. A further increase in PTFE content resulted in a lowered activity due to a decrease in the utilization of platinum clusters and also a decrease in the effective conductivity of the electrolyte. The latter resulted in a higher cell resistance as indicated from the slope of the linear part of I–E curves for 35 % PTFE content in comparison to that for 20 % PTFE. The treatment of the catalyst substantially increases the number of acidic functional groups leading to a more hydrophilic surface. The modified carbon surface therefore adsorbs water much more easily (to be discussed in section 2.3.3.4) and requires a higher PTFE content in the catalyst layer to achieve optimum performance.

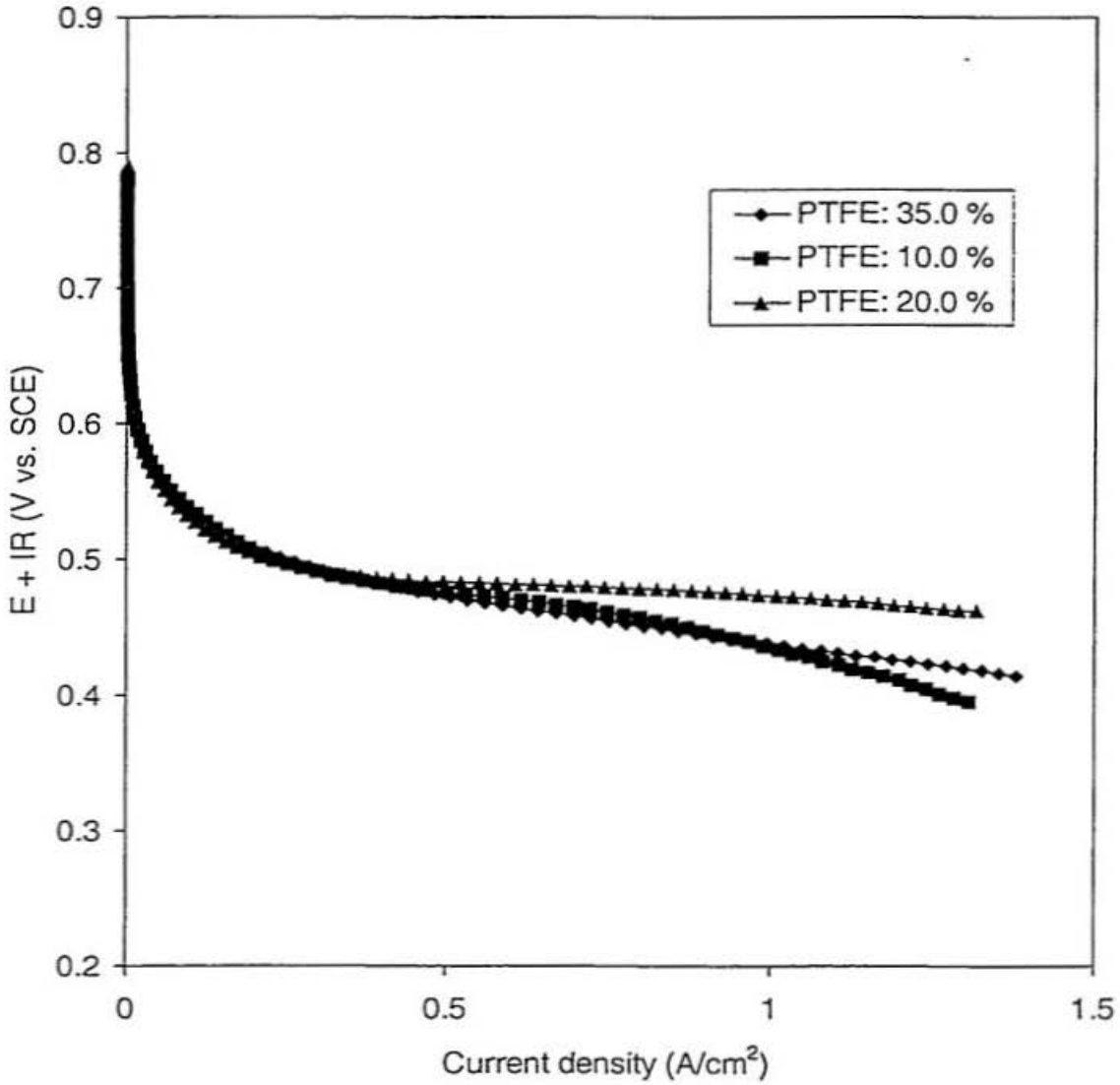

Fig. 2.22 Oxygen reduction performance for HNO_3 modified catalyst with different PTFE contents in the catalyst layer at 0.2 mg Pt/cm^2.

2.3.3.2 Effect of Nafion loading on the ORR performance

Nafion was impregnated into the modified catalyst to investigate its effect on the catalyst's ORR performance. The results are shown in **Fig. 2.23,** indicating that 0.13 mg/cm^2 Nafion in the modified catalyst layer decreased its performance. This observation is contrary to the fact that impregnation of Nafion into commercial carbon-supported catalysts usually improves the ORR performance (50). This is probably because the modified catalyst already provides enough ionic conductivity. Further addition of Nafion into the catalyst layer would block O_2 diffusion to the Pt surface and give a lower ORR performance. This advantage for modified catalysts will further reduce costs for PEMFCs since Nafion is one of their most expensive components.

2.3.3.3 CVs for modified catalysts

Fig. 2.24 displays CVs for modified and original catalysts, which indicate that the HNO_3 treated catalyst behaved somewhat differently from the original catalyst. The treated catalyst has larger hydrogen adsorption and desorption peaks corresponding to a higher active catalyst surface area. Charge integration of hydrogen adsorption for the treated and non-treated catalysts gave active surface areas of 140 cm^2 and 100 cm^2, respectively. Furthermore, there was a new (or enlarged) redox peak, most likely corresponding to a quinone/hydroquinone couple (5) associated with the treated catalyst. It can be concluded that the oxidation of the carbon support significantly increases the

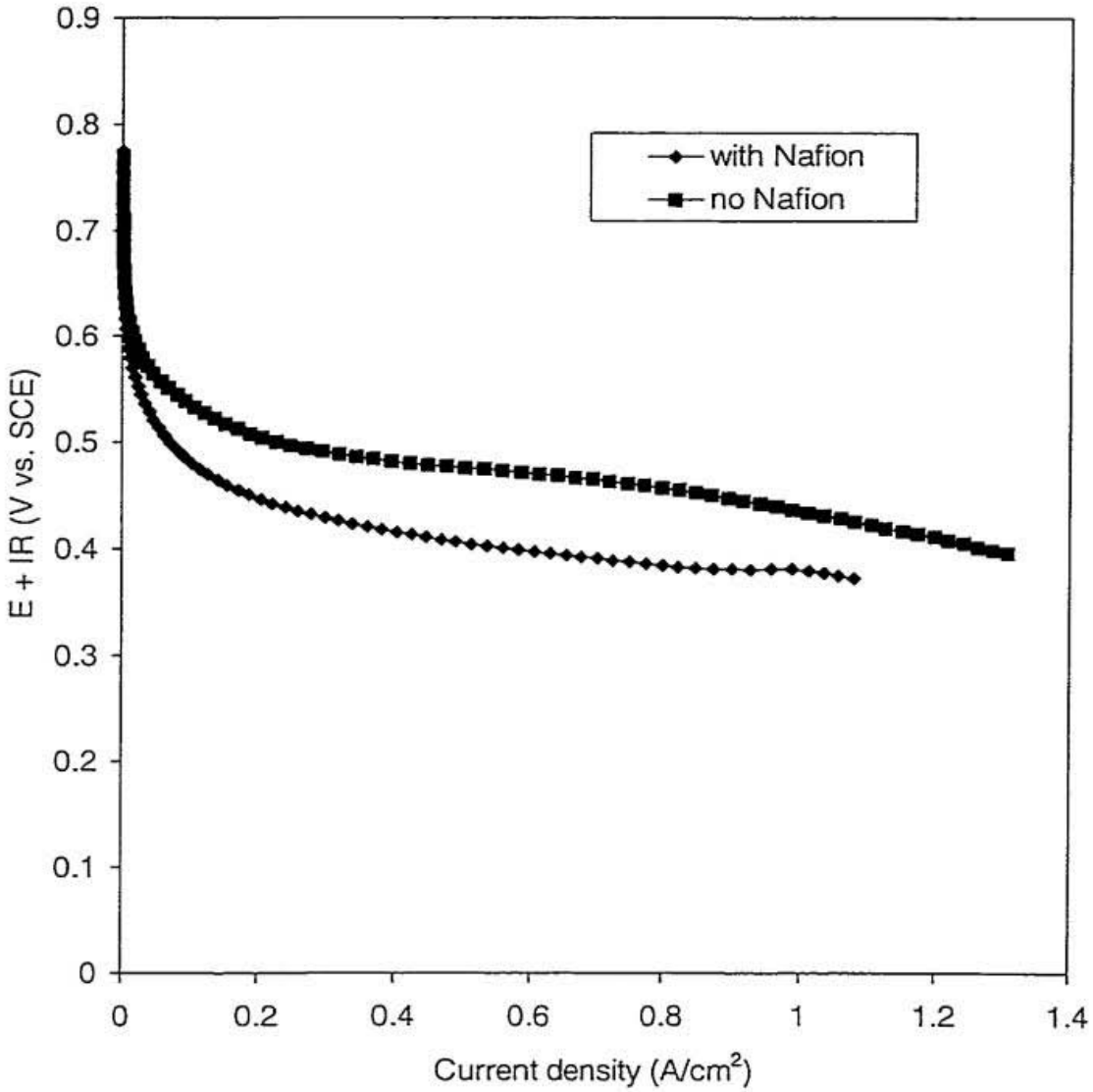

Fig. 2.23 Oxygen reduction performance for HNO_3 modified catalyst with Nafion impregnated in the catalyst layer at 0.20 mg Pt/cm^2. The electrode impregnated Nafion contains 0.13 mg/cm^2.

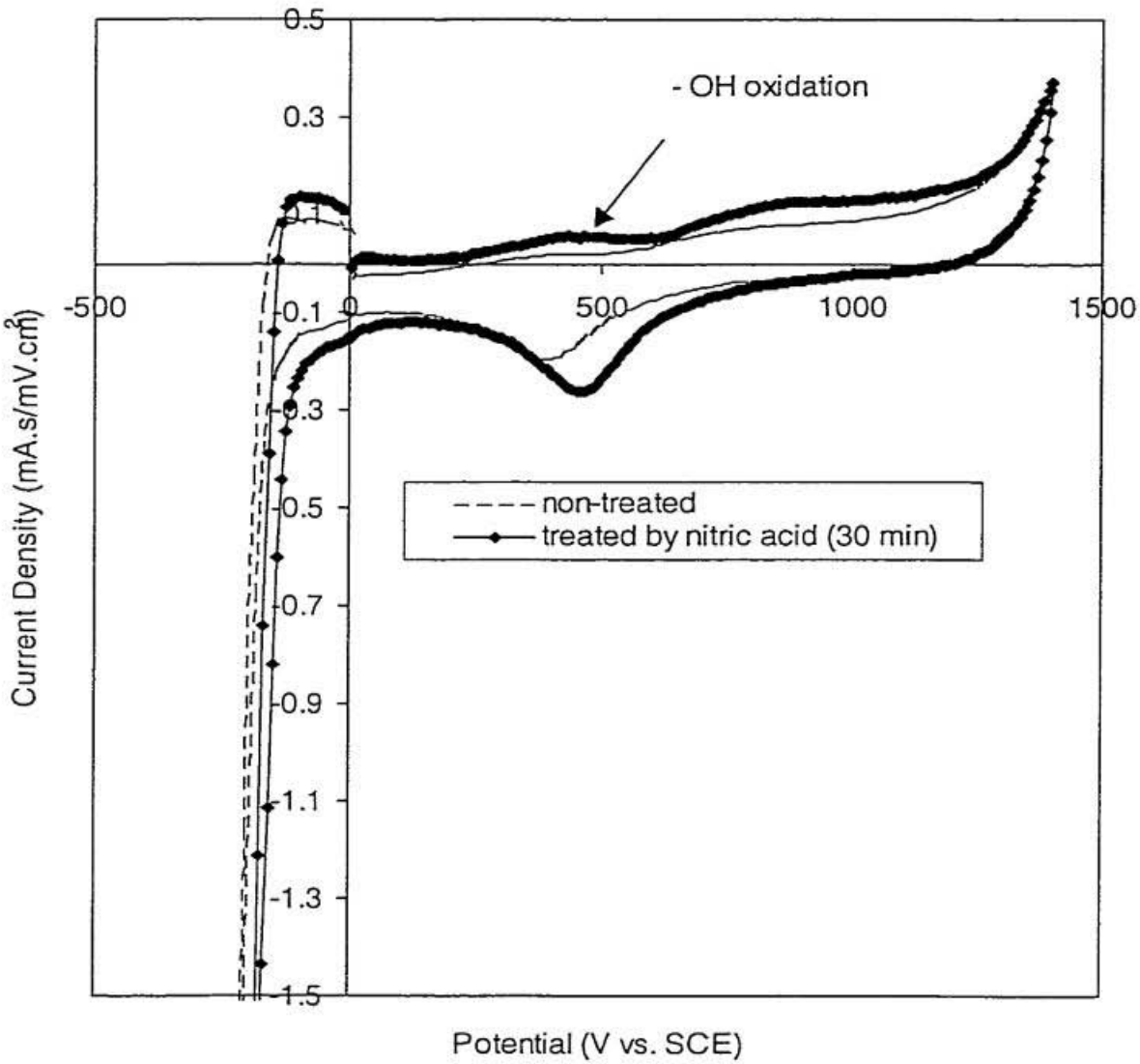

Fig. 2.24 CVs for treated and non-treated catalysts at 0.20 mg Pt/cm^2 and a scan rate of 10 mV/s. 20 % Pt/C refixed in HNO_3.

acidic functional groups such as - OH and – COOH so that proton access to the catalyst surface is much easier, leading to a larger active surface area. This is one of the reasons that the modified catalyst can improve ORR performance. The chemical oxidation also causes profound modification of the morphological characteristics of the carbon support (i.e., increase in microporosity) (25) and significantly increases its wettability because of the increased acidic functional groups. The increase in wettability is attributed to an increased pore volume and to the progressive build-up of oxygenated groups.

2.3.3.4 IR spectra of modified catalysts

Fig. 2.24 shows IR spectra for carbon-supported catalysts treated by HNO_3 and non-acidic chemicals. An almost no acidic functional groups were detected on the original catalyst surface. The HNO_3 treated catalyst showed a very strong absorption peak at 1618 cm^{-1}, which may be due to a mixture of carboxylic and carbonyl groups (56). A very strong absorption peak is also found at around 3400 cm^{-1} that may be related to a – OH stretch. This – OH peak may be due to water adsorption. In either case, it indicates that the modified catalyst becomes more hydrophilic. On the hand, the H_2O_2 and $(NH_4)_2S_2O_8$ modified catalysts showed a lower density of carboxylic acid groups on the surface, and the NaClO modified catalyst behaved the same as the original catalyst. This indicates that non-acidic oxidants can only slightly increase the acidic functional groups on the carbon surface.

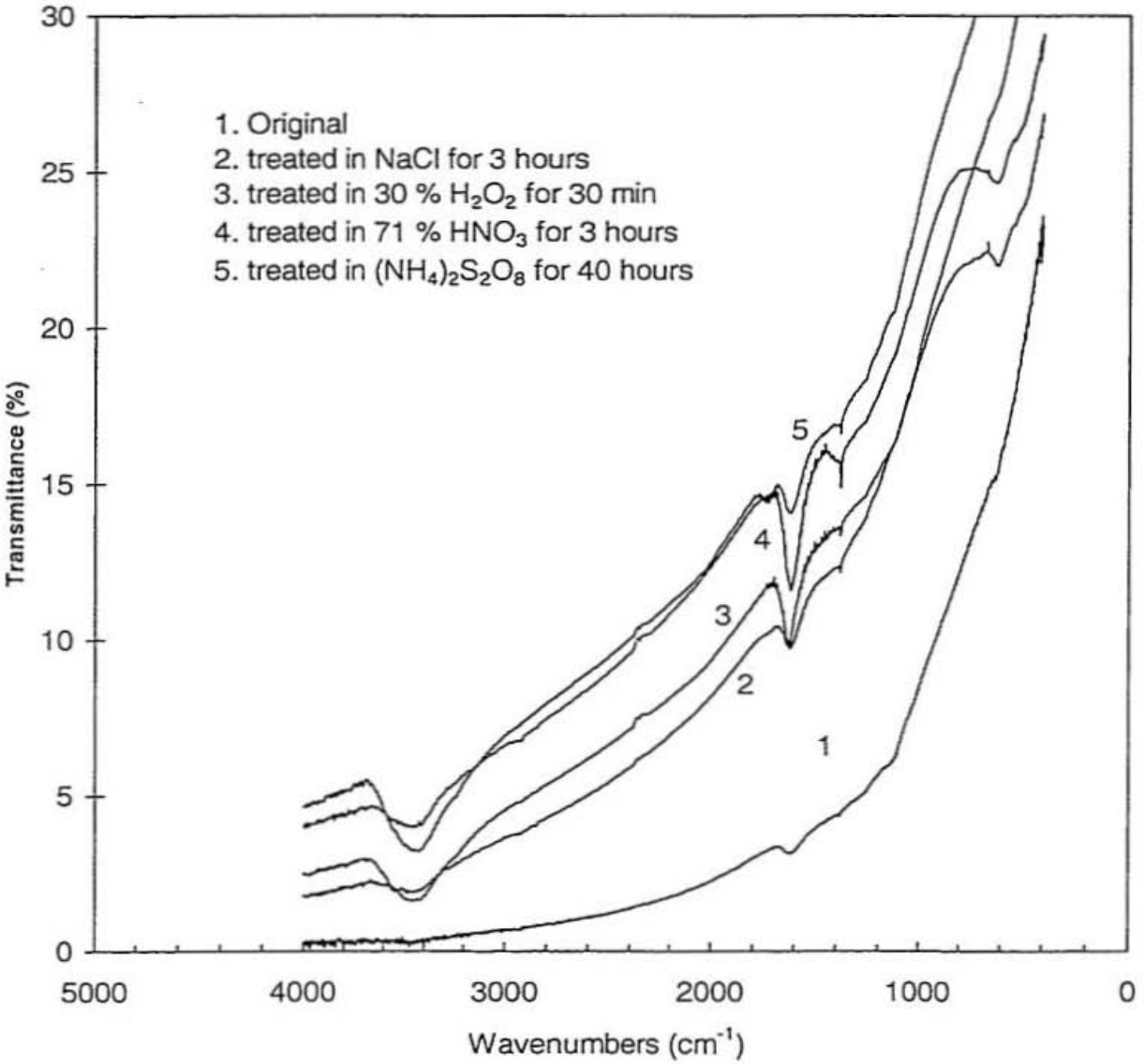

Fig. 2.25 IR spectra for different 20 % Pt on carbon-supported catalysts.

Oxidation of the carbon support in HNO_3 appears to produce a large increase in the concentration of surface oxide groups. This point has been proven by CVs for treated catalysts which showed an additional oxidation peak associated with –OH (**Fig. 2.24**). Furthermore, the pH of an aqueous slurry of carbon can also provide a convenient indicator of the surface groups. The pH of carbon slurries is thought to be a function mainly of the concentration of carboxylic acid groups. The complete titration of carbon slurries provides additional information on the surface properties. Accordingly, titration of a HNO_3-modified catalyst showed that it possessed an acidity twice as high as the non-treated catalyst (57). Therefore, it can be concluded that the modified catalyst improves ORR performance due to its increased proton accessibility to the catalyst surface, and increased proton concentration (**Eqn (2.1.3)**). This also supports the idea that non-acidic oxidants only can marginally increase the ORR performance due to less formation of the acidic groups on the carbon surface.

The increased concentrations of – OH and – COOH on the carbon surface also increase the ionic conductivity of the catalyst layer. This creates a potential advantage for systems using Nafion as a binder and ionic conductor in the catalyst layer since less will be required. This would decrease O_2 diffusion limitations. Moreover, a more hydrophilic carbon support will tend to associate with the sulfonic acid groups of the Nafion leaving the hydrophobic perfluorinated backbone to face the oxidant gas. This orientation will lead to a higher oxygen concentration in the catalyst layer (O_2 has a much higher solubility in non-polar backbone) and should produce a much improved ORR performance.

2.3.3.5 Conductivity measurements on modified catalysts

In graphite, the carbon-carbon bond length is 1.42 Å in the hexagonal rings and 3.354 Å in the direction of the c axis, which is perpendicular to the rings. The layer planes are composed of a hexagonal array of carbon atoms held by stable covalent bonds, but with weak Van Der Waals bonds between the layers. Therefore, some species can be easily inserted into the layers to change the carbon's conductivity. The four-probe method was applied to measure the electrical conductivity of the carbon-supported catalysts (as described in the experimental section). The results are given in **Table 2.2.**

Table 2.2 Electronic conductivities of the modified catalysts

Samples	Conductivity (σ, S/cm)
20 % Pt on Vulcan XC-72R	1.53
$HClO_4$ (refluxed 6 hours)	1.22
98 % H_2SO_4 (refluxed 6 hours)	0.27
85 % H_3PO4 (refluxed 6 hours)	1.83
71 % HNO_3 (refluxed 3 hours)	1.3
71 % HNO_3 (6 hours at RT)	1.31

The conductivity data indicate that all the modified catalysts possessed similar electronic conductivity to that of the original catalyst except the catalyst treated by H_2SO_4 which had a significantly lower conductivity. This may be due to the decomposition of intercalate-graphite bisulfate in the presence of water (58). The H_3PO_4 treated catalyst had slightly higher conductivity than the original one. A common technique to prepare graphite acid compounds is expressed by the general equation as follows (59):

$$C_x + A^- + yHA \longrightarrow C_x^+A^- \bullet yHA + e^- \qquad (2.2.5)$$

Where C_x is the host graphite and A^- is the anion of the acid (HA), e.g., NO_3^-.

The data also strongly indicates that the carbon support has a strong resistance to acid oxidation since the catalyst treated by hot HNO_3 solution showed the same conductivity as the catalyst treated in HNO_3 at room temperature. It is presumed that the electronic conductivity of the catalyst would decrease due to the oxidation of carbon. However, it is proposed that graphite intercalates are formed during the oxidation, and that their very good electronic conductivity maintains the catalyst conductivity. Therefore, oxidation of carbon-supported catalysts increases ionic conductivity without compromising electronic conductivity. This is another major reason that modified catalyst can improve ORR performance. Without graphite intercalates, IR drop would offset any improvement of the ionic conductivity increase.

2.4 Conclusion

The half-cell technique, with a self-designed gas diffusion electrode holder, was successfully used for the evaluation of catalyst performance. With the help of CV, the electrochemically active surface area can be measured by using the hydrogen adsorption peaks, although carbon features can mask these and make the method imprecise. The experimental data show that, in order to obtain the true active surface area, a slow scan rate should be applied so as to achieve a steady state on the electrode.

Polarization results indicate that the transient polarization can fully represent the electrode performance with the fast and reliable characteristics. AC impedance is a useful technique for measurement of the cell resistance.

Catalysts modified by both acidic and non-acidic oxidants can significantly improve the ORR performance. The catalysts treated by acids, especially by HNO_3, increase the number of carbon surface functional groups such as –OH and –COOH allowing protons more easy access to the catalyst surface. The improved ionic conductivity on the catalyst surface leads to a higher performance based on the triple contact mechanism for the ORR in the catalyst layer (8, 10, 34). Meanwhile, graphite intercalates are produced so that the catalysts maintains their electronic conductivity.

In conclusion, the modified catalysts improve ORR performance due to a higher ionic conductivity caused by the increase of surface functional groups.

References

(1) A. Damjanovic, in Modern Aspects of Electrochemistry, (J. O'M. Bockris and B. E. Conway, eds.), Vol. 5, p. 369. Plenum, New York, 1969.

(2) A. J. Appleby and A. Borucka, J. Electrochem. Soc. 122, 1212 (1969).

(3) S. -M. Park, S. Ho, S. Aruliah, M. F. Weber, C. A. Ward, and R. D. Venter, J. Electrochem. Soc. 133, 1641 (1986).

(4) H. R. Kunz and G. A. Gruver, Electrochim. Acta 23, 219 (1978).

(5) M. S. Wilson and S. Gotesfeld, J. Appl. Electrochem., 22, 1 (1992).

(6) S. J. Lee, S. Mukerjee, J. McBreen, Y. W. Rho, Y. T. Kho and T. H. Lee, Electrochim. Acta, 43, 3693 (1998).

(7) E. A. Ticianelli, C. R. Derouin and S. Srinivasan, J. Electroanal.. Chem. 251, 275 (1988).

(8) M. S. Wilson and S. Gottesfeld, J. Electrochem. Soc. 139, L284 (1992).

(9) E. J. Taylor, E. B. Anderson and N. R. K. Vilambi, J. Electrochem. Soc. 139, L45 (1992).

(10) D. Raistrick, U.S. Patent 4, 876115, 1990.

(11) E. A. Ticianelli, C. R. Derouin, A. Redondo and S. Srinivasan, J. Electrochem. Soc. 135, 2209 (1988).

(12) R. Liu, W. H. Her and P. S. Fedkiw, J. Electrochem. Soc., 139, 15 (1992).

(13) Kim Kinoshita, Electrochemical Oxygen Technology, A Wiley-Interscience Publication, John Wiley & Sons, Inc., 1992, p. 60.

(14) K. Kordesch and J. Gsellman, Proc. of the Workshop on The Electrochemistry of Carbon, S. Sarangapani, J. R. Akridge, and B. Schumn (eds.), August 17-19, 1993, p.221.

(15) H. P. Boehm, R. Setton, and E. Stumpp, Carbon, 24, 241 (1986).

(16) M. S. Dresselhaus and G. Dresselhaus, Adv. Phys., 30, 139 (1981).

(17) M. Noel, R. Santhanam, J. Power Sources, 72, 53 (1998).

(18) J. H. De Boer and A. B. C. Van Doon, Third Conference on Industrial Carbons and Graphites, Society of Chemical Industry, London, 1971, p. 303.

(19) D. Hadzi and A. Novak, Trans. Faraday Soc., 51, 1641 (195).

(20) E. Matuyama, J. Phys. Chem., 58, 215 (1954).

(21) A. Martin Rodriguez and P. S. Valerga Jimenez, Carbob, 24, 163 (1986).

(22) W. S. Hummers and R. E. Offeman, J. Am. Chem. Soc., 80, 1339 (1958).

(23) J. B. Donnet, A. Voet, P. Ehrburger, H. Dauksch, and P. A. Marsh, Carbon, 11, 431 (1973).

(24) K. Hondo and A. Shindo, Carbon, 24, 230 (1986).

(25) Y. Matsumura, S. Hagiwara, and H. Takahashi, Carbon, 14, 163 (1976).

(26) S. Hagiwara, K. Tsutsumi, and H. Takahashi, Carbon, 16, 89 (1978).

(27) J. B. Donnet, E. Papirer, and H. Dauksch, Carbon Fibers Their Place in Modern Technology, Plastics and Polymers Conference Supplement No. 6, The Unwin Brothers, Ltd., Surrey, England, 1974, p. 58.

(28) B. R. Puri and R. C. Bansal, Carbon, 1, 457 (1964).

(29)M. Wakizoe, O. A. Velve and S. Srinivasan, Electrochim. Acta, 40, 335 (1995).

(30) P. R. de Sena, E. A. Ticianelli, and E. R. Gontalez, J. Electroanal. Chem., 357, 225 (1993).

(31) Parthararathy, S. Srinivasan and A. J. Appleby, J. Electroanal. Chem., 339, 101(1992).

(32) S. Gilman, in Electroanal. Chem., Vol. 2 (A. J. Bard, ed.), Arnold Press, London, 1967, pp. 111 – 192.

(33) A. S. Arico, V. Alderucci, V. Antonucci, S. Ferrara, V. Recupero, N. Giordano, K.

(34) I. D. Raistrick, Electrochim. Acta, 35, 1579 (1990).

(35) W. Jenseit, O. Bohme, F. U. Leidich and H. Wendt, Electrochim. Acta, 38, 2115 (1993).

(36) A. Parthasarathy, B. Dave, S. Srinivasan, and A. J. Appleby, J. Electrochem. Soc., 139, 1634 (1992).

(37) A. Esoinola, P. M. Miguel, M. R. Salles, and A. R. Pinto, Carbon, 24, 337 (1986).

(38) L. J. Van der pauw, Philips Res. Repts 13, 1-9, 1958.

(39) Essalik, K. Amouzegar, O. Savadogo, J. Applied Electrochem., 25, 404 (1995).

(40) A. B. Sepa, M. V. Vojnovic and A. Damjanovic, Electrochim. Acta, 32, 129 (1987).

(41) J. Huang, R. K. Sen, and E. B. Yeager, J. Electrochem. Soc., 141, 786 (1979).

(42) M. R. Tarasevich, Electrokhimiya, 9, 599 (1973).

(43) E. B. Yeager et al, J. Serb. Chem. Soc., 57, 819 (1992).

(44) A. Damjanovic and V. Brusic, Electrochimica, 12, 615 (1967).

(45) A. J. Appleby, J. Electrochem., 117, 328 (1970).

(46) A. J. Appleby, J. Electrochem., 117, 641 (1970).

(47) A. Damjanovic and M. A. Genshaw, Electrochim. Acta, 5, 1281 (1970).

(48) A. C. Riddiford, Electrochim. Acta, 4, 170 (1961).

(49) A. Parathasarathy, C. R. Martin, and S. Srinivansan, J. Electrochem. Soc., 138, 916 (1991).

(50) Z. Poltarzewski, P. Staiti, V. Alderucci, W. Wieczorek, and N. Giordano, J. Electrochem. Soc., 139, 761 (1992).

(51) A. J. Appleby, J. Power Sources, 49, 15 (1994).

(52) E. E. Kadin, R. Faure, and R. Durand, J. Electroanal. Chem., 301, 177 (1991).

(53) N. M. Markovic, H. A. Gasteiger, and P. N. Ross, Jr., J. Phys. Chem., 99, 3411 (1995).

(54) Uchida, Makoto, Aoyama, Yuko, Nobuo, Ohta, Akita, J. Electrochem. Soc., 142, 4143 (1995).

(55) S. Srinivasan, E. A. Ticianelli, C. R. Derouin and A. Redondo, J. Power Sources, 22, 359 (1988).

(56) J. M. O'Reilly and R. A. Mosher, Carbon, 21, 47 (1983).

(57) R. Martin and P. G. Pickup, Personal Communication, 1998.

(58) H. L. Riley, Fuel, 24, 8 (1945).

(59) A. R. Ubbelohde, Carbon, 7, 523 (1969).

Chapter 3

Surface Characterization of Carbon-Supported Pt Catalysts by Reduced CO_2 Oxidation

3.1 Introduction

3.1.1 Hydrogen Adsorption

Noble metals such as platinum and ruthenium have wide applicability in electrochemistry. The search for more efficient catalysts for both fuel oxidation and oxygen reduction in fuel cells has led to a demand for a better understanding of the basic processes involved. This stimulated investigations into the role of adsorbed intermediates in hydrogen oxidation, the oxidation of organic fuels, and the reduction of oxygen. The considerable work directed toward elucidating the fundamental processes taking place at fuel cell electrodes has been reviewed by Breiter (1).

The real surface area of a catalyst can be orders of magnitude greater than the geometric area. Since adsorption and catalytic reactions depend on the real surface area of catalysts, it is important to be able to measure this quantity. Early measurements of the active surface area of the catalyst were referred to as "galvanostatic" with the recorded

transient as a charging curve (2), "cyclic voltammetry" with the recorded curves as cyclic voltammograms (3), and "ac impedance" for the measurement of pseudocapacitance as a function of potential (4-6). These three techniques for measuring active surface areas all depend on the adsorption and desorption of H atoms on the catalyst surface. Among them, cyclic voltammetry (CV) proved to be quite valuable and convenient for determining the electrochemically active surface area of electrodes. The CV technique has now been successfully used for the determination of the catalyst specific surface area supported on high-area carbons (7-18). However, it seems that large double-layer capacitance associated with these high-area carbons has a significant impact on the use of this method, particularly at low Pt loadings (see section 2.3.1.1).

The determination of surface area from hydrogen adsorption measurements depends on whether the quantity of charge $Q_{H,s}$, corresponding to saturation hydrogen coverage, can be obtained. In converting this quantity to the number of platinum surface sites, it is assumed that each surface platinum atom is associated with one chemisorbed hydrogen atom, and that the coverage with hydrogen atoms is zero at the inflection separating the "hydrogen" and "double-layer" regions (see **Fig. 2.4**). The determination of $Q_{H,s}$ from CV measurements also depends on whether the contribution due to hydrogen adsorption can be separated from contributions due to other processes occurring simultaneously, e.g., hydrogen evolution. In order to establish a method for comparing data obtained with different electrodes and by different workers, Gilman (19-20) suggested that the potential of the current minimum that follows the second cathodic

hydrogen peak be arbitrarily taken as an "end-point" for integration of the hydrogen adsorption charge for area determination.

Although the determination of electrode surface area from hydrogen adsorption has been widely used, especially for unsupported catalysts, this method presents a more difficult problem for supported catalysts because of overlap of H adsorption and the evolution of molecular hydrogen. The increase in current at potentials below - 0.20 V (SCE) in **Fig. 2.11** with carbon-supported catalysts is due to hydrogen evolution. It can be seen that there is a potential region in which both adsorption and evolution occur simultaneously. Consequently, cathodic current does not actually reach a minimum as the hydrogen atom deposition and molecular hydrogen evolution currents merge together. Thus, an "end point" for full hydrogen coverage determined from such a CV must be somewhat arbitrary.

In addition, electrochemical surface-area measurements are hard to make on carbon-supported electrocatalysts, especially those containing only a small weight fraction of Pt, due to interference from the double-layer charging current associated with the C support (21). The carbon features (double-layer charging and redox behavior of surface-active groups) mask the platinum hydrogen adsorption-desorption characteristics. Connolly et al. (22) and Urisson et al. (23) reported that the Pt surface area could be obtained by an electrochemical method (galvanostatic stripping of adsorbed H_2) if the content of Pt in the catalyst is greater than approximately 1 wt % Pt supported on C. However, Bett et al. (21) reported that the CV technique did not yield meaningful values of active surface areas of the Pt-C electrocatalysts containing 1 % Pt. In order to address

this problem, CO anodic stripping has also been using to accurately measure electrochemically active surface areas.

3.1.2 Potentiodynamic Stripping of Chemisorbed CO

In regards to limitations of the active surface area measurement for carbon-supported catalyst by H adsorption, especially at low Pt loadings, potentiodynamic stripping of chemisorbed CO on Pt has also been used to determine Pt electrocatalyst surface areas (24-28). Typically, CO molecules are adsorbed on Pt by holding the electrode potential constant at 0.05 V (vs. NHE), and the resultant current-potential curve for the oxidation of CO on Pt provides a sharper and better-defined peak than for H adsorption. One electron is transferred during the oxidation of adsorbed H, whereas two electrons are transferred when oxidizing CO to CO_2 on Pt. There have been considerable discussions in the literature on whether CO is bridged-bonded or linear on Pt, for which 210 $\mu C/cm^2$ and 420 $\mu C/cm^2$ are passed, respectively (29). Due to steric effects, not every surface atom can accommodate one CO molecule. Bett et al. (21) showed that electrochemical determinations of CO-H atom ratios were 0.87-0.89 for unsupported Pt blacks and 0.89-0.90 for Pt supported on graphitized Spheron 6 (a channel black).

CO oxidation by potentiometric stripping (or linear sweep voltammetry) provides a good method to determine the surface area of catalysts with less interference from the double layer charge and better resolution, since the CO oxidation peak replaces a flat shoulder due to H adsorption. However, as CO can adsorb directly onto bare Pt sites (3.1)

or Pt-H sites (3.2), the active surface area determined by CO can be much larger than that from H adsorption measurement. This overestimation may be due to CO reaching the embedded Pt surrounded by hydrophobic graphite in micropores that may not be accessible by protons.

$$CO + Pt \longrightarrow Pt = CO \qquad (3.1)$$

$$2CO + 2Pt\text{-}H \longrightarrow 2\ Pt{=}CO + H_2 \qquad (3.2)$$

However, the Pt sites that are not accessible to protons should not be electrochemically active in the fuel cell reactions. This implies that the active surface area determined by CO stripping may not represent the real surface area available for the ORR in PEMFCs.

3.1.3 Reduced CO_2 Oxidation

Considering the limitations of CO for measuring active surface areas, CO_2 may be an alternative candidate to replace CO without loss of high resolution of the CO method. CO_2 is adsorbed much less strongly than CO on the Pt surface, and it can only adsorb on the hydride Pt surface as in the equation (3.3) (30), which means that it would not adsorb on the Pt sites that are not accessible to protons.

$$CO_2 + 2\ Pt\text{-}H \rightarrow Pt{=}CO + H_2O + Pt \qquad (3.3)$$

This relationship is advantageous as it is more directly related to H adsorption and corresponds to the accessible surface area. Many studies have been conducted on smooth platinum electrodes in acid environments to evaluate the complex kinetic behavior of "reduced" CO_2, and the effects of experimental conditions on surface coverage and the nature of the reduced products (31-43). The products of CO_2 reduction are usually mixtures of H_2CO_4, CO, HCOOH, CH_3OH, HCHO and CH_4 depending on the catalysts and adsorption potential. However, it is believed that the reduction results in the formation of no more than a monolayer of adsorbed species. Therefore, oxidation of reduced CO_2 should be an effective alternative method to determine the active catalyst surface area. Although many studies have been conducted on Pt electrodes to examine the CO_2 reduction, CO_2 has not been used by others for active surface area measurement.

3.1.4 Scope of This Work

The charge required for oxidation of reduced CO_2 has been employed to determine the active surface area of unsupported and carbon-supported catalysts in gas diffusion electrodes using the CV technique. Due to the complexity of the products, relative oxidation charges for reduced CO_2 were used to compare active surface area for different catalysts and different Pt loadings. The factors affecting CO_2 adsorption on the Pt surface, such as adsorption potential and adsorption time, were evaluated to obtain saturation coverage of reduced CO_2 on the Pt surface. The scan rate dependence of the

stripping scan was also characterized so as to obtain true oxidation charges. Furthermore, as the products of reduced CO_2 are quite similar to those of partial oxidation of MeOH and CO adsorbed species on Pt surfaces, information on catalyst poisoning tolerance has been obtained from the potential shift of the oxidation peak and the onset potential for reduced CO_2 oxidation.

3.2 Experimental

The experimental setup and MEA preparation were the same as those described in the experimental section of Chapter 2. The potential program applied to the working electrode comprised of an initial potential step to 1.4 V vs. SCE for 5 minutes and holding of the potential at – 0.4 V (SCE) for 2 minutes for cleaning. This was followed by a potential step to the adsorption potential in a CO_2 environment for an adsorption time t_{ad}. Before the stripping scan, N_2 gas was used to flush CO_2 from the gas chamber. Cyclic voltammograms were recorded following application of different adsorption potentials (E_{ad}), adsorption time (t_{ad}), and by employing different scan rates. Supported (10 % and 20 % Pt on Vulcan XC-72R from Electrosynthesis Co, inc., 20 % Pt/Ru (a/o) on Vulcan XC-72 from E-TEK, Inc., and 20 % Pt on Vulcan XC-72R modified by HNO_3) and unsupported catalysts (platinum black and a mixture of the Pt black and another metal from Ballard Power Systems, Inc.) were evaluated in this study. All measurements were carried out at room temperature (23 ^{0}C ± 1 ^{0}C).

3.3 Results and Discussion

3.3.1 Unsupported Catalyst

3.3.1.1 Relationship between coverage and scan rate

It is generally assumed that CO_2 is electrochemically inert, so that only under very extreme conditions of potential may it be reduced. A CV for a 4 mg Pt/cm^2 Pt black electrode following CO_2 adsorption at a potential of – 0.2 V (SCE) for 30 minutes is displayed in **Fig. 3.1**. A pronounced peak due to oxidation of the reduced CO_2 occured at 0.55 V (SCE). This peak is due to a chemisorbed species that is formed when chemisorbed hydrogen (electrochemically formed) reacts with CO_2. The oxidation of the product is very irreversible. Compared with CO stripping from a Pt surface, reduced CO_2 behaves quite similarly. Therefore, oxidation of reduced CO_2 retains the high-resolution characteristic of the CO method.

In order to achieve the best resolution and saturation coverage, scan speed needs to be evaluated to investigate the relationship between the peak area and scan rate. **Fig. 3.2** shows partial CVs with different scan rates begun at an adsorption potential of – 0.2 V (SCE) for 30 minutes. It is found that the peak shape became sharper with decreasing scan rate, which indicates that slower scan rates provided a higher resolution, e.g., at 10

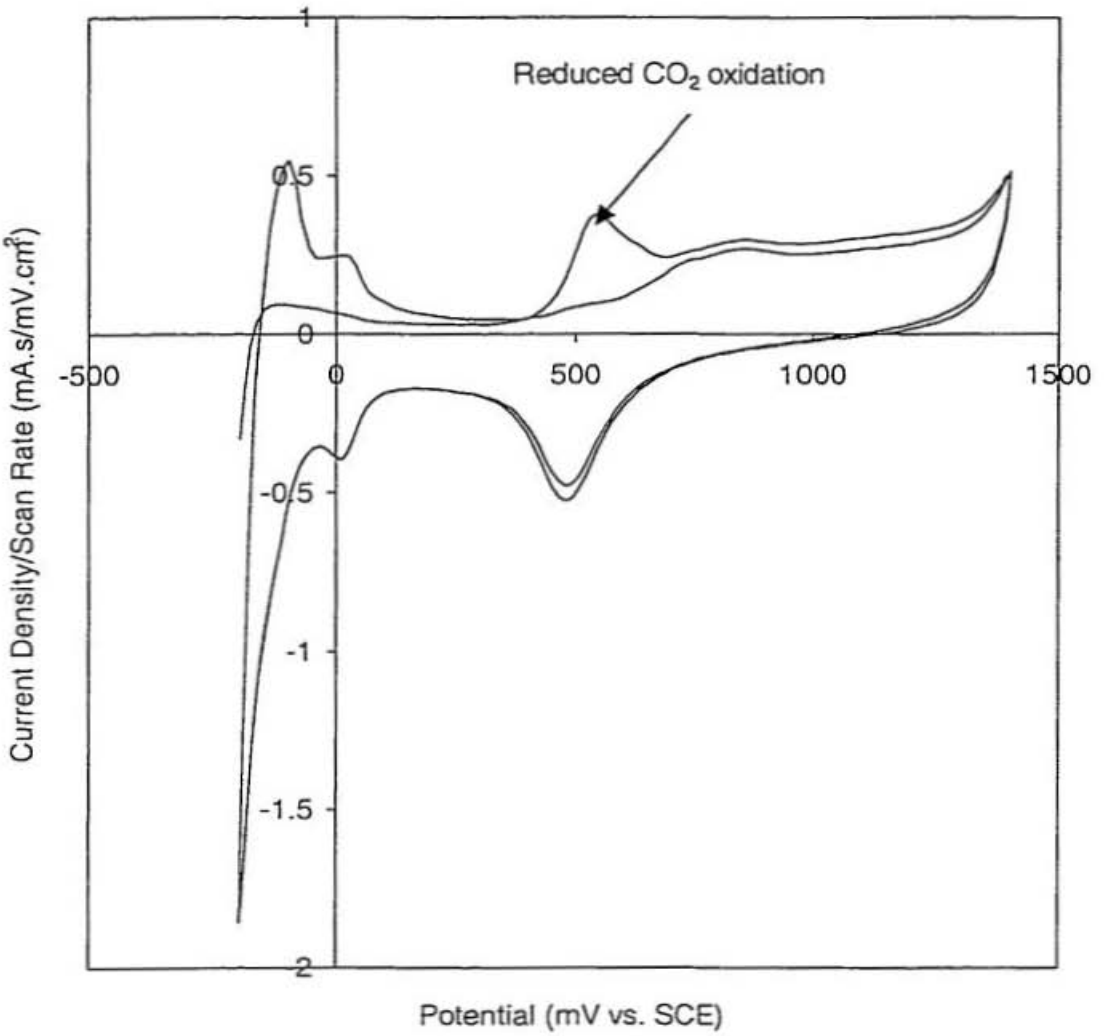

Fig. 3.1 Cyclic voltammograms for reduced CO_2 oxidation on 4 mg Pt/cm^2 at t_{ad} = 30 min and E_{ad} = - 0.2 V (SCE). Scan rate: 100 mV/s.

mV/s. It is also observed that the background in N_2 should be used as a baseline to calculate the oxidation charge for reduced CO_2, since using second scan as the background would cause underestimation of the oxidation charge as some reduced CO_2 still remains on the electrode surface.

Integration of peak areas of CVs for reduced CO_2 gives the oxidation charges for reduced CO_2 at different scan rates. The results are in **Fig. 3.3**. For the purpose of comparison, the H adsorption charge was also calculated to determine saturation coverage by CO_2 on the Pt surface. When performing calculations of CO_2 coverage, a one electron mechanism (31, 44-45) and the adsorption of one CO_2 molecule per H adsorption site has been assumed, although a two-electron mechanism has been suggested by another researcher (46). Hence, we assume that the adsorbed radical COOH is the main product of CO_2 and H_{ad} reaction on the surface of the platinum. The mechanism of its oxidation can be written as follows:

$$Pt - COOH \longrightarrow Pt + H^+ + CO_2 + e^- \qquad (3.4)$$

It can be seen from **Fig. 3.3** that the oxidation charge for reduced CO_2 increased with decreasing scan rate, but it approached a nearly constant value when the scan rate was below 40 mV/s. The hydrogen charge is almost independent of scan rate. Saturation coverage, Q_{CO2r}/Q_H by reduced CO_2, is about 0.5 at a scan rate of 10 mV/s. The slightly low coverage by reduced CO_2 is due to the competitive adsorption between H and reduced CO_2. This is supported by the fact that the H oxidation still occurs even with

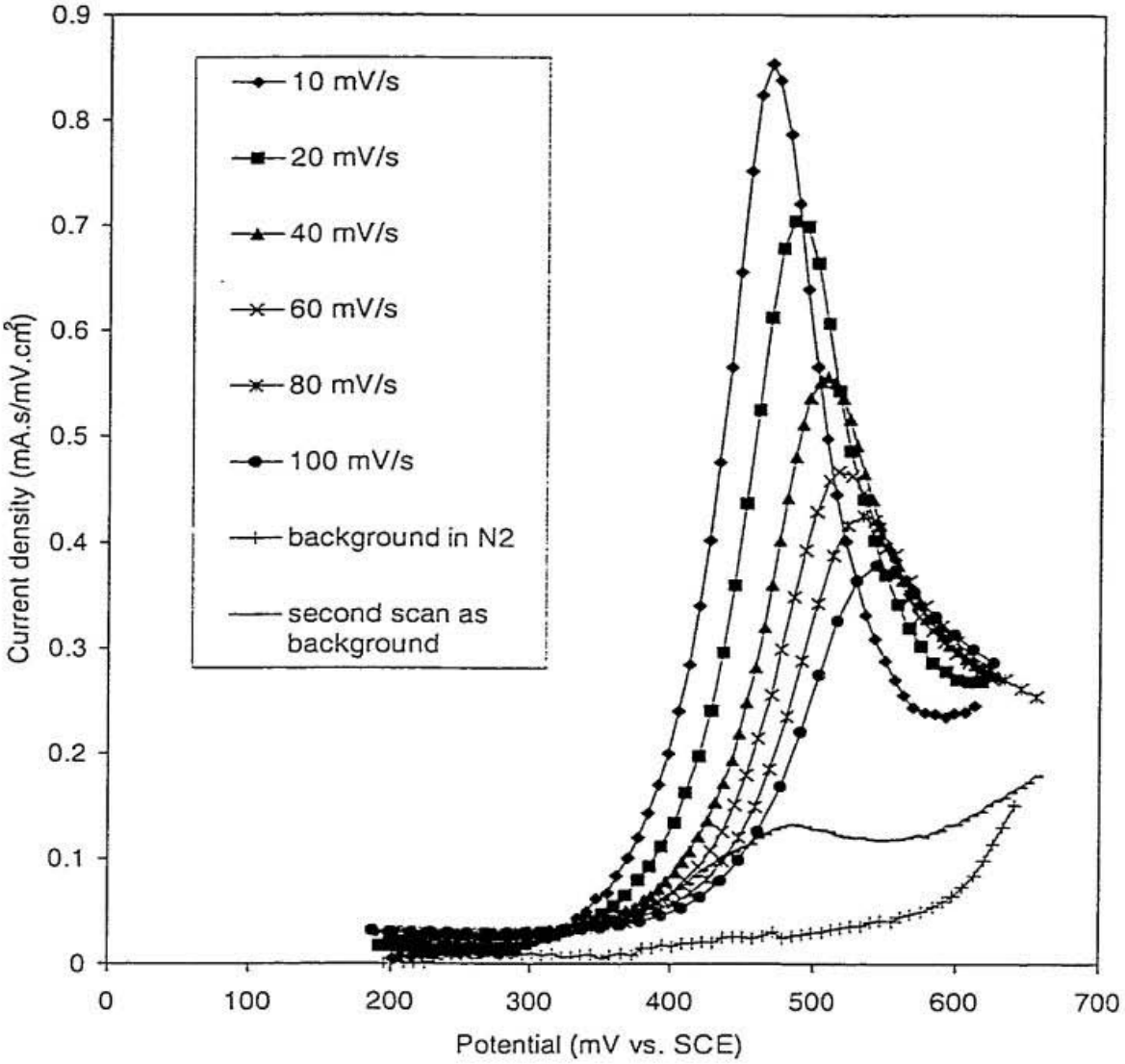

Fig. 3.2 Partial CVs for reduced CO_2 oxidation at different scan rates at E_{ad} = - 0.2 V (SCE) for 30 min.

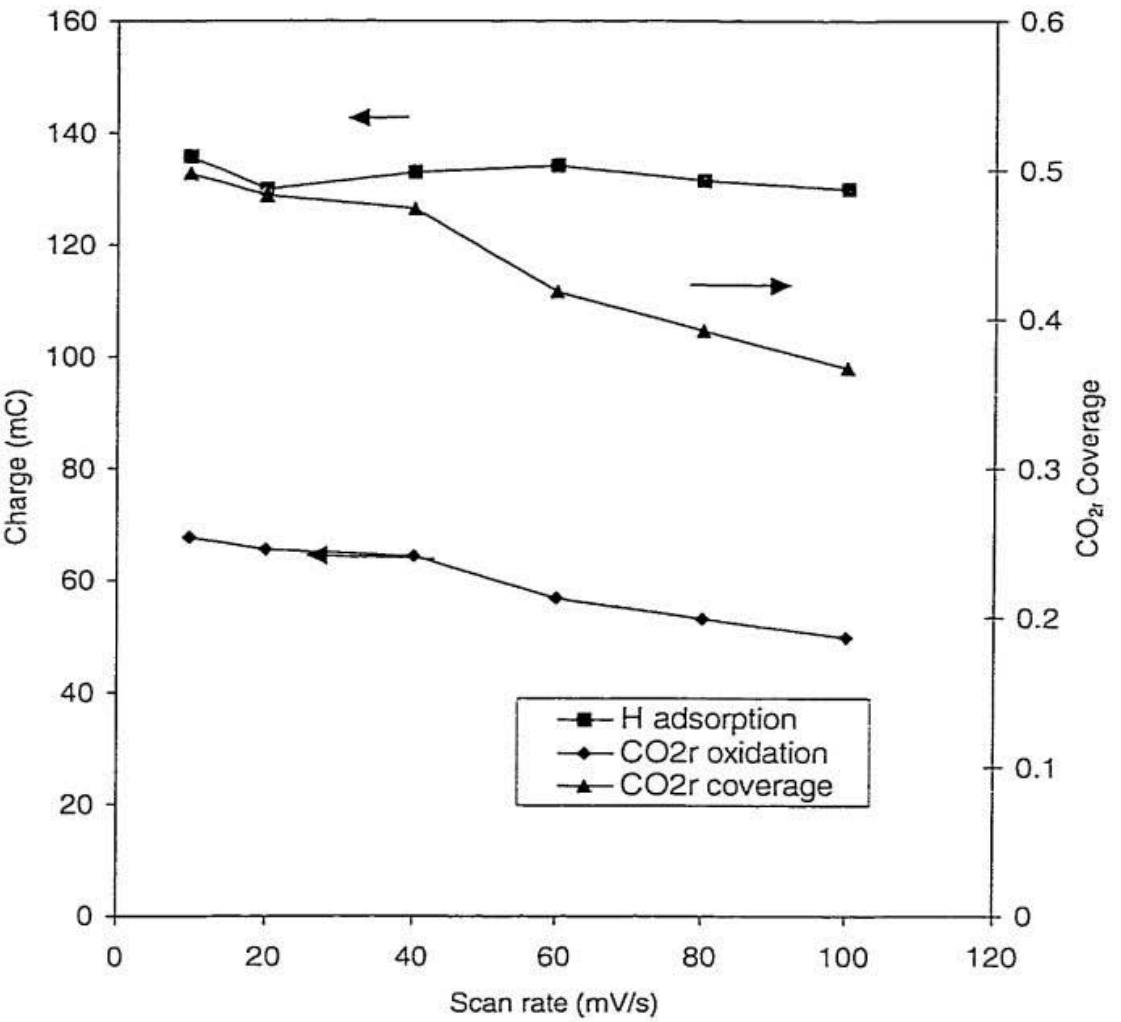

Fig. 3.3 The relationship between CO_{2r} oxidation charge and scan rate for E_{ad} = - 0.2 V (SCE) for 30 min. CO_{2r} means reduced CO_2. CO_{2r} coverage is defined as Q_{CO2}/Q_H.

reduced CO_2 adsorption (**Fig. 3.1**). The larger size of the CO_2 molecules also contributes to the low coverage on the Pt sites.

3.3.1.2 Adsorption time for CO_2 reduction

The adsorption time (t_{ad}) at - 0.2 V (SCE) was changed to obtain different CO_{2r} (reduced CO_2) surface coverages. These are estimated through the area of the positive potential sweeps between 0.25 and 0.75 V (SCE). CVs for different adsorption times are shown in **Fig. 3.4**, which indicates that the coverage by reduced CO_2 increases with increasing adsorption time. In order to obtain saturation coverage, a long adsorption time such as 80 minutes should be used to reduce CO_2 onto the Pt surface as the oxidation charge at 80 minutes approaches a constant value in comparison to that at 120 minute. This phenomenon also illustrates that the adsorption of CO_2 on the Pt surface is a very slow kinetically controlled process. Therefore, if enough adsorption time can be maintained to achieve the saturation coverage by reduced CO_2, the oxidation charge is a valuable representation of the real active surface area.

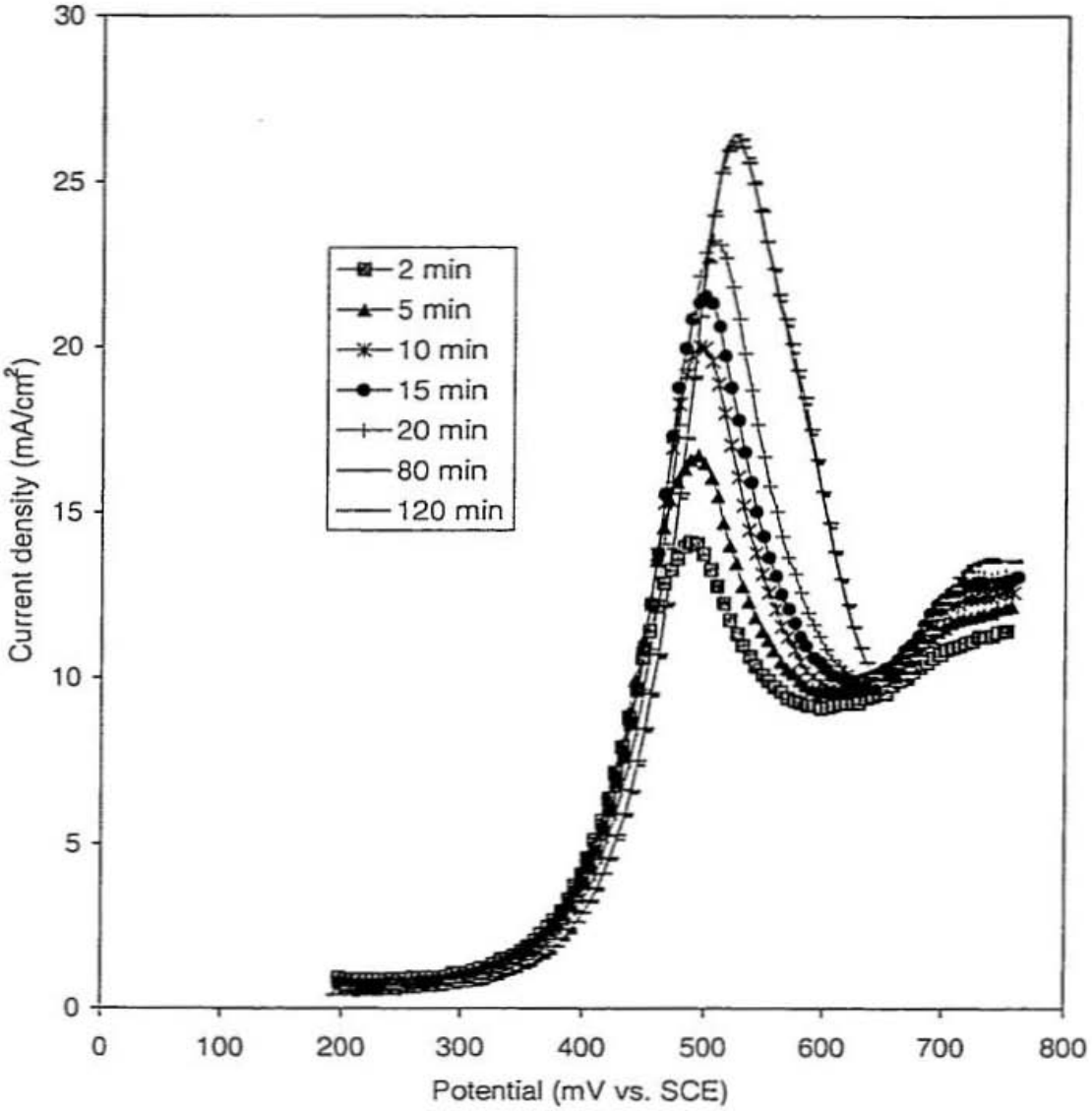

Fig. 3.4 Partial CVs for different adsorption times with 4 mg Pt/cm^2 at E_{ad} = - 0.2 V (SCE) and a scan rate of 40 mV/s.

3.3.1.3 Adsorption potential for CO_2 reduction

Fig. 3.5 shows CVs for a 4 mg Pt/cm^2 (Pt black) electrode following CO_2 reduction at different potentials for 30 minutes. It was found that the peak potentials were approximately constant at 0.5 V (SCE) when E_{ad} was between 0.1 and - 0.1 V vs. SCE although the peak height increased with decreasing adsorption potential. There is much less CO_2 reduction occurring on the Pt surface when at 0.1 V. When the adsorption potential was shifted to more negative potential such as – 0.2 V, the peak area maintained the same value as that at – 0.1 V, but the peak potential shifted negatively to 0.48 V. This can be explained by different bonding states for hydrogen at different E_{ad} values. The hydrogen will be strongly (-s) or weakly (-w) bonded to the Pt surface at potentials from – 0.1 to 0.1 V and from – 0.1 V to - 0.2 V (SCE), respectively (43). Therefore, $\theta_{s\text{-}H}$ and $\theta_{w\text{-}H}$, the degree of surface coverage by either s-H or w-H adatoms, respectively, depends on E_{ad}, the adsorption potential. CO_2 can react with s-H or w-H atoms to form strongly and weakly bound reduced CO_2 adsorbates, respectively. This explains why reduced CO_2 coverages on the Pt surface are related to the adsorption potential. **Fig. 3.6** displays the relationship between the oxidation charge for reduced CO_2 and the adsorption potentials. Saturation adsorption can be achieved at potentials below - 0.1 V (vs. SCE).

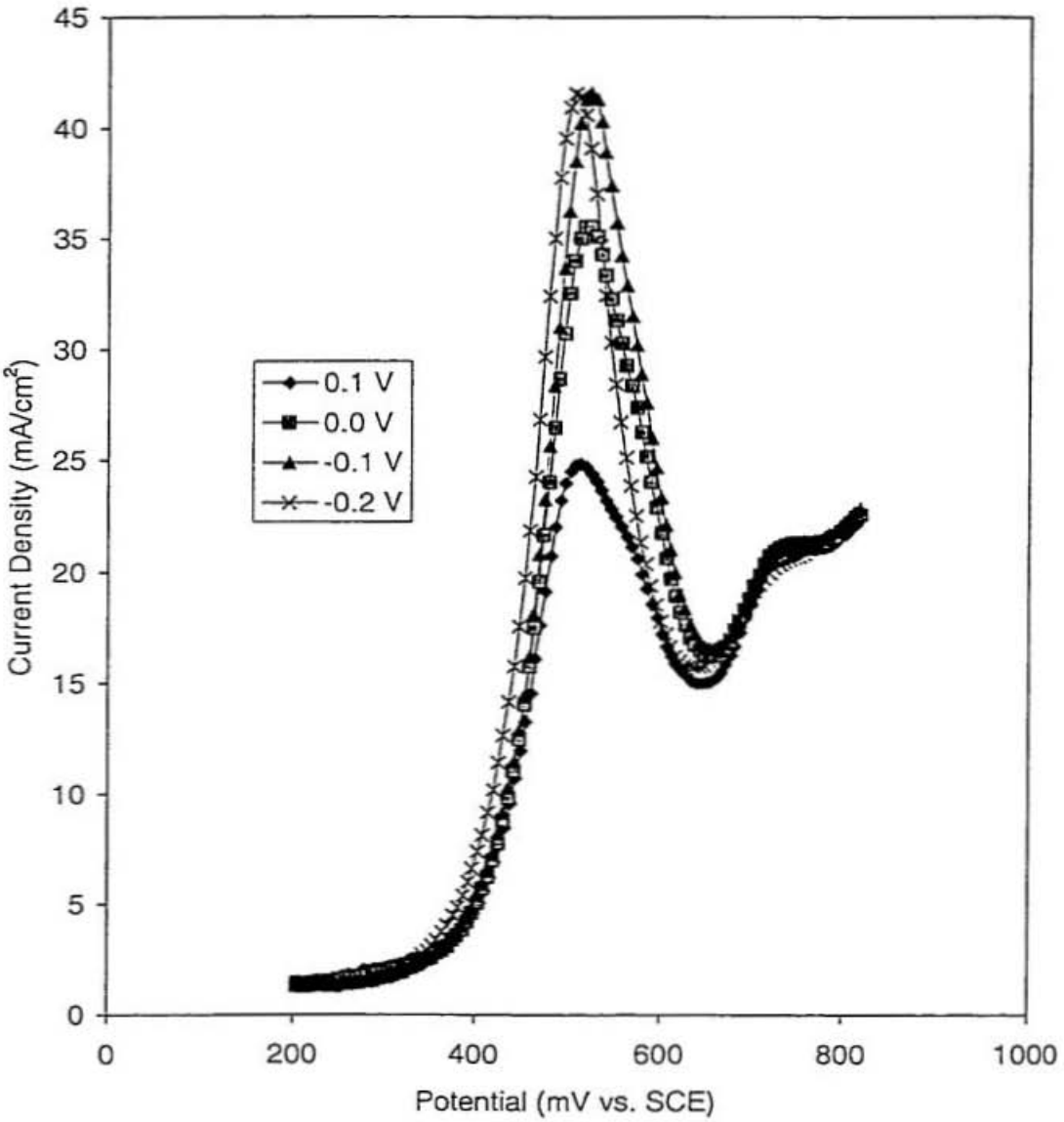

Fig. 3.5 Partial CVs for reduced CO_2 oxidations for different adsorption potentials at 4 mg Pt/cm^2, t_{ad} = 30 min, and a scan rate of 40 mV/s.

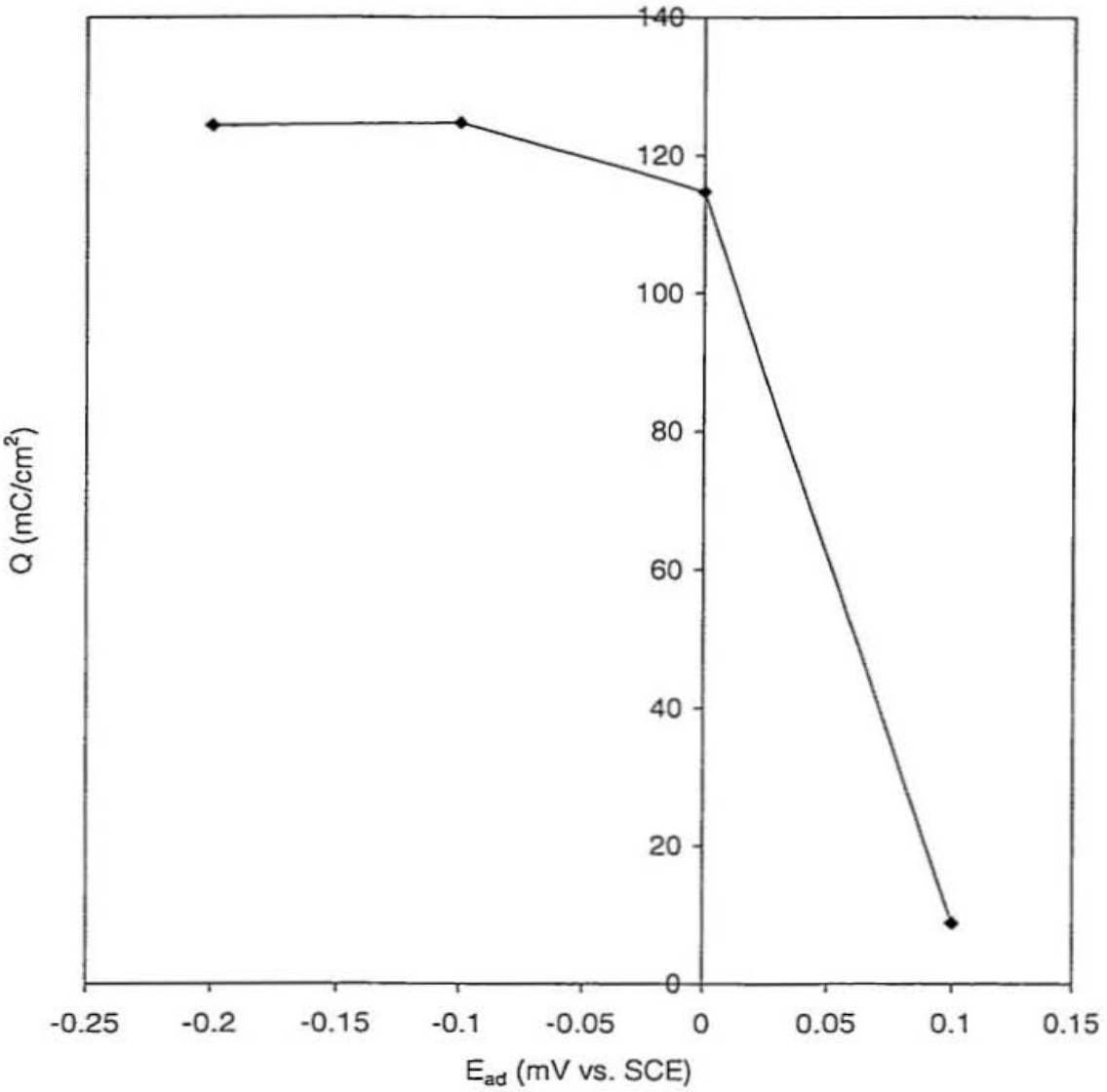

Fig. 3.6 The oxidation charge for reduced CO_{2r} following different adsorption potentials at t_{ad} = 30 min and a scan rate of 40 mV/s.

3.3.2 Carbon-Supported Catalysts

Fig. 3.7 shows partial CVs for reduced CO_2 on 10 % and 20 % Pt on Vulcan XC-72R, both at 0.4 mg Pt/cm^2 loadings. It was found that the reduced CO_2 oxidation peaks were much more well-defined than the H adsorption peaks, as for the Pt black catalyst. The peak area for the 20 % Pt carbon-supported catalyst is much larger than that for the 10 % Pt/C catalyst as expected. Integration of peak areas gave the reduced CO_2 oxidation charges of 39.1 mC and 69.9 mC for the 10 % and 20 % Pt catalysts, respectively. The higher resolution of the peak creates a more accurate determination of oxidation charge relative to the H adsorption charge. Applying this method to determine the active surface area for a 20 % Pt/C catalysts modified by HNO_3 (see section 2.3.3.3) showed that the modified catalyst has a similar behavior to the non-treated catalyst. However, the reduced CO_2 oxidation charges were significantly larger than non-treated catalyst (64.1 mC and 89.3 mC for the modified catalyst at 0.2 and 0.4 mg Pt/cm^2, respectively, in comparison to 50.9 mC and 72.3 mC for the non-treated catalyst). The reduced CO_2 oxidation charge gave the same trend as the measurement by H adsorption. Furthermore, it also supports our conclusion that the performance gain with the modified catalyst is partially due to an increase in the active surface area as described in the chapter 2.

Different catalysts such as 10 % and 20 % Pt on Vulcan XC-72R, 20 % Pt/Ru, Pt black, and a mixture of Pt black and another metal at different loadings were also evaluated. The results are summarized in **Table 3.1**.

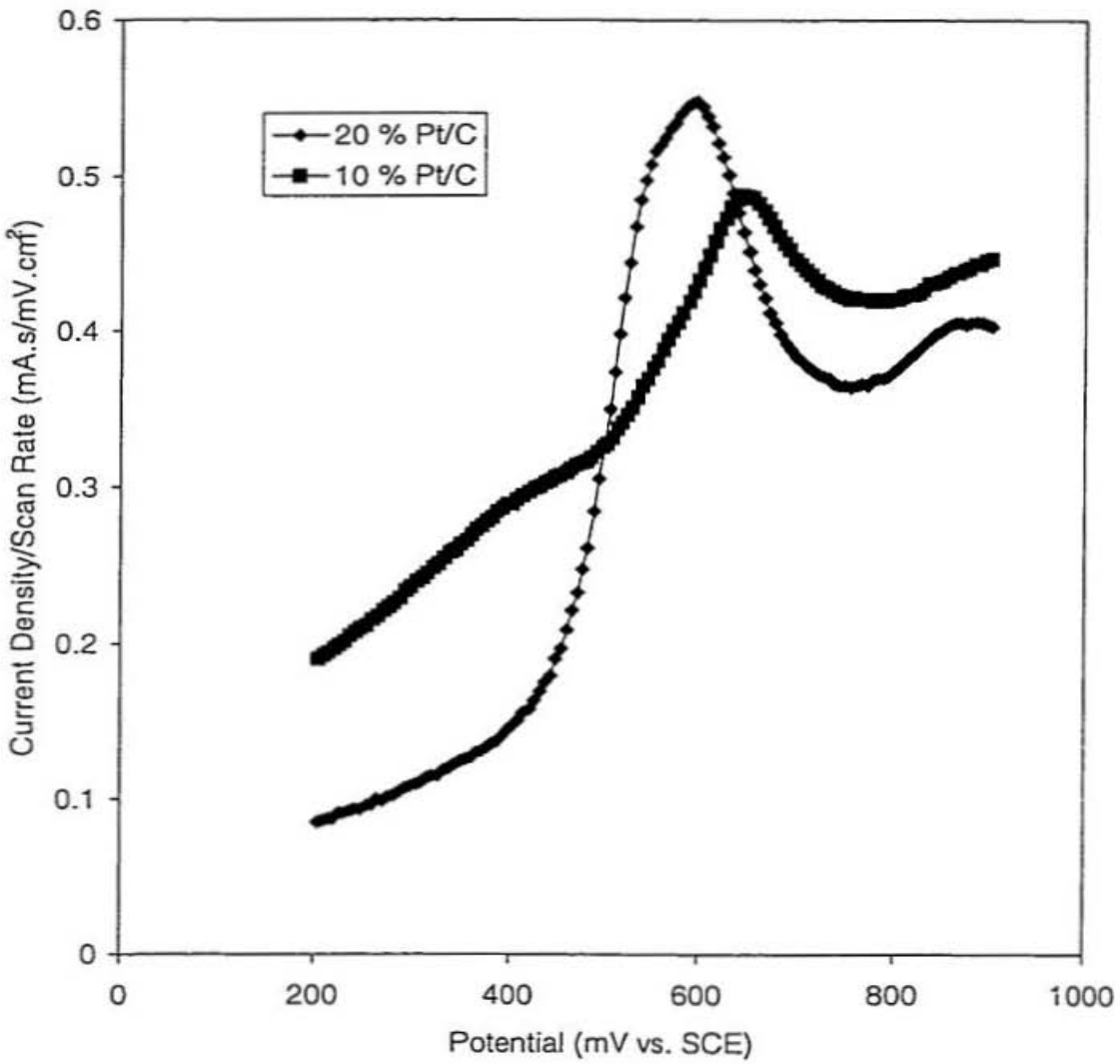

Fig. 3.7 Partial CVs of reduced CO_2 oxidation at 10 % and 20 % Pt/C for 0.40 mg Pt/cm^2 with E_{ad} = - 0.2 V (SCE) and t_{ad} = 80 min. Scan rate: 40 mV/s.

Table 3.1 Oxidation charge for reduced CO_2 for different catalysts at different loadings

Catalyst	Pt	Pt+ X	20 % Pt (1)		20 % Pt (2)		10 % Pt (1)		20% Pt/Ru
Loading (mg/cm^2)	4	4+ 1.33	0.2	0.4	0.2	0.4	0.2	0.4	0.17+ 0.088
Charge (mC)	74.5	196.5	56.2	69.9	63.8	80.1	22.7	39.1	57.3
SP (mV)	320.0	250	422.0	418.0	432.0	412.6	437.1	444.8	346.5
PP (mV)	522.0	552.0	593.0	594.0	599.0	602.0	641.4	649.0	514.7

SP: starting potential for reduced CO_2 oxidation; PP: peak potential for reduced CO_2 oxidation; 1: commercial catalysts; 2: catalyst treated in HNO_3; X: a metal.

It can be seen from **Table 3.1** that, for the same type of catalyst group such as Pt black and a mixture of Pt black and another metal , a higher Pt loading usually leads to a higher oxidation charge. 10 % Pt on Vulcan XC-72 showed lower charge values relative to 20 % at two different Pt loadings. The treated catalyst gave higher oxidation charges in comparison to non-treated catalyst at different Pt loadings. It is a common point that, for all different types of catalysts, the reduced CO_2 oxidation charge increases with increasing Pt loading. 20 % Pt/Ru gives a slightly higher value than 20 % Pt catalyst due to a slightly higher Pt + Ru loading. These observations lead to the conclusion that

reduced CO_2 oxidation is a reliable method for the evaluation of active surface areas for different unsupported and carbon-supported catalysts.

As for peak potentials, it was observed that the catalysts with a higher percentage of Pt showed low peak potentials (20 % Pt at 0.6 V vs. SCE) compared to a higher value for lower Pt percentages of Pt (10 % Pt at 0.650 V vs. SCE). Meanwhile, the starting oxidation potential (defined as the potential that oxidation current begins to rise) for reduced CO_2 showed the same trend as the peak potential. Modification of carbon supported catalyst with HNO_3 did not significantly affect the peak potential and starting oxidation potential positions. The 20 % Pt/Ru catalyst demonstrated significantly lower peak and starting oxidation potentials in comparison to the 20 % Pt catalyst, e.g., 0.515 V and 0.35 V instead of 0.60 V and 0.42 V, respectively for the different loadings. A mixture of Pt black and a second metal also gives a much lower starting oxidation potential of 0.25 V in comparison with 0.32 V for pure Pt black.

Therefore, the starting oxidation potential for reduced CO_2 can be an important parameter to indicate the catalyst's tolerance to MeOH and CO poisoning. It is well-known that catalysts with lower oxidation potentials for MeOH and CO possess higher tolerance to them as MeOH and CO are much more easily oxidized on their surfaces.

3.4 Conclusions

The reduced CO_2 oxidation charge can be used to compare the active surface areas of different catalyst although the relative charge should be used due to the complexity of the products of CO_2 reduction. This method retains the resolution advantage of the CO stripping method, and avoids the overestimation of active surface area. The saturation coverage is close to 0.5 relative to hydrogen adsorption. Furthermore, peak and oxidation starting potentials for reduced CO_2 are two representative parameters to explain catalyst tolerance to MeOH and CO, especially the oxidation starting potentials.

References

(1) M. W. Breiter, Electrochemical processes in fuel cells, Springer-Verlag, New York, 1969.

(2) F. P. Bowden, Proc. Roy. Soc., Ser. A, 125, 446 (1929).

(3) F. G. Will and C. A. Knorr, Z. Electrochem., 64, 258 (1960).

(4) M. Breiter, in Trans. Symp. Electrode Process, edited by E. Yeager, Wiley, New York, 1961, p. 307.

(5) B. E. Conway, J. Electroanal. Chem., 8, 486 (1964).

(6) D. Gilroy and B. E. Conway, Can. J. Chem., 46, 875 (1968).

(7) K. Kinoshita, J. Lundquist, and P. Stonehart, J. Catalysis, 31, 325 (1973).

(8) E. A. Ticianelli, C. R. Derouin and S. Srinivasan, J. Electroanal. Chem., 251, 275 (1988).

(9) S. Mukerjee, S. Srinivasan and A. J. Appleby, Electrochim. Acta, 38, 1661 (1993).

(10) N. Giordano, A. S. Arico, S. Hoxevar, P. Staiti, P. L. Antonucci and V. Antonucci, Electrochim. Acta, 38, 1733 (1993).

(11) N. Giordano, E. Passalacqua, P. L. Antonucci, L. Pino, M. Vivaldi, A. Patti and K. Kinoshita, Electrochim. Acta., 38, 913 (1993).

(12) N. Giordano, E. Passalacqua, L. Pino, A. S. Arico, V. Antonucci, M. Vivaldi and K. Kinoshita, Electrochim. Acta., 36, 1979 (1991).

(13) V. Alderucci, P. L. Antonucci, D. L. Cocke, H. Kim and N. Giordano, J. Appl. Electrochem., 24, 58 (1994).

(14) J. A. Poirier and G. E. Stoner, J. Electrochem. Soc., 141, 425 (1994).

(15) J. Perez, A. A. Tanaka, E. R. Gonzalez ans E. A. Ticianelli, J. Electrochem. Soc., 141, 431 (1994).

(16) D. Desoete, R. Gijbels and J. Hoste, "Neutron Activation Analysis" J. Wiley & Sons, New York (1972), p. 478.

(17) L. Zinkowsky, Nucl. Inst. Meth. Phys. Res. B4, 421 (1994).

(18) A. Essalik, K. Amouzegar and O. Savadogo, J. Applied Electrochem., 25, 404 (1995).

(19) S. Gilman, in Electroanalytical Chemistry, Vol. 2 (A. J. Bard, ed.), Arnold Press, London, 1967, pp. 111 – 192.

(20) R. Woods, in Electroanalytical Chemistry, Vol. 9, edited by A. J. Bard, p.1-162, 1975.

(21) J. Bett, K. Kinoshita, K. Routsis, and P. Stonehart, J. Catal., 29, 163 (1973).

(22) J. F. Connolly, R. J. Flannery, and G. Aronowitz, J. Electrochem. Soc. 113, 577 (1966).

(23) N. A. Urisson, L. N. Mokrousov, G. V. Shteinberg, Z. I. Kudryavtseva, I. I. Askakhov, and V. S. Bagotskii, Kinet. Katal., 15, 1000 (1974).

(24) K. F. Blurton, P. Greenberg, H. G. Oswin, and D. R. Rutt, J. Electrochem. Soc., 119, 559 (1972).

(25) T. R. Ralph, G. A. Hards, J. E. Keating, S. A. Campbell, D. P. Wilkinson, M. Davis, J. St-Pierre, and M. C. Johnson, J. Electrochem. Soc., 144, 3845 (1997).

(26) K. F. Blurton, P. Greenberg, H. G. Oswin, and D. R. Rutt, J. Electrochem. Soc., 119,

59 (1972).

(27) K. Kunimatsu, K. Shimazu and H. Kita, J. Electroanal. Chem., 256, 371 (1988).

(28) T. Iwasita-Vielstich, in C. Tobias and H. Gerischer (eds.): Advance in Electrochemical Science and Engineering, Vol. 1, VCH Weihnleim, p. 127 (1990).

(29) Y. Ikezawa, H. Saito, H. Fujisawa, S. Tsuji and G. Toda, J. Electroanal. Chem., 240, 281 (1988).

(30) R. J. Bellows, E. P. Marucchi-Soos, and D. T. Buckley, Ind. Eng. Chem. Res., 35, 1235 (1996).

(31) J. Giner, Electrochim. Acta, 8, 857 (1963).

(32) J. Giner, Electrochim. Acta, 9, 63 (1964).

(33) M. W. Breiter, Electrochim. Acta, 12, 1213 (1967).

(34) Yu. B. Vassiliev, V. S. Bagotzky, N. V. Osetrova, O. A. Khazova and N. A. Mayorova, J. Electroanal. Chem., 189, 271 (1985).

(35) Yu. B. Vassiliev, V. S. Bagotzky, O. A. Khazova and N. A. Mayorova, J. Electroanal. Chem., 189, 295 (1985).

(36) J. Sobkowski and A. Czerwinski, J. Electroanal. Chem., 65, 327 (1975).

(37) A. M. Baruzzi, E. P. M. Leiva and M. C. Giordano, J. Electroanal. Chem., 158, 103 (1983).

(38) A. M. Baruzzi, E. P. M. Leiva and M. C. Giordano, J. Electroanal. Chem., 189, 257 (1985).

(39) J. Giner, Electrochim. Acta, 9, 63 (1994).

(40) M. L. Marco, J. Gonzalez-Velasco, J. M. Vara, M. C. Giordano and A. J. Arvia, J.

Electroanal. Chem., 270, 205 (1989).

(41) M. L. Marco, J. Gonzalez-Velasco, J. M. Vara, M. C. Giordano and A. J. Arvia, J. Electroanal. Chem., 287, 99 (1990).

(42) Z. Nikolic, H. Huang, D. Gervasio, A. Lin, C. Fierro, R. R. Adzic, and E. B. Yeager, J. Electroanal. Chem., 295, 415 (1990).

(43) M. L. Marco, J. Gonzalez-Velasco, J. M. Vara, M. C. Giordano and A. J. Arvia, J. Electroanal. Chem., 281, 257 (1990).

(44) V. N. Kamath and H. Lal, J. Electroanal. Chem., 19, 147 (1968).

(45) S. B. Brummer and K. Cahill, J. Electroanal. Chem., 21, 463 (1969).

(46) P. Stonehart, Electrochim. Acta, 18, 125 (1973).

Chapter 4

Methanol Crossover Inhibition in Liquid-Feed Direct Methanol PEM Fuel Cells (DMFCs)

4.1 Introduction

4.1.1 Current DMFC Status

PEMFC technology has advanced in the last few years to the point of being considered a viable option for primary power sources in electric vehicles. Current systems are based on either hydrogen carried on board the vehicle, or the steam reforming of methanol to generate hydrogen (and CO_2) as the fuel. However, the complexity and additional weight and volume associated with the reformer on board the vehicle to make hydrogen-rich fuel presents significant challenges in the implementation of this option. The DMFC can be fed directly from a fuel tank that is filled from a service station pump. The operation of this design involves mixing the methanol with water and circulating it directly through the anode chamber of the fuel cell. This advantage has attracted many automobile makers to take efforts to develop the DMFC.

Currently, there are two obstacles inhibiting the application of PEM DMFCs, namely, the low activity of methanol electro-oxidation catalysts and the phenomenon of methanol

crossover through the polymer electrolyte membrane from the anode to the cathode side. Both the diffusion (1) and the electro-osmotic drag (2) of the methanol contribute to the latter.

Efforts have been expended in developing new anode catalysts and, to some extent, methanol impermeable membranes for DMFCs. In order to reduce and even to prevent the detrimental effect of methanol crossover, four possibilities can be considered: the use of anode catalysts insensitive to methanol, the development of membranes not permeable to methanol, the modification of current membranes, and optimization of operating conditions.

4.1.2 Inhibition Strategies for Methanol Crossover

Among the above four possibilities, the approach for solving methanol crossover mainly relies on the electrolyte membrane properties. The electrolyte currently being used in DMFCs is a Nafion based membrane with void cages of ~40 Å (3,4) and channels of 10 Å (5) between the cages. In a mixture of water and alcohol, swelling of the membrane with solvent increases the size of the void cages. Therefore, the reason for methanol crossover through the membrane is due to the hydrophilic channels caused by ionic aggregates (5). Accordingly, it should be possible to reduce the pore/channel size within the membrane without significantly compromising its proton conductivity.

In an attempt to inhibit methanol crossover, it was reported that the thicker Nafion with a high equivalent weight, e.g., 1500 EW exhibits lower methanol crossover due to

its lower porosity (6). Moreover, new types of membrane have been synthesized to minimize methanol crossover. A polybenzimidazole (PBI) membrane doped with phosphoric acid has been used for the development of a polymer electrolyte DMFC operating at temperatures close to 200 ^{0}C (7-9). Methanol crossover is minimized by the low mobility of methanol in the nonswollen PBI membrane, and a negligible electro-osmotic drag number (10). Perfluorinated sulfonamides polymer electrolyte membranes were reported (11,12) as a means of reducing the impact of methanol crossover. Buchi et al (13) considered a cross-linked poly (tetrafluoroethylene-hexafluoro-propylene) copolymer (FEP). The membranes were tested for their ability to decrease methanol crossover. Cross-linked membranes with a strong resistance to swelling are potentially useful (14).

New membrane concepts and the modification of existing membranes often cause the protonic resistance to increase as methanol crossover is reduced. In the case of the DMFC, since the typical current density is significantly lower than in the H_2/air PEMFC, the focus of transport studies is on methanol crossover and developing strategies to minimize its effects. Strategically, one might be willing to accept some loss in cell performance because of a higher membrane resistance to lower the penalties associated with methanol crossover.

4.1.3 Conducting Polymer Doped Ion Exchange Membranes

In order to reduce methanol crossover, the size of the channels in the Nafion membrane needs to be decreased, while maintaining similar ionic conductivity to that of the original membrane. Conducting polymers such as polypyrrole (PPy) and polymethylpyrrole (PMPy) could play this kind of role since they can be easily doped into the Nafion membrane (15,16). They are also mechanically and chemically stable and can stand up to 350 ^{0}C (17). Their best electronic conductivities are in the range of 10^2 – 10^3 S/cm although the different oxidant agents that can be used for their synthesis, e.g., Fe^{3+}, Fe^{2+}, $(NH_4)_2S_2O_8$, $K_2S_2O_8$, Cu^{2+} (18-20) can have a substantial influence on their electronic conductivity. Additionally, conducting polymer doped Nafion has another potential advantage in that it can enhance the anodic performance of Pt/Ru particles inserted into the modified membrane by hot bonding. According to reported results (21-28), conducting polymers containing nanodispersed Pt particles can catalyze the hydrogen evolution reaction (HER) and methanol oxidation reaction. This fact indicates the conducting polymers on the surface of the Nafion membrane can extend the electrochemical reaction zone.

4.1.4 Scope of This Work

Based on the advantages of conducting polymers, Nafion membranes modified by PPy and PMPy with different polymerization methods were tested for the optimization of

polymerization conditions in the terms of the proton conductivity of the modified membrane. As well, methanol crossover and oxygen reduction performance were also tested in the half-cell. Preliminary results are reported in this chapter.

4. 2. Experimental

4.2.1 Electrochemical Measurements of Methanol Permeability Through DMFC-like Cells

In this test, the cell shown in **Fig. 2.3(b)** of Chapter 2 was used to evaluate methanol permeation through the membrane. Electrochemical experiments were performed by using a Hokuto Denko HA-301 potentiostat and HB-104 function generator with a BBC MDL 780 X-Y recorder. Chronoamperometric data were collected and analyzed by using a Tron microcomputer with a Data Translation DT2801 ADC/DAC card. Electrodes from Ballard Power Systems (high loading advanced anode) consisted of two distinct layers, a (gas diffusion) backing layer and a thin film composite layer of interspersed catalyst and PTFE.

The cell conditions used for methanol permeation experiments were the same as those used for a liquid-feed DMFC, other than the replacement of oxygen by nitrogen. The nitrogen was not humidified as the membrane was contacted by an aqueous sulfuric acid electrolyte containing 1 M methanol. The permeation of methanol was measured

electrochemically by monitoring methanol electrooxidation at the "nitrogen electrode." The methanol flux through the membrane is determined from the measured mass transport limited current, i.e., the plateau of a steady-state voltammogram. Assuming that the Nafion membrane is pinhole free, the observed i_{lim} from methanol permeation through the membrane can be expressed, in general, as follows (29)

$$1/i_{lim} = d/nFAD_mC_m \qquad (4.1)$$

Where, D_m is the diffusion coefficient of methanol in the membrane; C_m is the methanol concentration in the membrane; d is the thickness of the membrane. $1/i_{lim}$ denotes as the resistance of methanol transport through the membrane.

The methanol flux obtained from the above permeation experiments can be further dissected into corresponding partition and diffusion coefficients, based on values of $C_mD_m^{1/2}$ obtained, according to the Cottrell relationship, from potential step experiments:

$$i = nFAC_m (D_m)^{1/2}/(\pi t)^{1/2} \qquad (4.2)$$

We solve for D_m and C_m using D_mC_m values obtained from the limiting currents and $C_mD_m^{1/2}$ values obtained from the Cottrell analysis.

4.2.2 Modification of Nafion Membrane by Conducting Polymers

Commercial Nafion®117 membranes were loaded with the conducting polymer in the following ways. The membranes were soaked in different oxidant solutions including 0.173 N ferric chloride (J. T. Baker, ACS) or 0.2 M ammonium persulfate ($(NH_4)_2S_2O_8$, Fisher, ACS) for a given time. Then, those membranes were exposed to 0.745 M aqueous pyrrole solution (Aldrich, 99%, CAS) or 0.745 M N-methylpyrrole (dissolved in ethanol first, then diluted to 0.745 M by distilled water) for a certain time to allow their polymerization. For use of H_2O_2 as the oxidant, the membrane was first soaked in the monomer solution, and then transferred to H_2O_2 (aq). The doped Nafion membranes were washed several times with deionized water after polymerization to remove the unreacted monomers and oxidants. Pyrrole and N-methylpyrrole were also polymerized by UV irradiation for 24 hours by Dr. Qi.

4.2.3 Ionic Conductivity Measurement on Modified Nafion Membrane

An experimental apparatus for determining the resistivity for proton transport through the membrane is shown in **Fig. 4.1** (30-31). Two PTFE blocks with cavities are bolted together around two glass slides with holes, which sandwich the membrane. SCE reference electrodes are positioned either side of the membrane, and the steady-state potential difference between them, induced by a constant current (10 mA) between the Pt electrodes, is measured by using an Orion Research 601 Digital Ion Analyzer. Ohm's law

is applied to compute the resistance of the membranes. The electrolyte was a 1 M H_2SO_4 solution. The exposed area of membrane was 0.145 cm^2.

Ionic resistance of membrane = $\Delta E/I$ (constant) (4.3)

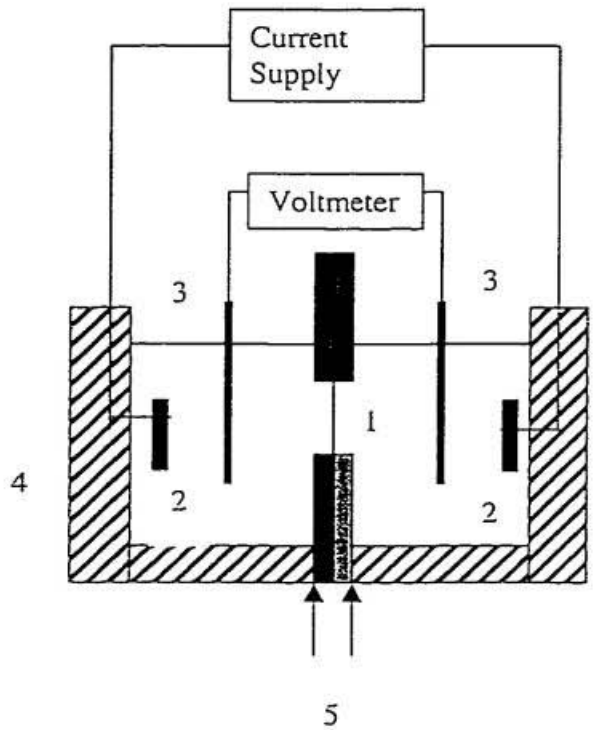

Fig. 4.1 Experimental apparatus for determination of membrane ionic resistance. 1. polymer membrane; 2. platinized Pt disc electrodes; 3. SCE electrodes; 4. PTFE block; 5. Glass slides.

4.3 Results and Discussion

4.3.1 Polymerization of Pyrrole and Methylpyrrole on/within Nafion Membrane

4.3.1.1 Pyrrole polymerization using Fe^{3+} as an oxidizing agent

Several pieces of Nafion 117 were equilibrated with 0.174 N Fe^{3+} solution for 12 hours. Then, they were immersed into 0.754 M pyrrole solution. The ionic resistance was measured by using the experimental setup in **Fig. 4.1**. The results are presented in **Table 4.1**.

Table 4.1 Membrane ionic resistance at different contact times with pyrrole

Contact time (hrs)	0	4	24
Ionic resistance (Ω)	1.7	1263	2030

It was found from **Table 4.1** that the PPy deposited on the membrane surface resulted in a large increase of ionic resistance. This is due to a prolonged immersion time of the Nafion membrane into the Fe^{3+} solution leading to a high concentration of Fe^{3+} in the membrane. A long contact time with the pyrrole solution also caused too much PPy formation on the Nafion surface. When a Nafion membrane containing ferric ions

contacted an aqueous pyrrole solution, pyrrole polymerized easily and quickly and formed a PPy layer in the membrane matrix beginning from the membrane surface following **Scheme 1** (16, 32)

Scheme 1

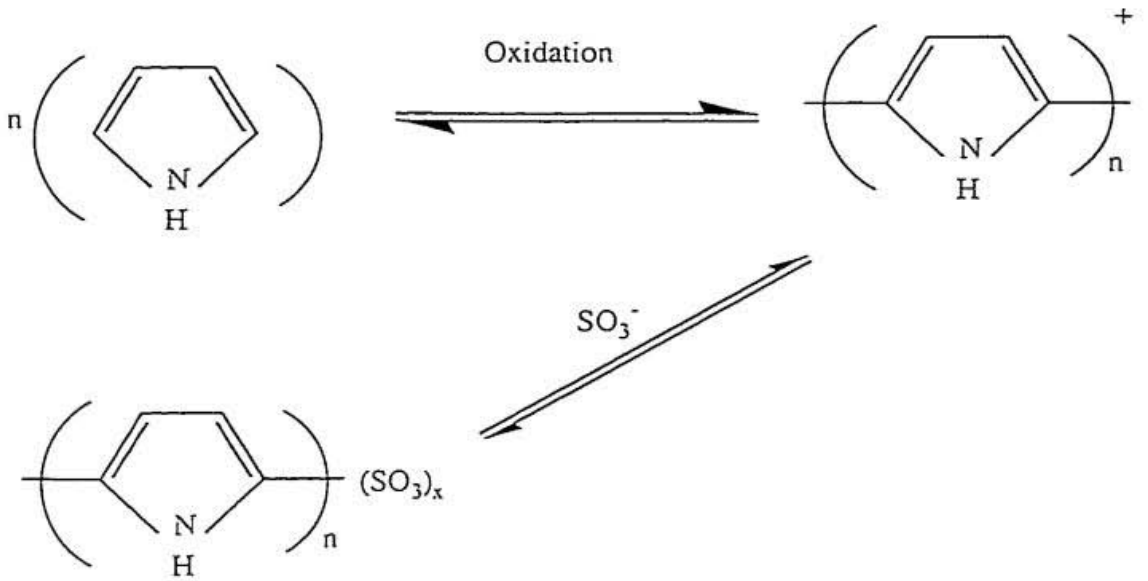

Doped

The doping of the partially oxidized PPy is maintained by the deprotonated sulfonic acid groups of the polymeric backbone of Nafion (33). Therefore, it is expected that both the proton conductivity and the permeability of the Nafion will decrease with increasing PPy contents. Black coloration and stiffness of the resulting membranes indicate heavy PPy deposition on/within the membrane. This layer of PPy blocks the channels for proton

conduction leading to a higher ionic resistance. Therefore, we needed to find the optimum conditions for pyrrole polymerization without significantly increasing the ionic resistance. In order to realize this, short immersion times in the oxidizing agent solution and contact times with the pyrrole should be applied.

Table 4.2 shows the ionic resistance of Nafion membranes for different immersion times in ferric ion solution following a 30 s contact time with a pyrrole solution.

Table 4. 2 Ionic resistances for different immersion times in Fe^{3+} solution

T (min)	0	5	10	30	120	240	720	1440
$R_{ionic,\ Fe}$ (Ω)	1.6	2.3	2.7	2.7	2.5	2.3	2.4	2.5
$R_{ionic,\ Pol}$ (Ω)	1.6	3.1	2.5	2.9	2.4	2.1	2.4	2.9

Note: T- Immersion time in Fe^{3+} (min); $R_{ionic,\ Fe}$ - Ionic resistance after Nafion membrane was immersed in Fe^{3+} solution; $R_{ionic,\ Pol}$ – Ionic resistance after polymerization for 30 s.

It is seen from **Table 4.2** that the ionic resistance of Nafion membranes increased slightly due to the absorption of Fe^{3+}, but it hardly changed with immersion time. When the Nafion membranes containing Fe^{3+} were contacted with the pyrrole solution, their color changed from light yellow to green indicating some PPy formation. The PPy modified Nafion membranes possessed almost the same resistance as the Fe^{3+} loaded ones due to the very short polymerization time (30 s). This fact indicates that a thin layer

of PPy formed on/within the Nafion membrane does not affect its proton conductivity drastically, but a large amount of PPy results in low proton conductivity. It can be speculated that a high percentage of the sulfonic acid groups serve as dopants for the oxidized PPy in the latter case and that a lower water content of the Nafion membrane decreases its proton conductivity (34). The modified membranes with light conducting polymers were used to test methanol crossover (section 4.3.3).

According to reported data (33), metal cations will be trapped in the Nafion membrane resulting in a resistance increase. Although Fe^{3+} inclusion into the membrane does not increase its resistance greatly under non-operating conditions, it will significantly increase the membrane resistance and decrease cell performance as metal ions, especially high valent cations, are electro-osmotically dragged into the inside membrane leading to the loss of membrane conductivity and poisoning of the catalysts. Fe^{3+} could be extracted from the membrane afterwards. Therefore, it is best to use low valent metal ions or non-metal ion oxidants to polymerize the pyrrole.

4.3.1.2 Pyrrole polymerization using $(NH_4)_2S_2O_8$ as an oxidizing agent

$(NH_4)_2S_2O_8$ was used to polymerize pyrrole onto/within the Nafion. **Table 4.3** lists the relationships between the membrane resistance and the immersion time in $(NH_4)_2S_2O_8$ solution, and also following 30 s contact with the pyrrole solution.

Table 4. 3 Ionic resistance at different immersion times in $(NH_4)_2S_2O_8$ solution

T (min)	0	5	15	30	60	120	300	420	1440
I_{Ionic} (Ω)	1.6	1.9	2.4	2.6	2.0	2.2	2.6	2.1	2.1
$I_{ionic,\ Pol}$ (Ω)	1.6	2.0	2.4	2.7	2.8	2.8	2.9	2.7	2.7

It is seen from **Table 4.3** that the membrane contacted with $(NH_4)_2S_2O_8$ showed the same behavior as with Fe^{3+}, in which the resistance only increased slightly after it was soaked in $(NH_4)_2S_2O_8$ solution. It also showed that PPy on/within membrane increased the ionic resistance slightly. There appears to be little difference between the effects of two oxidants. Although the PPy modified membranes have higher ionic resistance, it will still be beneficial for the DMFC if this kind of membrane can significantly reduce methanol crossover. Reduction of methanol crossover will greatly improve the DMFC performance resulting in the offset of the IR loss due to the resistance increase. This results from the low current density operation in DMFCs.

However, it was still highly desirable to obtain a method to deposit a layer of polymer onto/within the Nafion surface without compromising ionic conductivity. On the other hand, it is very difficult to control the polymerization of pyrrole in air as pyrrole is quite easily polymerized by oxygen. Therefore, considering this, N-methylpyrrole was used to replace pyrrole due to its stability in air. In order to polymerize N-methylpyrrole, H_2O_2 can be used as the oxidant without introducing metal cations into the Nafion membrane.

4.3.1.3 Methylpyrrole polymerization using H_2O_2 as an oxidizing agent

When H_2O_2 was used to oxidize N-methylpyrrole, the membranes were firstly soaked into methylpyrrole solution. Then were contacted with H_2O_2 solution for a 30 s period. Resistances for different immersion times in N-methylpyrrole and polymerization times with H_2O_2 are presented in **Table 4.4.**

Table 4.4 Resistance for different immersion in N-methypyrrole and polymerization times with H_2O_2

T (min)	0	5	30	120	270
I_{ionic} (Ω)	1.6	1.8	1.6	1.7	1.6
$I_{ionic,\ Pol}$ (Ω)	1.6	1.8	1.6	1.7	1.6

The results showed that the ionic conductivity of the Nafion did not change with the polymerization of N-methylpyrrole. However, PMPy did form on the Nafion as the color of the membrane changed from light yellow to brown. The resistances of the PMPy doped Nafion membrane are the same as for the original membrane. The data also showed that immersion time did not affect the conductivity. Therefore, H_2O_2 is a good candidate for the polymerization of N-methylpyrrole.

4.3.1.4 Pyrrole and methylpyrrole polymerization by UV irradiation

In order to avoid the detrimental effect of metal ions on the conductivity of the resulting membrane, oxygen in the air can be a possible choice to polymerize pyrrole and methylpyrrole onto the Nafion surface with the help of UV irradiation. Nafion membranes were soaked in pyrrole or N-methylpyrrole solutions for 30 min, then irradiated under UV light for 24 hours. The resistances of the modified membranes are presented in **Table 4.5**.

Table 4.5 Resistance of membranes modified by PPy and PMPy formed by UV irradiation

Membranes	Nafion	Pyrrole	Methylpyrrole
I_{ionic} (Ω)	1.6	1.6	1.6
$I_{ionic,\ Pol}$ (Ω)	1.6	1.7	1.6

The membranes with deposited PPy and PMPy retain the same resistance as the original Nafion membrane. Since these membranes can reduce the methanol crossover significantly (section 4.3.3), the UV irradiation method will be an attractive manufacturing process.

4.3.2 Methanol Crossover Measurement for Nafion Membrane

To obtain the steady state current, a potential step method with a long polarization time (e.g., typically 30 min) was applied. **Fig. 4.2** demonstrates the relationship between methanol crossover and temperature.

It was found that the methanol started to oxidize at ca. 0.2 V, and approached a constant limiting current dependent on operating temperature. The limiting current for methanol oxidation was reached when the potential was over 0.4 V (SCE), with values of 47 mA/cm^2 and 68 mA/cm^2 being obtained at 50 ^0C and 70 ^0C, respectively. The results indicate that a higher operating temperature leads to a larger methanol crossover in DMFC operation. However, it is desirable to use a high temperature in the DMFC to increase the kinetics of methanol oxidation. This is supported by the fact that the half-wave potential shifts from 0.35 V (SCE) at 50 ^0C to 0.30 V (SCE) at 70 ^0C, which shows that a higher operating temperature enhances the kinetics of methanol oxidation. Therefore, for a high temperature operation, the membrane should be modified to reduce methanol permeation across the membrane.

4.3.3 Methanol Crossover Inhibition by Modified Membranes

Results of methanol crossover experiments on PPy and PMPy modified membranes at 50 ^0C and 70 ^0C are shown in **Fig. 4.3** and **Fig. 4.4**, respectively. It is seen that the conducting polymer-doped Nafion membranes significantly reduced methanol

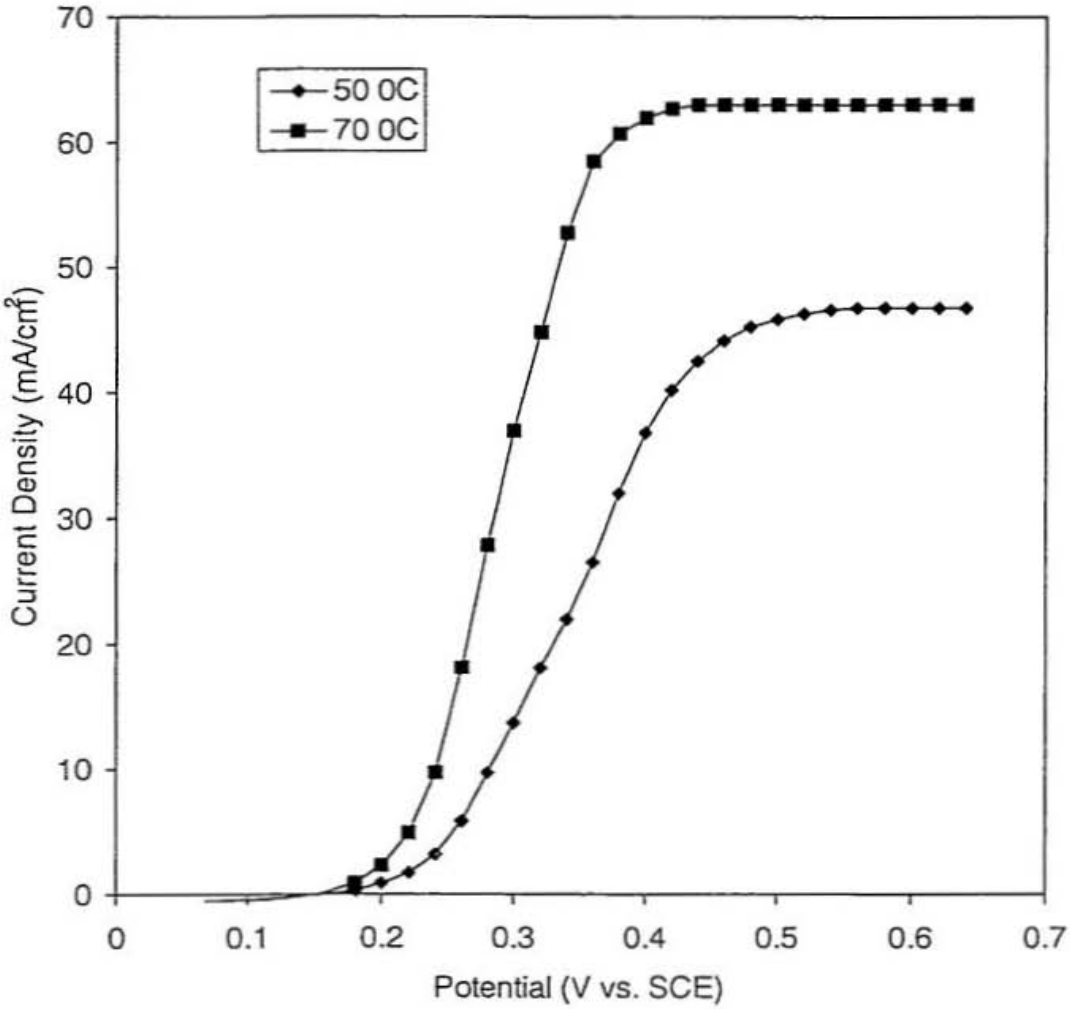

Fig. 4.2 Current-potential relationship for MeOH oxidation at different temperatures. Ballard anode. N117 membrane. 1 M MeOH in 1 M H_2SO_4.

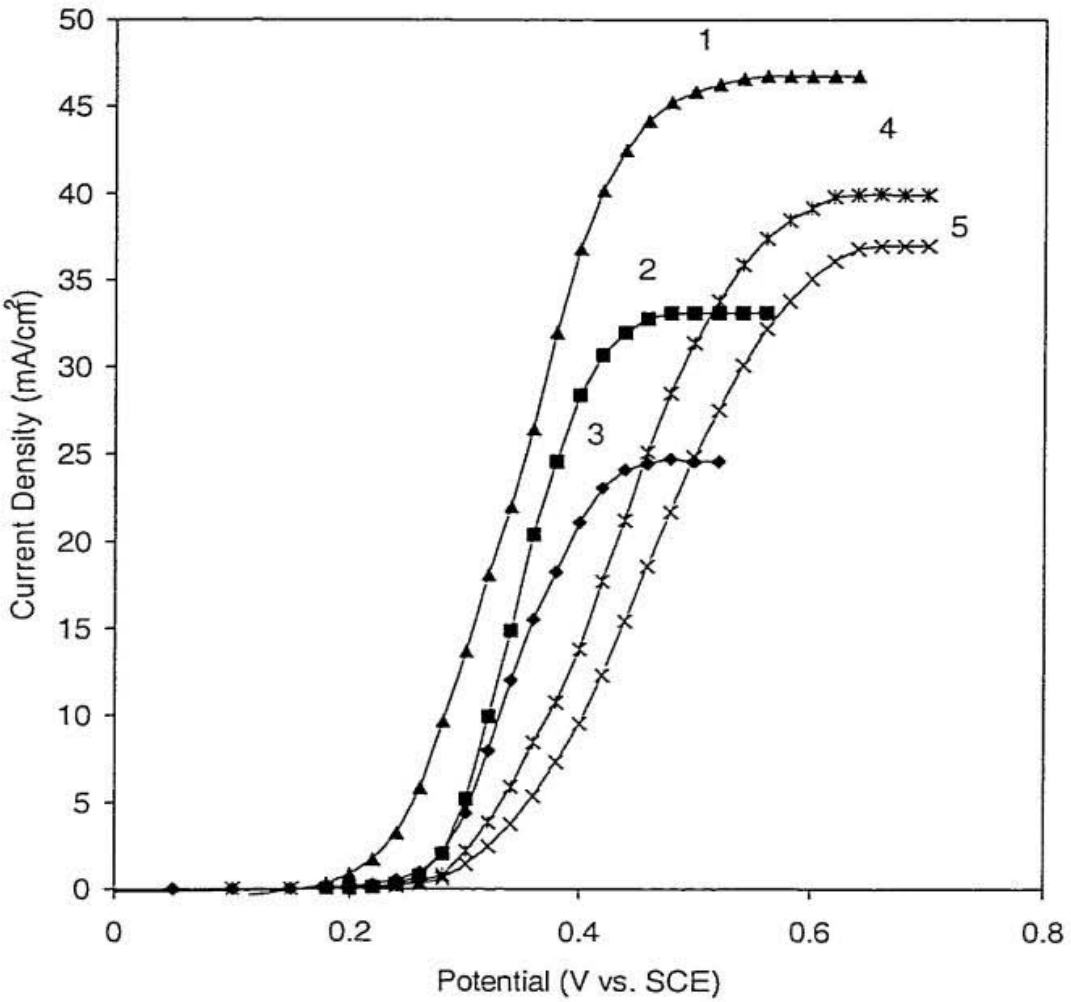

Fig. 4.3 MeOH crossover for different membranes at 50 ^{0}C in 1 M MeOH. Ballard anode. N117 membrane. 1. Nafion membrane. 2. PPy polymerized by Fe^{3+}, then immersed in water. 3. PPy polymerized by Fe^{3+}, then immersed in HCl. 4. PPy polymerized by UV. 5. PMPy polymerized by UV.

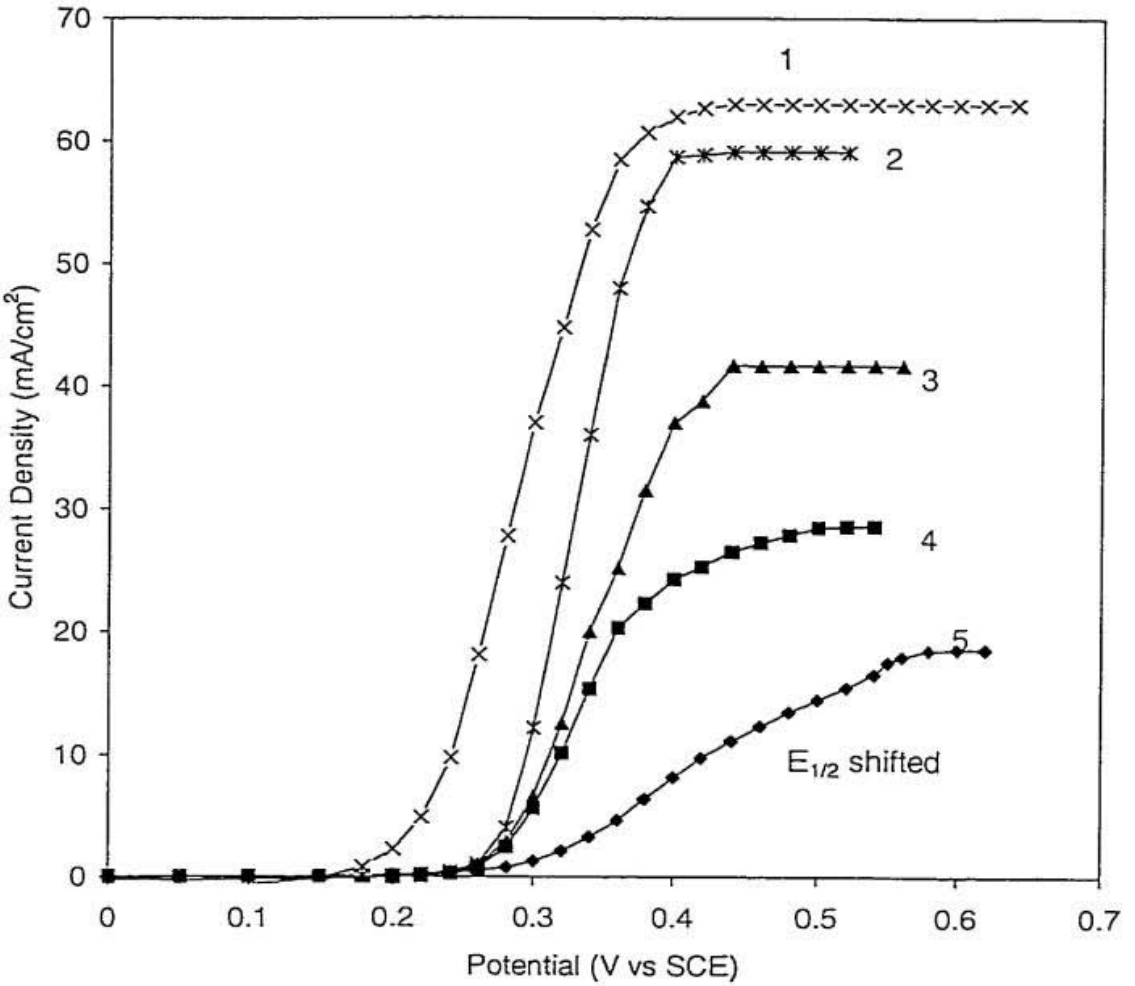

Fig. 4.4 MeOH crossover for different membranes at 70 ^{0}C in 1 M MeOH. Ballard anode. 1. Nafion membrane. 2. PPy polymerized by H_2O_2. 3. Ppy polymerized by Fe^{3+}, then immersed in water. 4. PPy polymerized Fe^{3+}, then immersed in HCl. 5. PMPy polymerized by H_2O_2

crossover. A 60 % reduction of methanol crossover was achieved by using PPy deposited with Fe^{3+} following immersion in HCl solution. It appears that treating the membranes with acid can help to form a more uniform conducting polymer on/within the membrane. Deposition of a layer of PPy or PMPy on/within the Nafion membrane by chemical oxidation did not change the catalytic activity of the catalyst since all half-wave potentials remained quite close to that for the original Nafion. However, the membranes modified by the UV irradiation method behave differently, which may be related to different polymer structures and surface properties such as hydrophobicity. Complete explanation still requires further investigations. Based the above discussions, therefore, PPy and PMPy membranes modified by UV seem not suitable for application in DMFCs.

It is seen from **Fig. 4.4** that a PMPy modified membrane from H_2O_2 oxidation showed the largest inhibition of methanol crossover (ca. 70 %). However, it should be emphasized here that there were a lot of gas bubbles adsorbed on this membrane surface. Therefore, the electrode area reduction caused by bubble adsorption may contribute to the lower methanol crossover to some extent. As for different oxidants, the membrane modified by Fe^{3+} also showed better methanol inhibition than H_2O_2 for PPy. This is probably related to the formation of different PPy microstructures on the Nafion surface with different oxidants.

4.3.4. Methanol Diffusion Coefficient in Nafion and Modified Membranes

A set of typical Cottrell plots, obtained in response to a potential step from 0 to 0.70 V (SCE) with Nafion 117, and PPy, and PMPy modified membranes operating at 70 ^{0}C, is shown in **Fig. 4.5**. If it is assumed that the rate of methanol transport through the cell is practically controlled by the membrane only (**Eqn (4.1)**) (29), D_m values can be obtained by combining the limiting current and the slope of Cottrell plot for each membrane. The results are summarized in **Table 4.6**.

Table 4.6 Methanol diffusion coefficients from electrochemical measurements at various temperatures

Temperature (^{0}C)	Membrane	Diffusion Coefficient (10^5, cm^2/sec)
50	Nafion	0.89
	Ppy/Nafion	0.39
	PMPy/Nafion	0.38
70	Nafion	2.48
	Ppy/Nafion	0.79
	PMPy/Nafion	1.32

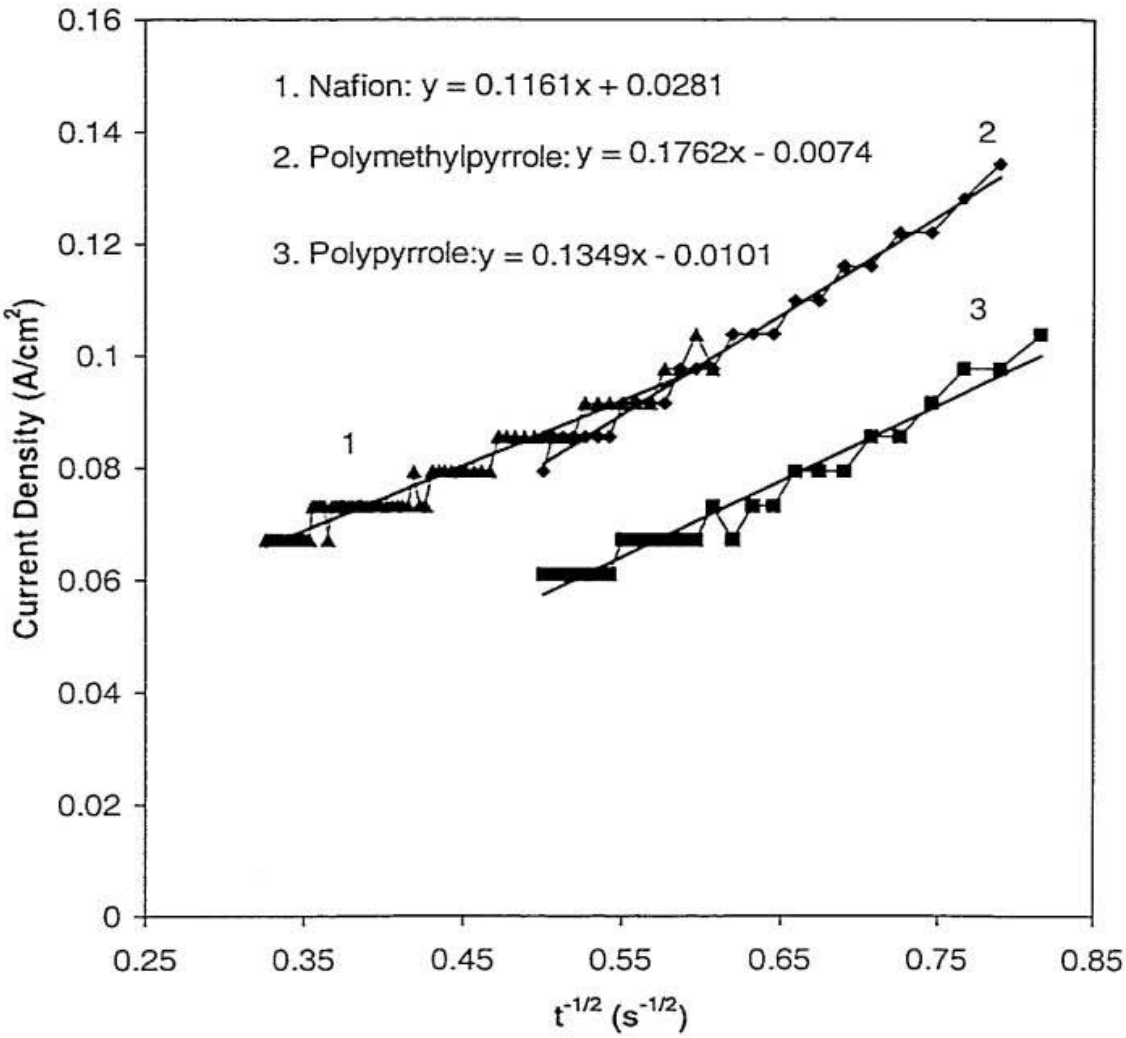

Fig. 4.5 Linear regression of Cottrell relationship for different membranes. Ballard anode.

It can be seen that the modified membranes had a lower diffusion coefficient within the membranes. The higher inhibition of methanol crossover for the modified membranes is due to the lower diffusion coefficient. Therefore, it can be deduced that the methanol crossover inhibition for the modified membranes is realized by blocking of the channels in the Nafion membrane by the conducting polymers. Therefore, the modification of Nafion membrane by conducting polymers such as PPy and PMPy is a quite promising method, although the stability of modified membranes still needs to be evaluated based on the practically operating conditions of DMFCs.

4.3.5 Oxygen Reduction Performance for Modified Membranes

Although the modified membranes have demonstrated a high inhibition of methanol crossover, the ORR performance on the cathode should not be affected. Otherwise, it will be without commercial value. Fig. 4.6 shows the ORR performance for modified membranes. It is seen that, after correction for the IR drop, the ORR performance for the modified membranes was quite similar to that of original Nafion membrane. This strongly indicates that the modified membranes do not affect the kinetic performance of the catalysts. This phenomenon is very important as the current density is usually lower, i.e., below 400 mA/cm^2 in the DMFC. Therefore, as far as the kinetic performance of the catalysts can be maintained, the slight increase in membrane resistance would not significantly affect DMFC performance. The thin layer of

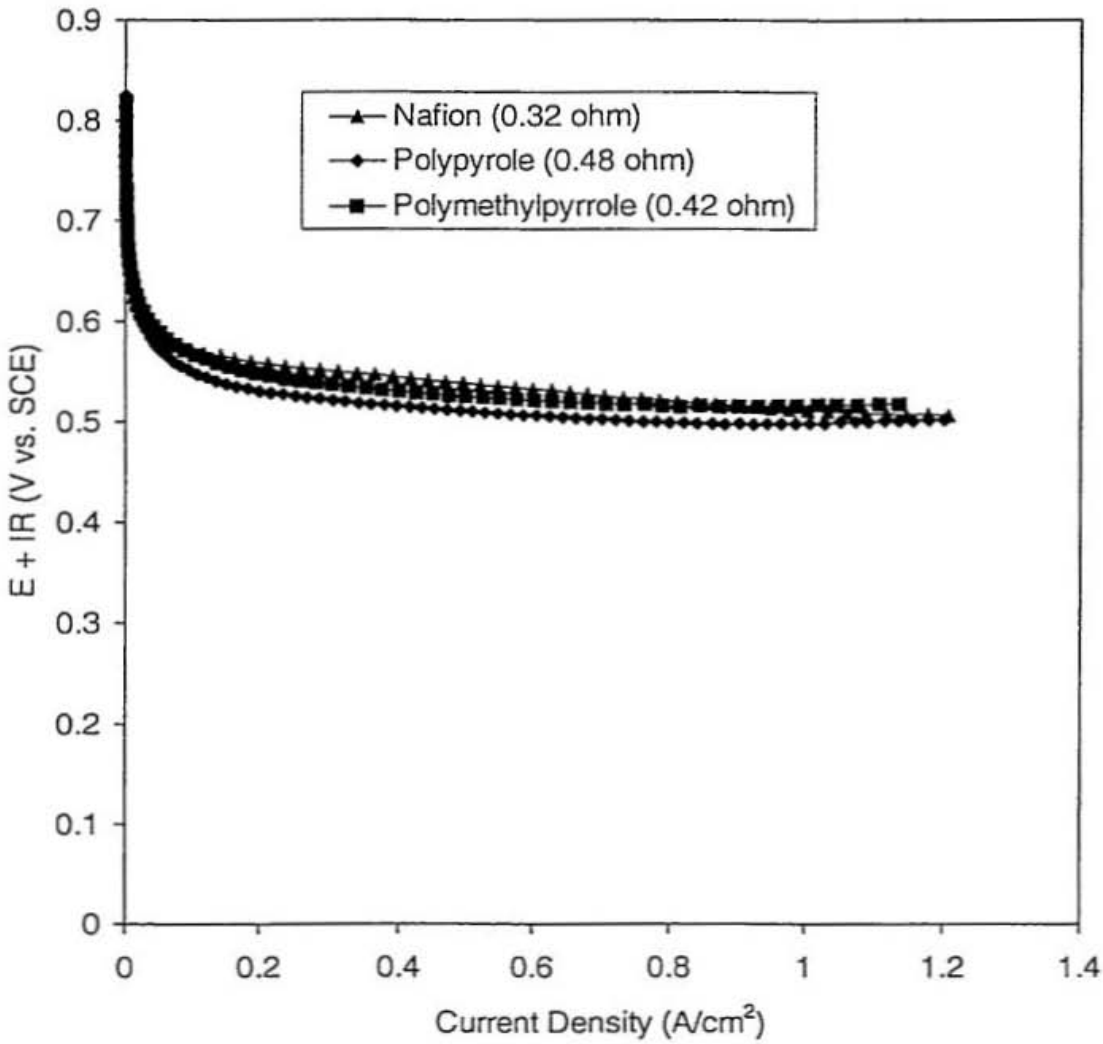

Fig. 4.6 Oxygen reduction performance for different membranes. 4 mg Pt/cm^2 electrode.

conducting polymers on/within the Nafion membrane would not short out the cell since monomers are hardly permeate through the membrane (15, 16). This indicates that all conducting polymers formed close to the surface.

4.4 Conclusions

PPy and PMPy were deposited on/within Nafion® 117 membranes by chemical oxidation with either Fe^{3+}, $(NH_4)_2S_2O_8$, H_2O_2 or O_2 with UV irradiation. The modified membranes showed similar resistance to the original membranes if polymerization conditions are controlled properly. Modified membranes inhibit methanol crossover to different extents. PPy polymerized by Fe^{3+} demonstrated the highest inhibition of methanol crossover. The inhibition of methanol crossover is realized by a lower methanol diffusion coefficient in the modified membranes. The modified membranes do not affect the cathode kinetic performance for the ORR although a small additional ohmic loss is caused by the slight increase in resistance of the modified membranes.

References

(1) M. R. Verbrugge, J. Electrochem. Soc., 136, 417 (1989).

(2) D. L. Maricle, B. L. Murach, and L. L. Van Dine, Abstract 35, p. 58, The Electrochemical Society Extended Abstracts, Vol. 94-1, San Francisco, CA, May 22-27, 1994.

(3) Akiko Aramata, Takuro Kodera, Makihiko Masada, J. Appl. Electrochem., 18, 577 (1988).

(4) K. A. Mauritz, C. J. Hora and A. J. Hopfinger, Advs. Chem. Ser. ACS, 187, 123 (1980).

(5) T. D. Gierke and W. Y. Hsu, ACS Symp. Ser., 180, 283 (1982).

(6) S. R. Narayanan, A. Kindler, B. Jeffries-Nakamura, W. Chun. H. Frank, M. Smart, T. I. Valdez, S. Surampudi, and G. Halpert, 11th Annual Battery Conference Applications and Advances, 1996, p. 113-122.

(7) R. F. Savinell, E. Yeager, D. Tryk, U. Landau, J. S. Wainright, D. Weng, K. Lux, M. Lit, C. Rogers, J. Electrochem. Soc., 141, L46 (1994).

(8) J. –T., Wang, J. S. Wainright, R. F. Savinell, M. Litt, J. Appl. Electrochem., 26, 751 (1996).

(9) J. S. Wainwright, J. –T. Wang, D. Weng, R. F. Savinell and M. Litt, J. Electrochem. Soc., 142, L121 (1995).

(10) D. Weng, J. S. Wainright and R. F. Savinell, Ext. abstract 667, 188th Electrochemical Society Meeting, Chicago. IL, 8 –13 Oct. (1995).

(11) Executive Summary, Direct Methanol Fuel Cell Review Meet., Dept. of Energy and Advanced Research Projects Agency, Baltimore, 26-27 Apr. 1994.

(12) K. Scott, W. Taama, J. Cruickshank, J. Power Sources, 65, 159 (1997).

(13) F. N. Buchi, B. Gupta, O. Haas and G. G. Scherer, J. Electrochem. Soc., 142, 3044 (1995).

(14) C. Lamy and J-M. Leger, 1st International Symposium on New Materials for Fuel Cell System, O. Savadogo, P. R. Roberge and T. N. Vezirogln (Eds.), p. 296, Editions de l'Ecole Polytechnique de Montreal, Canada (1995).

(15) Toshikatsu Sata, Chem. Mater., 3, 839 (1991).

(16) Toshitatsu Sata, J. Membrane Science, 72, 43 (1992).

(17) R. Ansari, W. E. Price and G. G. Wallace, Polymer 37, 917 (1996).

(18) S. Y. Luk, W. Lineton and M. Keane, C. Dearmitt and S. P. Armes, J. Chem. Soc. Faraday Tran., 91, 905 (1995).

(19) S. K. Dhawan, M. K. Ram, B. D. Malhotra, S. Chandra, Synth. Metals, 75, 119 (1995).

(20) K. Nishio, M. Fujimoto, O. Ando, H. Ono, T. Murayama, J. Appl. Electrochem., 26 425 (1996).

(21) Steve Holdcroft and B. Lionel Funt, J. Electroanal. Chem., 240, 89 (1988).

(22) R. Kostecki, M. Ulmann, J. Augustynski, D. J. Strike and M. Koudelka-Hep, J. Phys. Chem., 97, 8113 (1993).

(23) M. Ulmann, R. Kostecki, J. Augustynski, D. J. Strike, M. Koudelka-Hep, Chimia 46, 138 (1992).

(24) C. C. Chen, C. S. C. Bose and K. Rajeshwar, J. Electroanal. Chem., 350, 161 (1993).

(25) C. S. C. Bose and K. Rajeshwar, J. Electroanal. Chem., 333, 235 (1992).

(26) H. Laborde, J-M. Leger, C. Lamy, J. Appl. Electrochem., 24, 219 (1994).

(27) D. J. Strike, N. F. De Rooij, N. Koudelka-Hep, M. Ulmann, J. Augustynski, J. Appl. Electrochem., 22, 922 (1992).

(28) C. T. Hable and M. S. Wrighton, Langmuir, 9, 3284 (1993).

(29) Xiaoming Ren, T. A. Zawodzinski Jr., F. Uribe, Hongli Dai and S. Gottesfeld, Proton Conducting Membrane Fuel Cells I, edited by S. Gotesfeld, G. Halpert, and A. Landgrebe, Proceedings Volume 95-23, The Electrochemical Society, Inc., 1995, p. 284.

(30) Burgmayer, P and Murray, R. W., J. Phys. Chem., 88, 2515 (1984).

(31) Chris D. Paulas and P. G. Pickup, J. Phys. Chem., 92, 7002 (1988).

(32) G. Schwitzgebel and F. Endress, J. Electroanal. Chem., 386, 11 (1995).

(33) H. L. Yeager, in Perfluorinated Ionomer Membranes, edited by A. Eisenberg and H. L. Yeager, (1982), p. 3.

Chapter 5

A Summary of This Research and Future Work

In this thesis, half-cell techniques with transient polarization have been demonstrated to provide fast evaluating the catalysts for PEMFCs. By using this setup, the catalysts can be evaluated without using complicate humidification systems for reactant gases. Furthermore, with this method, catalysts modified by chemical oxidation, especially in acidic environment, have been successfully characterized. The modified catalysts showed a higher proton conductivity while maintaining their electronic conductivity, and therefore showed improved kinetic performances as well as higher performances at high current densities. The idea of modifying commercial catalysts can be extended to many chemicals which can react with carbon to give products with a higher proton conductivity and/or a higher O_2 solubility. For instance, Br_2 and F_2 can react with carbon to produce -CF_2- and –CBr_2- groups which can give a higher oxygen solubility in the catalyst layer. This direction remains open for further investigations. Moreover, although the modified catalysts have demonstrated improved short-term performances in a half cell, they still need a long-term evaluation to confirm their stability under true PEMFC operating conditions.

The reduced CO_2 reoxidation method showed better resolution than conventional H_2 adsorption or desorption for active area determination of carbon-supported catalysts. It

is easily applied in real systems due to its non-toxicity in comparison to the CO stripping method. Additionally, the peak and onset potentials for reduced CO_2 oxidation can provide two significant indications of the catalyst's tolerance towards CO and CO_2. However, it can only be used for relative comparison of active surface area among different catalysts. Therefore, the measurement of absolute surface area by this method remains a goal for further studies.

Nafion membranes modified by conducting polymers have been found to significantly decrease MeOH crossover without affecting cathode performance. Less MeOH crossover could substantially increase DMFC performance. However, the modified membranes were only tested at temperatures up to 70 ^{0}C in a half-cell. In a real DMFC, the temperature can go higher than 120 ^{0}C, which requires the modified membrane to stand a high temperature. Therefore, the high temperature stability needs to be tested in the future. Furthermore, in order to avoid the impact of bubble adsorption on the membrane at high temperatures, the half-cell setup should be modified to allow the electrolyte to flow in the cell.